Report on

Modeling and management of erosion and sedimentation processes in a stretch of Gandak River using morphodynamic modeling

A Purpose Driven Study under National Hydrology Project

PDS Code: NIH-34 _ 2019 _107

NATIONAL INSTITUTE OF HYDROLOGY
ROORKEE – 247 667 UTTARAKHAND
Oct, 2024

Modeling and management of erosion and sedimentation processes in a stretch of Gandak River using morphodynamic modeling

Study Sponsored by
National Hydrology Project
Ministry of Jal Shakti
Department of Water Resources, River Development & Ganga Rejuvenation

Study carried out at
Centre for Flood Management Studies
National Institute of Hydrology
Patna, Bihar
Oct, 2024

Study Group

Lead Organization: National Institute of Hydrology, Roorkee

Principal Investigator:	**Dr. Pankaj Mani, Scientist G**
Co. PI:	**Dr Rakesh Kumar, Scientist G (Retd.)**
	Sh. J. P. Patra, Scientist E
	Dr Biswajit Chakravorty, Scientist G (Retd.)

Partner Organization: Flood Management Improvement Support Centre, Water Resources Department, Patna, Bihar

Principal Investigator:	**Md. Parwez Akhtar, Deputy Director**
Co. PI:	**Er. Bindiya Gupta, Assistant Directo** **Er. Manish Kumar, Assistant Director**

Acknowledgement

The study group at NIH has made its best efforts in carrying out the study entitled **"**Modeling and management of erosion and sedimentation processes in a stretch of Gandak River using morphodynamic modeling**"** sponsored by National hydrology Project. However, it would not have been possible without the support and help of many individuals and organizations. I would like to extend my sincere thanks to all of them.

I express gratefulness towards the partner agency Flood Management Improvement Support Centre, Water Resources Department, Patna, Bihar for providing logistic help and support for the study. I am thankful to NHP officials for providing fund and other support to carry out the study. I also thank NHP division of NIH who provided necessary support in carrying out the river cross section survey work though outsourcing, hydrological data collection work. I also express my gratitude to Director NIH, officials of PDS NIH for their contributions through constant support and constructive suggestions.

(Pankaj Mani)
Scientist G & Principal Investigator
Centre for Flood management Studies
National Institute of Hydrology, Roorkee

Contents

List of Figures

List of Tables

List of Annexure

1 PDS PROPOSAL & RELEVANCE

1.1 About PDS Proposal

A project proposal entitled "Modelling and management of erosion and sedimentation processes in alluvial river using morphodynamic modelling" was submitted to National Hydrology Project (NHP) as Purpose Driven Study (PDS) in May 2019. National Institute of Hydrology (NIH), Patna is the lead organization and Water Recourses Department (WRD), Government of Bihar (GoB) is the partner organization in this PDS study. WRD nominated officials from Flood Management Improvement Support Centre (FMISC), WRD GoB as Principal Investigator (PI) and Co-PI (Annexure-I). The partner organization has the responsibility of providing the logistic support during field visit, data support and identification of a study site. Altogether 15 vulnerable sites (8 on Gandak river, 6 on Kosi river and one on Ganga river) were intimated by FMISC (Annexure-II). For this study the site one Gandak river from Kunwari village (near 47 km. of Saran Embankment) in u/s of Rewa Ghat up to Baligaon (near 30 km. of Saran Embankment) in d/s of Rewa Ghat bridge was finalized in consultation with FMISC. The main reason for selection of this stretch was its vulnerability to bank erosion at several locations and many anti-erosion works have been carried out in this stretch. However, the problem is not limited to this stretch and is widely spread over the entire alluvial stretch of Gangetic plain, and therefore, the lesson learnt from the specific study may be transferred to other reaches aslso.

1.2 The Gangetic Plain

The Gangetic Plain is developed mainly by the alluvium of the Ganga and its tributaries. The catchment area of Ganga basin is 10.86 lakh Sq. Km, out of which 8.61 lakh Sq Km lies in India, which is nearly 26% of the total geographical area of the country. The basin is spread over 11 States namely, (i)Uttarakhand, (ii)Himachal Pradesh,(iii)Haryana, (iv)Delhi, (v)Uttar Pradesh, (vi)Rajasthan, (vii)Madhya Pradesh, (viii)Chhattisgarh, (ix) Bihar, (x)Jharkhand and (xi)West Bengal. The important tributaries which join the Ganga in its course are the Ramganga, Gomati, Ghaghra, Gandak, BurhiGandak, Kosi, Kamla, Bagmati and Mahananda on the left and Yamuna, Tons, Sone, Punpun, Kiul, Ajoy, Damodar and Rupnarayan on the

right. The historical evidences show that the alluvial plain has remained the initiator of agriculture since neolithic period. The availability of extensive fertile land, perennial water and the conducive climatic condition might have allured the early settlement to conceive agricultural practices in the region. The archaeological investigations suggest several early civilizations have flourished in the region where the agricultural was the main occupation of human population (Singh 2012). Since long, the agricultural practices have transformed to the tradition and passed from generation to generation. The Indo Gangetic Plain is one of the most extensive fluvial plains of the world where the ancient agricultural activities have progressed to well develop agricultural practices (Pal et al., 2009). Within Ganga basin in Indian Territory, coverage of agricultural land accounts to 65.57% of the total area (GFCC, 2023). The Agriculture Sector occupies centre stage in Indian economy encompassing three thrust areas; (1) to promote inclusive growth, (2) to enhance rural income, and (3) to sustain food security. It accounts for nearly 14% of GDP, about 13 % of exports and supports half of the country's population as its principal source of income (58% of workforce). As per Census 2011, the total number of agricultural cultivators and agricultural laborers increased from 234.1 million in 2001 to 263.0 million in 2011. The share of agri-exports in total exports increased from 12.81% in 2011-12 to 13.08% (Rs 231,992 Cr) in 2012-13, a record level. Agriculture industry greatly add to the economy of India, providing direct benefit of employment and livelihood to its practitioners and supporting food demand for major chunk of country's population. In the Ganga basin, there are several major systems of canals which cater to almost 28 percent of the net irrigated area. There are 478 major and medium irrigation projects that represent a command area of about 36.12 percent of the basin. The agriculture and its allied sector greatly add to the Gross Domestic Product of India and consequently leads to benefits to the economy such as an increased multiplier effect (Sehgal et al., 2013). The contribution of Ganga basin states in agricultural and allied sectors at current price is about 46.7 % of the national contribution (NSO, 2022).

1.2.1 Tributaries originating from Nepal

The Ganga is the main drainage line flowing west to east while the several tributaries originating from north in Nepal mostly creates flood havoc. The average annual rainfall in the basin varies from 600 mm to 1900 mm and about 80% of it occurs during the south west monsoon. The rainfall increases from West to East and from South to North. The flood problem is mostly confined to the areas on the northern bank of the river Ganga. In the basin

States, Bihar (northern part), Uttar Pradesh (eastern part) and West Bengal are the worst flood affected states. The main reasons of flooding in these states are; intense and prolonged rainfall in the catchments (Nepal) of the tributaries, high spate of Ganga during floods tributaries causing inundation due to back water effect, excessive silt load in the tributaries causing erosion and sedimentation in rivers, reduced carrying capacity of rivers due to silting, meandering and bank line shifting of rivers adversely affecting the flood protection measures and thus causing loss of land, property and life. The damage by the northern tributaries is aggravated not only by spilling over their banks but also due to changing of their courses. The excessive erosion and siltation coupled with inadequate maintenance also adversely impact the operation and efficiency of existing flood control structures.

Mostly the flooding problems in Ganga river basin are located in middle and lower reach where the slope of Ganga river is flat to very flat. The eroded materials from the upper reach are carried downstream and deposited in these reach causing river aggradation and bank erosion in middle reach and accretion in the lower reach. Moreover, the north bank tributaries of Ganga river in the middle and lower reach, originating from Nepal brings excessive silt with flood due to climatic, geological and topographical conditions. These tributaries while travelling from very steep slopes in mountainous region to comparatively milder slope in tarai region and further very mild slope in their lower reaches brings down the sediments causing river meandering, bank line shifting, river aggradation and bank erosion. In general, the flood problem increases from the West to the East and from South to North. In the North Western parts of the region and some eastern parts, there is the problem of drainage congestion. GFCC reports that about 24 million ha (approximately 50%) flood affected areas lies in Ganga basin out of the total flood affected area of 50 million ha in the country.

1.3 Nature and hydrological problems of alluvial rivers

The word ‘alluvial’ means made up of sand and earth left by rivers, floods, etc. The bed and bank materials of the river beds are made out of sands and gravels transported and deposited by river over a period of time. Another interesting meaning of ‘alluvial’ is carried by moving water. The most prominent characteristics in alluvial rivers are its natural and continuous erosion and sedimentation process. Its second marked characteristic of alluvial river is that it hardly flows in straight path. They mostly flow in meandering and/ or braiding pattern. In fact, the alluvial rivers acquire the shape and planform through a balancing process of erosion

and sedimentation. Unlike non-alluvial rivers which make their way by cutting the landscape, the alluvial rivers evolve their own landscape. The development of floodplain of an alluvial river over the time is a part of its landscape formation until unless perturb through anthropogenic interference. When flood exceeds the bankfull capacity, the river spills over and inundates the adjoining relatively flat floodplain on regular basis, may be in some cases, several times in a year. The floodplain is the natural buffer river space available for excess floodwater. When water spreads over the floodplain, the flow velocity reduces and the suspended sediments (sand and silts) get deposited. Sometimes sedimentation followed by inundation also fills up the abandoned channel within the floodplain. Thus the floodplain is also made up of alluvial soil. Within the floodplain, the river channel may shift its course/ bank by erosion of river bank and or river bed and thus supplying the same alluvial soil to the river. Over time the alluvial river builds its channel with sediment it carries and continuously reshapes its cross section to obtain depths of flow and channel slopes that generate the sediment-transport capacity needed to maintain the stream channel.

The alluvial river flow over the unconsolidated sediment called valley fill, lying above the bedrock. The thickness of valley fill may range from few meters to hundreds of meters. The floodplain of a river is an area of low relief adjacent to the river channel, which is inundated at times of high river stage. During floods the floodplain receives a layer of fine sediment that settles out of suspension as the flood waters spread over the floodplain with reduced velocity. Due to frequent flooding and siltation, the floodplains are very fertile and heavily vegetated. The natural levee along the alluvial channel is formed due to deposition of the finer fraction of suspended sediment of the flood waters passing across the river banks during high flood stage. Once the floodwater crosses over the bank and spread in floodplain, the flow velocity reduces drastically inducing deposition at the junction which in turn forms the ridge line also known as natural levee.

1.3.1 Erosion and sedimentation in alluvial rivers

The major three processes in alluvial rivers are erosion, transportation and deposition. These three processes depend on the amount of energy associated with flowing water. The bed and banks can be eroded making it wider, deeper and longer. The headward erosion occurs near its source and makes the river longer. The vertical (bed) erosion makes the river channel deeper. This happens more in the upper stages of a river. The lateral (bank) erosion makes the

river wider. This occurs mostly in the middle and lower stages of a river. The four main processes of erosion in alluvial rivers are (i) hydraulic action, (ii) abrasion / corrosion, (iii) attrition, and (iv) corrosion. Through hydraulic action, the alluvial particle materials of river bed and banks are detached and moved away with the flow. Sometimes it may also lead to undercutting and bank collapse. If the river slope is steep/ or at falls, the flow may erode the river bed causing bed scour. In abrasion, the sediments cause development of potholes where depressions exist in the channel floor. The attrition is the process in which the larger sediment (rocks) particles collide and breaks into smaller particle and with the movement; its surface becomes smooth and round. Thus when the river moves downstream, the sediment particles becomes more and more smooth and round. Hence, through attrition, the flow energy is decreased and also the sediment particles become smaller and smoother leading to reduce the eroding power of stream. In corrosion the erosion occurs through chemical process as some of the rocks particles are soluble in water/ fluid media. The river erosion in limestone region is due to this reason.

Transportation of the eroded (detached) material with flow starts when frictional force is overcome. The four main processes of transportation are; (i) Suspension (suspended load), (ii) saltation, (iii) traction, and (iv) solution (solution load). In suspension very fine particles (sand, silt and clay etc.) is lifted up due to turbulence and transported with the river flow. If the turbulence is not enough to lift the heavier particles in suspension, they may bounce up and down in the fluid media and move downstream with the flow. Through traction, large materials (boulders etc.) rolled and move downstream with the stream force. Through solution, the dissolved materials are transported with flow.

Deposition occurs when the river loses its energy. This may occur due to several reasons; reduced inflow (rainfall), excessive evaporation, region of high frictional resistance (at river bank), region of reduced velocity (river stretch where its slope drops; shallows area like wider river reach, floodplain, or sea mouth; location of bars in meandering river) etc. (Richards, 1982)

1.3.2 Fluvial depositional landforms

The river moving downstream on a level plain brings down a heavy load of sediments from the upper course. The decrease in stream velocity in the lower course of the river reduces the transporting power of the streams which leads to deposition of this sediment load. Coarser materials are dropped first and finer silt is carried down towards the mouth of the river. This

depositional process leads to the formation of various depositional landforms through fluvial action such as Delta, Levees and flood Plain etc.

Two distinctive depositional process, lateral accretion and overbank sedimentation are responsible for development of various fluvial landforms. In lateral accretion processes, coarser sediment (and bed load) is deposited along the stream. The sedimentation of specific particle size occurs when the flow boundary shear is overcome by the channel frictional force (channel boundary shear). The sediment depositional pattern follows the distribution of channel boundary shear distribution. Thus, the courser sediments are deposited in the channel thalweg and the finer sediments get deposited along the margins as flow depth and velocity reduces. Through, overbank sedimentation are responsible for creating natural levee, infilled channels and floodplain. In this process, the coarse sediments are transported as bedload while the fine grained sediments are transported as suspended load. Once, the flow overtops the channel and moves to wider floodplain, the flow velocity reduces rapidly. This causes deposition of coarser sediments along the channel margin or sometimes transported within the floodplain forming features like dunes and ripples. This sedimentation process depends upon the floodplain hydraulics like; topography, hydrology and vegetation cover. (Hudson,2017)

Natural levees form along channel-floodplain margins and slope towards floodplain bottoms. Natural levees represent the aggregate construction of numerous individual sedimentation events occurred over hundreds of years. They are especially associated with flood-prone rivers dominated by suspended sediment transport, and coastal plain meandering rivers in particular. The slopes of natural levees between the channel and flood basins are related to sediment size, with coarse sediments associated with steep natural levees while fine-grained sediments are more associated with broad low sloping natural levees (Cazanacli and Smith 1996). From the standpoint of humans, natural levees are among the most important landforms within an active floodplain, as their higher surface and permeable soils permit settlement and, especially, agricultural activities with minimal flood risk. Channel bars develop as ripples and dunes are successively deposited along the flanks of shallow channel margins, resulting in lateral accretion. The presence of multiple channel bars in the floodplain indicates the historical channel activity and helps to investigate the historical hydro-climatic conditions. Further, the various landforms of the alluvial rivers are of immense economic

value. The deposition of sediment particle in floodplain is the natural replenishment of soil fertility. The alluvial aquifers are mostly a good source of ground water reserves. The alluvial rivers (channel bar deposits) are the major source of sand (building materials).

1.3.3 Morphological behaviour of alluvial rivers

One of the prominent characteristics of alluvial river is its meandering flow path. A meandering river is a single channel that flows in a curve, bendy path like a snake. Within floodplain the rivers tries to follow the path of least resistance. As the river flows through a relatively flat terrain of loose alluvial soil, it triggers erosion and adopts curved path. Once the meander starts, the process get amplified. Thus in meandering river, the distance 'as the stream flows' is greater than 'linear distance.' The water is flowing at faster rates (higher velocity) at the outer edge of meander compared to the inner edge. This higher velocity induces erosion on the outer edge (cut bank) and contrarily depostio on the inner edge (point bar). The formation of oxbow lake in meandering river is again a widely recurrent phenomenon. The oxbow lakes are formed when the bends of two meanders are close enough, the river bypass the curve. During course of time, the oxbow lake may be filled up with alluvial sediments that are available during flood events. The meandering manage the energy of water, as it moves through and over channel terrain, by increasing resistance and reducing channel gradient. The geometry of the meander minimizes the amount of work, or energy expended, while using that same energy uniformly. Streams meander to maintain equilibrium – a dynamically stable form and function. The water flow through alluvial channel is generally turbulent and so always have some swirling eddies. This turbulence further amplifies, quantitatively and qualitatively, due to presence of channel bed and bank surface irregularities. In some places, this turbulence concentrates the erosive energy on a specific bank causing the river to erode on that bank. The process accelerates the amount of water flowing on this bank, also the channel becomes deeper on this bank. As the stream erodes outward, this bank no longer remains straight and develops a curvature. The curved flow path further develops centrifugal force on the flow mass. The water on the top surface, in turns, heads up towards outer bank while the water at the bottom layer is pulled towards curvature of the stream, to relieve the pressure. The net result of this is that the secondary flow perpendicular to the main flow. The secondary flow is spiral in nature descending along the bank. On the shallower opposite side of the channel, the water velocity will be comparatively lower, allowing sediment to deposit, building a gravel bar. The gravel bar

formation is amplified by the spiral flow of the main current, as it tends to move the eroded material away from the outer bend and back towards the opposite side, dropping some of that material on the end of the bar. In this manner, natural turbulence, combined with the river's ability to erode transport and deposit sediment, develops a meander bend on outer bank while develops gravel bar on the inner bank, called a point bar (Leopold Wolman, 1957; Kumar et al., 2015).

Another major characteristic of alluvial river is its braiding. When the bedload sediment is higher compared to suspended sediment, rivers develop a network of interconnected unstable threads, separated by islands or bars. The total discharge and sediment is conveyed through these threads. Braiding occurs in the river stretch of steep gradient and high flow velocity. The exposed bars appearing in the river during lean flood period may be fully covered during the high flood period. The braided channels undergo rapid changes in morphology associated with channel network dynamics, bar development and migration, local scour and fill, and channel bifurcation. This set of very active channel processes, associated with intense bedload transport, leads to the morphological development and inherent (autogenic) instability of braided river morphology. At high flow where many bars are partially submerged, flow and bedload transport in a braided channel remains divided among several branches with inactive bar surfaces between them, and it is under these conditions that braiding is most active and the morphology is developed. Thus, braiding involves active morphological development at channel-forming flows and is not the consequence of incidental low-flow dissection of bars. (Ashmore, 2013).

1.4 Flood management in Ganga basin

The flood management practices adopted in India may be classified broadly under two categories; structural measures and non-structural measures. Under the structural measures, construction of reservoirs, detention pond, interlinking of rivers, flood diversion channel etc. are planned wherein the inflow flood is controlled and moderated. Some other structural measures like; construction of levee, embankment, floodwall, channel and drainage improvement measures etc. are also adopted to protect the area wherein, although the flood is not reduced, the river banks are artificially raised to prevent spilling. Watershed management practices through forestation, soil conservations and vegetation covers and construction of check-dams, detention basins, diversion channels, and other structures to arrest flow velocity and silt on the hill slope are part of the structural measure of flood management practices in

hilly areas. Among the non structural measures, flood forecasting and early warning system, flood hazard mapping and risk assessment, floodplain zoning, development of guidelines for building construction in flood prone areas, development of emergency action plan, performance evaluation and efficiency assessment of existing structural measures are in practice. In some of the states, raising of villages in flood prone areas has also been attempted that may be considered as a way forward towards "living with flood concept'. As per the CWC report (CWC, 2018), the total flood protected area in three worst flood affected states of Uttar Pradesh, Bihar and West Bengal is 8.97 ha. This has been achieved by construction of embankment (18,113 km), improvement of drainage channel (11,752 km), raised villages (4, 511), town protection works (343), and raised platforms (65). The flood protection measures adopted in these states are able to reduce the flood impact considerably. The year-wise flood affected area has been reduced as shown in Figure 1.1. Among the various flood management practices, construction of embankments is widely practiced. They are cost and time effective and can be constructed using locally available construction materials and manpower.

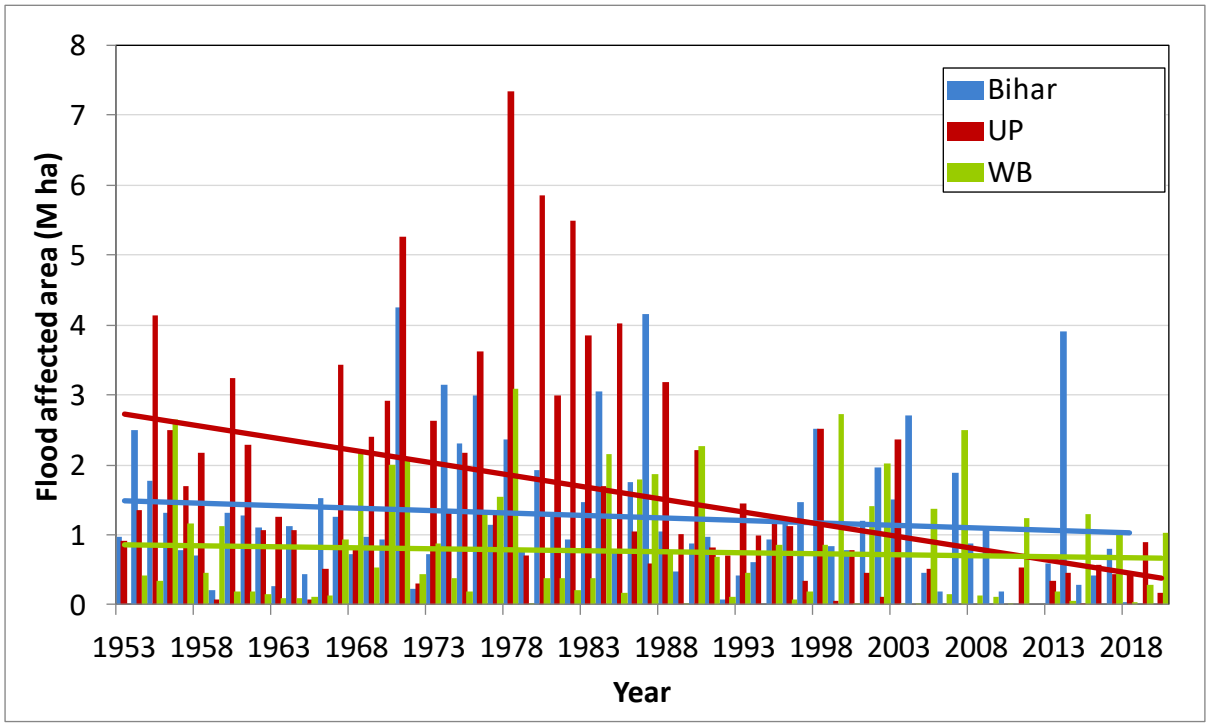

Figure 1.1: Flood affected area from 1953 to 2018 in states of Bihar, UP and WB (source: CWC, 2022)

However, construction of embankment may also induce adverse affect to the river and floodplain. The river and floodplain are the integral part in alluvial river system connected

laterally and hydrologically. For extreme floods, the floodplain acts as valley storage, hold significant amount of sediments and the acts as recharge zone for ground water. The construction of embankment impedes all these process. The confinement of the river flow within embankment cause high flow velocity and flood level. The embankments may be vulnerable to river action particularly during high floods. In such cases, the cost intensive anti-erosion works may be warranted at the short notice. It may also obstruct the countryside drainage and therefore provision of flood sluices is made. Thus along with the embankment several allied structures becomes the integrated part of the complete flood protection system. Hence, its planning, design and regular operation and maintenance plays a vital role to maximize the benefit from this flood protection measure. In absence of preventive measure, either, flood risk is transferred in the downstream river reach or its failure may pose more severe flood hazard in the protected area (Habersack, 2015). The erosion/ sedimentation in alluvial river system are a complex process involving a number of factors including fluvial erosion, seepage erosion, and cantilever mass failure. To predict the rate of bank erosion/ sedimentation with these complexities, a morphodynamic modeling is suitable approach. The morphology of an alluvial river channel affects the movement of water and sediment along it, but in the longer run is shaped by those processes. The problem of erosion and siltation in a river reach are equally disastrous and need engineering interventions (river training works) at critical locations. The river training works may serve the following objectives or advantages:

1. To prevent the river from changing its course and to avoid outflanking of structures like bridges, weirs, aqueducts, etc. (guide bunds)
2. To prevent flooding of the surrounding countries by providing a safe passage for the flood waters without overtopping the banks (embankment).
3. To protect the river banks by deflecting the river away from the attacked banks (Groynes or Spurs)
4. To ensure effective disposal of sediment load (river bank pitching.
5. To provide minimum water depth required for navigation (dredging etc.).

These measures are cost intensive. A well designed structure has to take care of obstruction induced silting and proportionate withdrawal of silt with water so as not to affect the river regime beyond a controlled area upstream or downstream. Similarly, other human interferences such as removal of bed and bank materials through mining, dredging for removal of silt near outlets or for maintaining a specified depth of channel for navigation etc,

should also conform to river regime. For providing dependable protection, scientific approach is required for understanding the river morphodynamics and thus to estimate the suitable hydraulic design parameters for anti-erosion works and silt management measures. 2D morphodynamic models are better replica of flow conditions and velocity distribution in alluvial river to understand the river regime and flow characteristics. The understanding of morphological behaviour of river will help in design a corrective measure to reduce the impact of overall flood disaster.

1.5 Objectives of the study

Understanding of the fluvial process as a result of sediment deposition and erosion, is necessary for management of alluvial river. Flood, avulsion and sediment transportation and deposition are the natural processes in alluvial rivers while the water diversion, channelization, and navigation are human disturbances to rivers. The fluvial process is the macroscopic view and long-term consequence of sediment movement. The braided rivers are naturally unstable, causing frequent bank erosion in different reaches and at varying rate. If the bank is composed of finer non-cohesive material, the erosive activity could take a serious turn. Therefore, arresting the erosive activity is given high importance. Anti-erosion works are normally costly and therefore, such measures are executed mainly at critical locations. For providing dependable protection, scientific approach is required for understanding the river behaviour at the critical location. The morphodynamic modelling helps in quantitative estimation of the flow and sedimentation/ erosion characteristics of river that can be used for adopting suitable engineering measures and their design. This study is proposed for problematic reach of alluvial river where severe bank erosion has been observed. The flood and erosion characteristics are proposed to be investigated using morphodynamic modelling in the study reach using MIKE 21C model. The study would identify if some engineering measure are necessary in the reach and also to estimates the design parameters of those engineering measure.

The draft policy of silt management 2017 (MOWR, RD and GR) suggested various approach of sediment management in river flowing through floodplain where it has meandering characteristics with fine sand bed, wide river width and interacting flood plain. For this reach the report suggests the sediment management practice through river training works such as bank protection, spurs etc, sand mining, desiltation/dredging etc. However, the reports

advocates to carry out a study of the river reach selected for desiltation/ dredging by appropriate mathematical and/ or physical model studies by employing consistent practices. The de-silting of any river reach needs to be justified bringing out clearly the flooding caused due to siltation along with technical comparisons of the alternative flood mitigation measures with "do nothing" or "proposed de-silting/ dredging" being other options. It should invariably be associated with sediment flux studies and morphological studies to confirm no significant adverse effect on downstream or upstream reach of the river including the safety and effectiveness of river crossings, water intakes, existing river bank / flood protection measures etc. Further, post dredging, sediment flux studies should also be carried out to quantify the amount of silt likely to be deposited in future i.e. Sediment modelling studies for the river may be done before taking up any such project. Presently most of the river training works are designed based on prevailing guidelines (CWC, etc.) and no specific studies are carried out for the purpose. As the erosion problem and its management is varying from case to case the scientific study of erosion is required which is generally done by suitable river model embedded with a sediment transport model. Such model is able to describe the variation in hydrodynamic characteristics i.e. water level and flow velocity and morphological characteristics such as helical flow, sediment transport, scour and deposition, bank erosion and plan form change of a river etc. The present study proposes to use a 2D curvilinear flow model to study the flow and sediment dynamics in an alluvial river. The objectives of the studies are:

1. To develop the flow field and carrying out the flood studies of river channels and adjacent floodplains using a curvilinear grids that follow the bank lines (to compute the flow characteristics like maximum flood level, flow velocity, flow direction, etc.).
2. To forecast of morphological changes over 2-3 years in the mobile braided river (The analysis would useful for planning and execution of river training works).
3. To prepare design criteria for river training works in terms of flow velocities, flow depths, scour depths, bank line retreat rates, shoaling, etc.
4. To analyse of sediment deposition (and erosion) in the study stretch, particularly at the meandering portion, bifurcations, confluences etc. and prediction of required annual volume of silt for dredging and sand mining etc.

The flow model developed and simulated for design flood estimates will be used to compute the flow characteristics like maximum flood level, flow velocity, flow direction, etc. and may

be used to for design of infrastructures. The design criteria for river training works depends on flow velocities, flow depths, scour depths, bank line retreat rates, shoaling, etc. The short term morphological characteristics are useful for planning and execution of river training works. The silt balance study are useful in deciding the location and quantification of required annual volume of silt for dredging and sand mining etc. The river flow models along with sediment transport model (morphological model) are used to predict the above characteristics.

2 STUDY AREA

2.1 General

Gandak River known as Kalie or Krishna Gandaki in the upper reaches rises in the glacial of southern Tibet at altitude of 7,620 m near Tibet Nepal border to the south east of Dhaulagiri at north latitude 29°18” and east longitude 83°85”. After receiving a number of tributaries like Mayangadi, Bari and Trisuli, Gandak debouches into the plains of West Champaran district of Bihar at Triveni (Valmikinagar). At this point two more tributaries viz. Panchand & Sarhad join the river. The entry point of the river at the Indo-Nepal border is also the confluence called Triveni with rivers Pachnad and Sonha descending from Nepal. Further downstream, the river flows into Bihar (India) from Nepal in the eastern end of the Valmiki Sanctuary and meets Masan. The Gandak flows southeast 300 kilometres across the Gangetic plain of Bihar state through West Champaran, Gopalganj, Saran and Muzaffarpur districts. It joins the Ganges near Patna just downstream of Hajipur at Sonepur (also known as HariharKshetra). The catchment area of the basin is 45,731 Sq. km, (5,687 sq. km is in Tibet, 30,882 sq. km in Nepal, 1,874 sq. km in U.P. and 7,288 sq. km in Bihar). This area is 6.96% of the total Ganga Basin catchment. It runs a course of 380 km in Tibet & Nepal and about 250 km in India. The basin map of the Gandak river is shown in Figure 2.1.

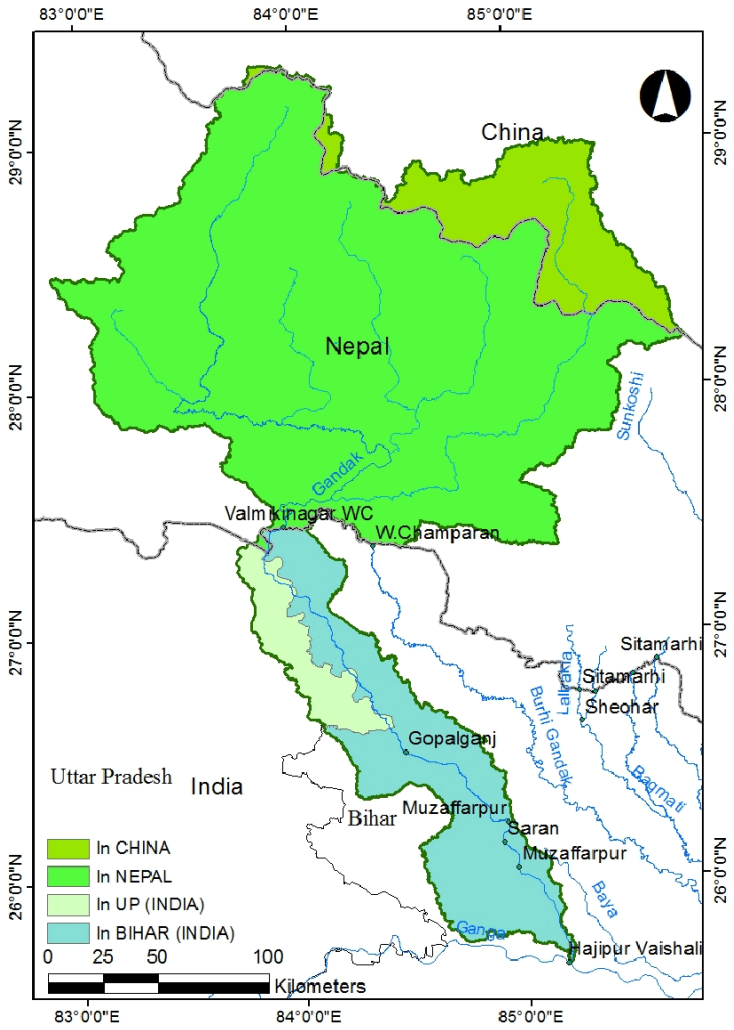

Figure 2.1: Basin area map of Gandak River.

The area of interest (study stretch proposed by WRD, Bihar) is located on the Gandak river between Kunwari village (near 47 km. of Saran Embankment) in upstream of Rewaghat up to Baligaon (near 30 km. of Saran Embankment) in downstream of Rewaghat. The Gandak river in this stretch is located in Muzaffarpur and Lalganj district on the left bank and Saran district on the right bank of Gandak river. The location map of the study stretch is shown in Figure 2.2. However, the hydrological data is available at Dumariaghat in the upstream reach and Lalganj and Hajipur in the downstream reach as shown in this figure. Considering the availability of the hydrological data, the study stretch has been thus extended on either side of the area of interest, i.e. from Dumariaghat to Hajipur. The locations of GD sites are also shown in the figure, Dumariaghat and Lalganj as GDSQ sites and Rewaghat and Lalganj as Gauging sites. The river is embankment in the entire stretch; the left bank embankment is

known as Tirhut embankment while the right bank embankment is known as Saran embankment. The left and right bank embankments are shown in Figure 2.2 by green and blue lines, respectively. The spacing of the embankment in the upper reach (upstream of Rewaghat) is more compared to downstream reach. Even in the downstream reach, the spacing is higher at the meandering locations. Due to bank erosion and river shifting, the river is flowing very close to embankment at few locations endangering its safety and therefore, anti-erosion works have been carried out either to protect the embankment or to deflect the river away from embankments.

In this stretch, the river bank erosion is very prominent causing major damages to the adjoining villages/ settlement. Several anti-erosion and flood control structural measures have been constructed from time to time by WRD Bihar to mitigate the damages. The details of anti-erosion work is obtained from WRD (Bihar Embankment Assets Management System) and incorporated in the modeling study. Three structures namely, two spurs on the right bank of Gandak river at Baligaon and one bed bars at Phular on the left bank of the Gandak river exists in the study stretch, as shown in Figure 2.3.

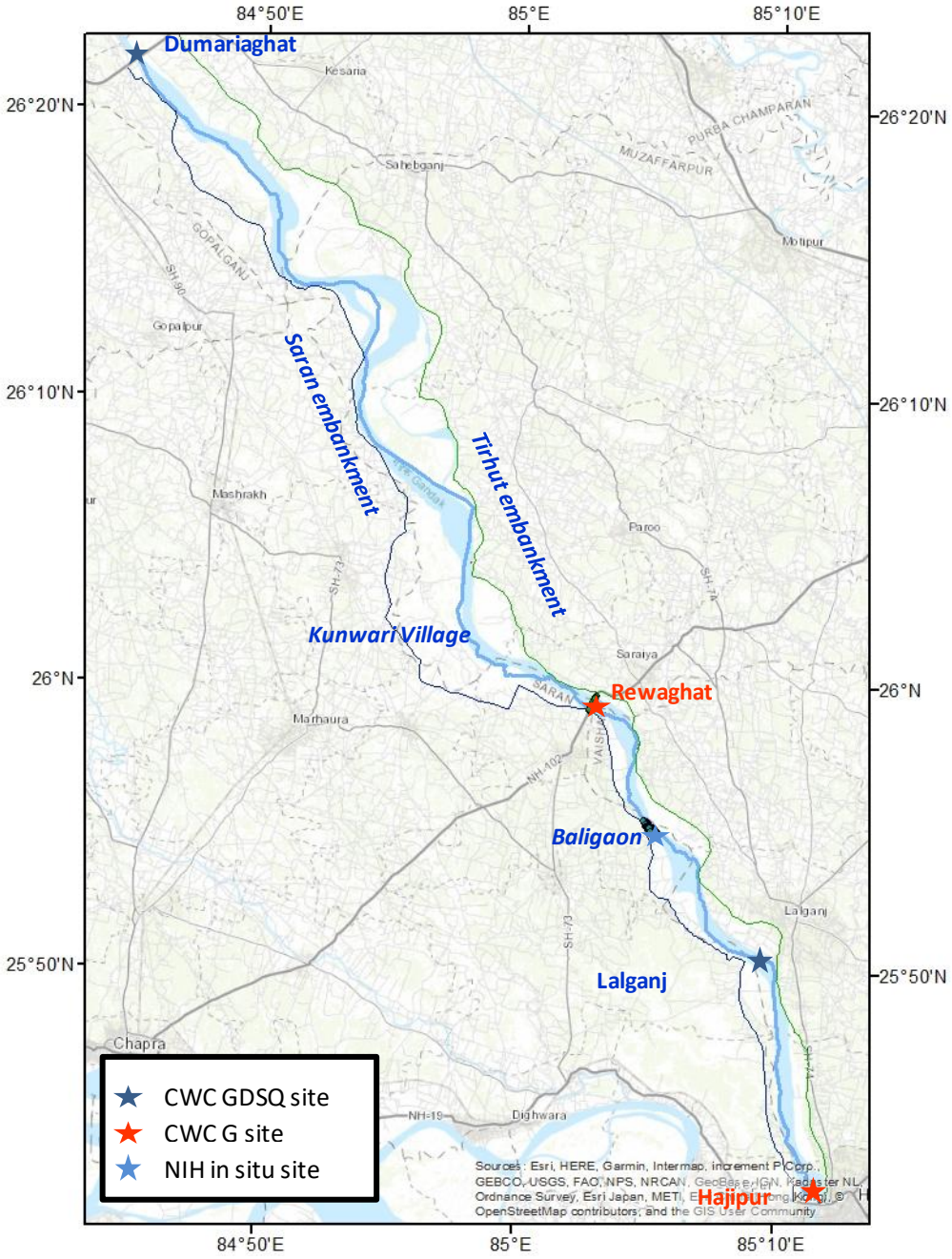

Figure 2.2: Study stretch in Gandak river.

The river length from Dumariaghat to Hajipur gauging sites is 99.8 km This stretch is used for development of 1D flow model.

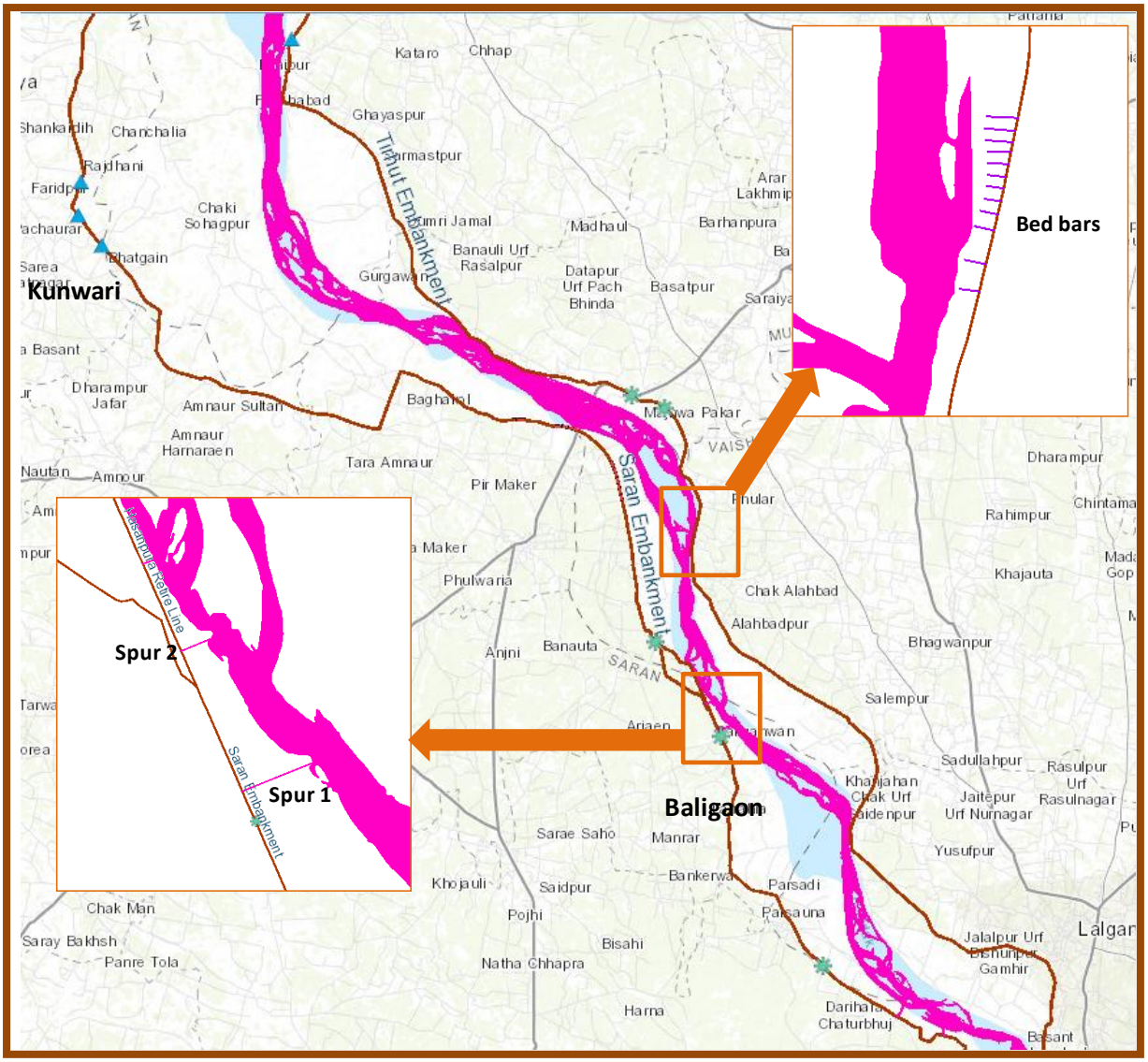

Figure 2.3: location of anti-erosion structures in the study reach.

The river length from Kunwari village to Baligaon is about 20 km. This stretch is used for development of curvilinear 2D flow model.

3 DATA AVAILABILITY

The data used in the study comprises of satellite images, hydrological data and river geometry data. The open source satellite images are downloaded from USGS web sites. The hydrological data are obtained from Central Water Commission (CWC). Site specific hydrological data at Baligaon site is collected by Centre for Flood Management Studies (CFMS), National Institute of Hydrology (NIH), Patna during 2022 monsoon. The river geometry data (river cross section data is obtained by field surveying through outsourcing. In addition, the locations of anti-erosion works are obtained from WRD Bihar (through site visit and online resources on Embankment Assets Management System). The details of data used in the study are described in this section.

3.1 Satellite data

It was proposed to use the satellite images for river morphological analysis. The satellite images for the study reach are downloaded from USGS web site during the period of 1975 to 2020 at an average interval of 5 years. The cloud free satellite images are selected generally for post monsoon period for extraction of river bank line. The details of data used in the study is given in Table 3.1

3.2 Hydrological data

3.2.1 Hydrological data from CWC

The gauge discharge and silt data for various gauging sites in the study reach are obtained from CWC. The gauge (G) discharge (D) and silt (S) data are available at Dumarighat and Lalganj sites while only gauge data is available at Rewaghat and Hajipur sites. The locations of hydrological data stations are shown in Figure 2.2. The details of data obtained from CWC are shown in Table 3.2. The data availability for GD and S are shown in Figure 3.1 and Figure 3.2, respectively. Considering the data availability, the hydrodynamic flow model could be generated for 2015 to 2019 while sediment transport model could be generated for 2019 only.

Table 3.1: Details of satellite images used for morphological analysis.

Date	Satellite	Sensor	Spatial Resolution (m)
03 Nov 1975	Landsat 2	MSS	60
16 Oct 1980	Landsat 3	MSS	60
22 Nov 1991	Landsat 5	TM	30
17 Nov 1995	Landsat 5	TM	30
13 Oct 2000	Landsat 5	TM	30
12 Nov 2005	Landsat 5	TM	30
25 Oct 2010	Landsat 5	TM	30
08 Nov 2015	Landsat 8	OLI	30
21 Nov 2020	Landsat 8	OLI	30

Source: https://earthexplorer.usgs.gov/

Table 3.2: Hydrological data as obtained from CWC.

SN	Name of Site	Data type	Data frequency	Year (monsoon only)	Remarks
1	Dumariaghat	G & D	Daily	2015-2020	Full
		S	Daily	2019	Full
2	Rewaghat	G	Daily	2015-2020	Full
3	Lalganj	G& D	Daily	2015-2020	Full
		S	Daily	2015-2016 2019-2020	Partial Full
4	Hajipur	G	Daily Hourly	2019-20 2019-20	Full

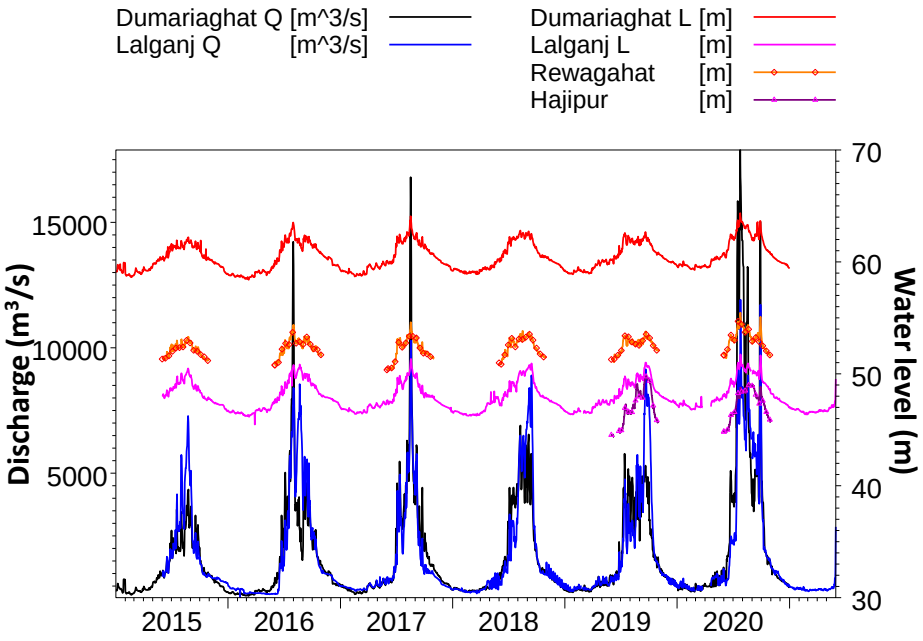

Figure 3.1: Availability of gauge and discharge data.

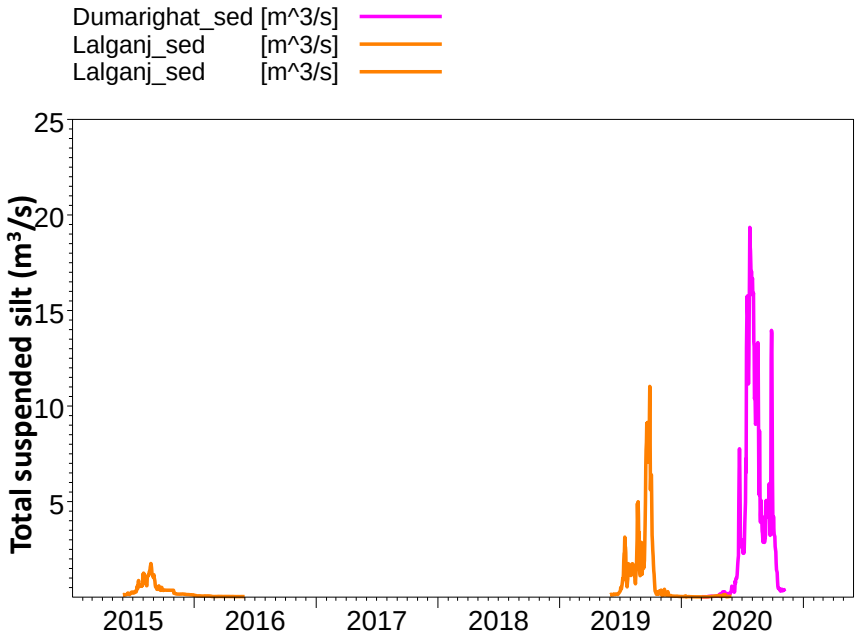

Figure 3.2: Availability of silt data.

Further, the annual peak discharge data for the priod of 1990 to 2020 at Dumarighat and Lalganj sites are also obtained for carrying out flood frequency analyse to estimate flood of various return period. The annual peak data is shown in Figure 3.3. In addition the annual silt (suspended sediment) load at Lalganj site is also obtained as shown in Figure 3.4.

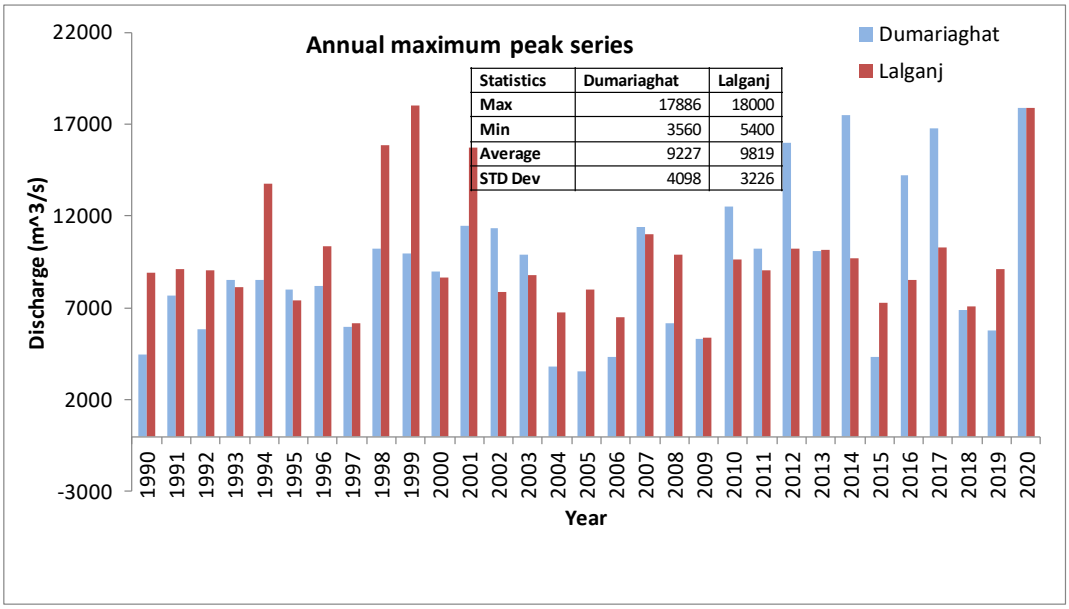

Figure 3.3: Annual peak discharge data at Dumarighat and Lalganj sites.

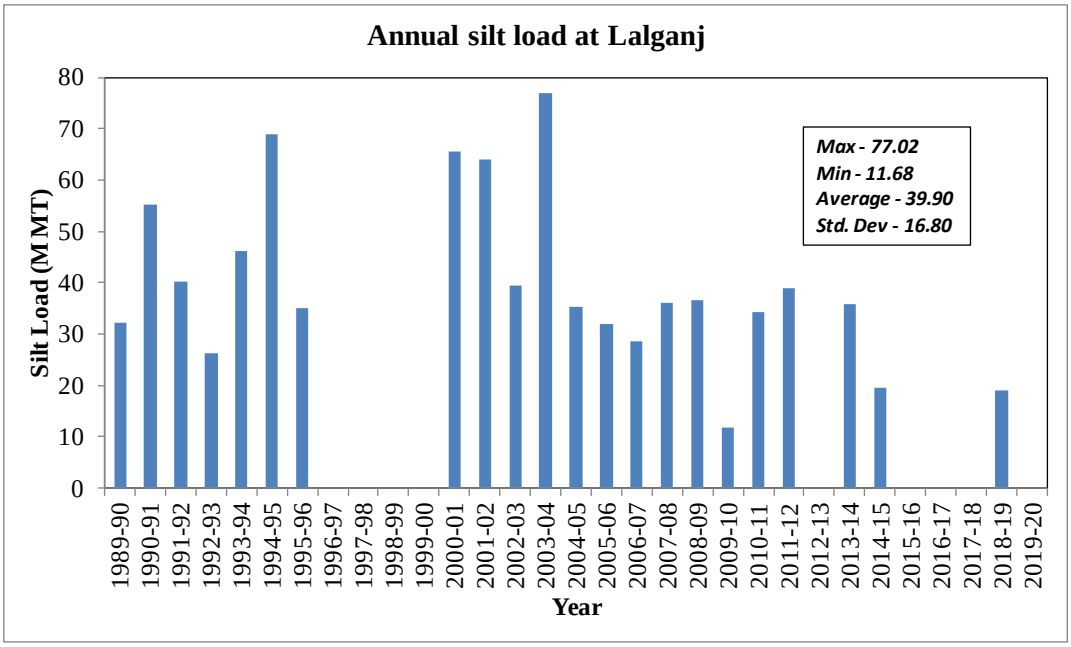

Figure 3.4: Annual silt load in million metric ton at Lalganj site.

3.2.2 Hydrological data collected by NIH

NIH established a gauging site at Baligaon to collect the hydrological data during monsoon period of 2022 to collect water level, discharge, flow velocity and silt data. The location of the established site is shown in Figure 3.5 and the river cross section is shown in Figure 3.6. The river width is about 400 m at this section while the embankment spacing is 2.6 km. The left and right banks are at elevation of 53.344 m and 53.725 m, respectively while the left and

right bank embankments are at elevation of 56.54 m 55.637 m, respectively. The temporary bench mark at this location was transferred from CWC GD sites using DGPS survey and the water level gauge was established (**Figure 3.7**). The active flow width is divided at every 50 m interval and its geographical coordinates are computed and feed into GPS. This GPS in turn is used to place the boat at specified point to take observations for flow depth, velocity (at d_{60}), and sediment samples (**Figure 3.8** to **Figure 3.10**). The sediment samples are collected at every 100 m, while flow depth and flow velocity is measured at every 50 m interval. The hydrological data collected by NIH at Baligaon site is given in Figure 3.11.

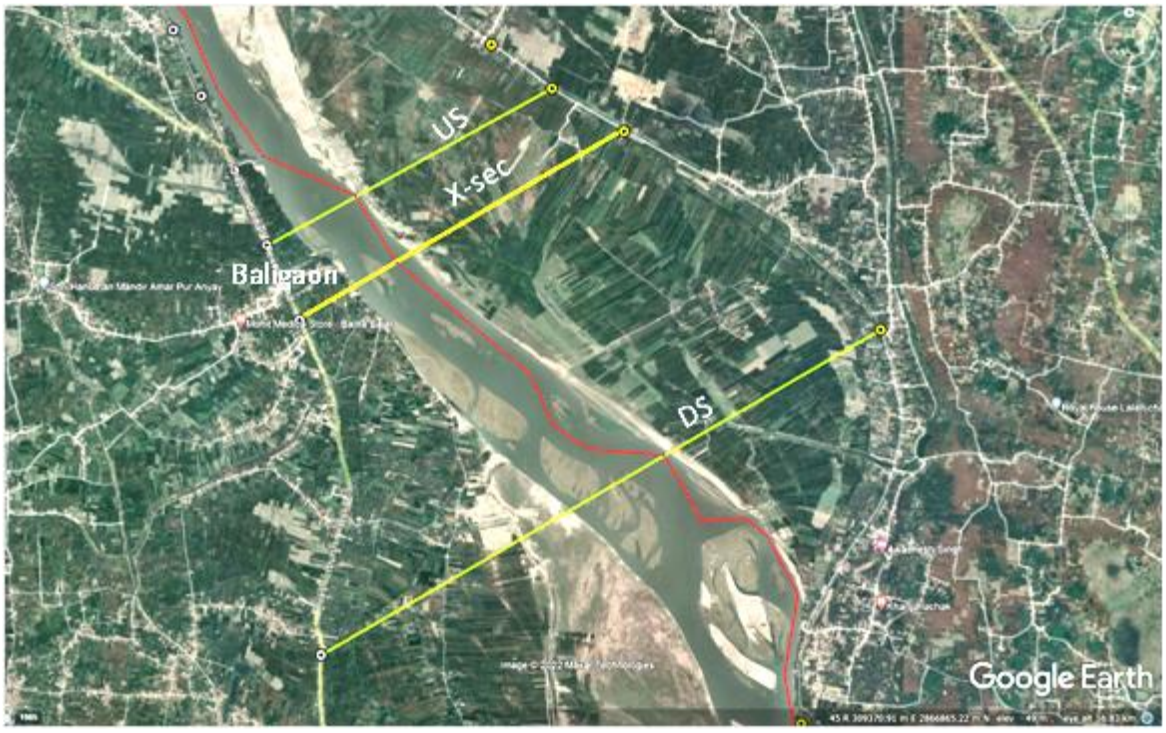

Figure 3.5: Location of GD site established at Baligaon.

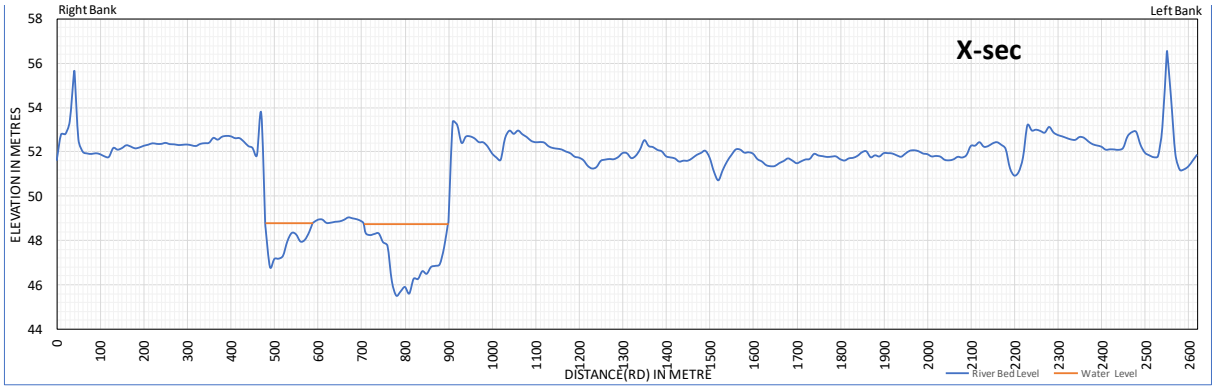

Figure 3.6: River cross section at the Baligaon site

Figure 3.7: Gauges established at site

Figure 3.8: Velocity measurement

Figure 3.9: Sediment sampling

Figure 3.10: Boat alignment in river using GPS

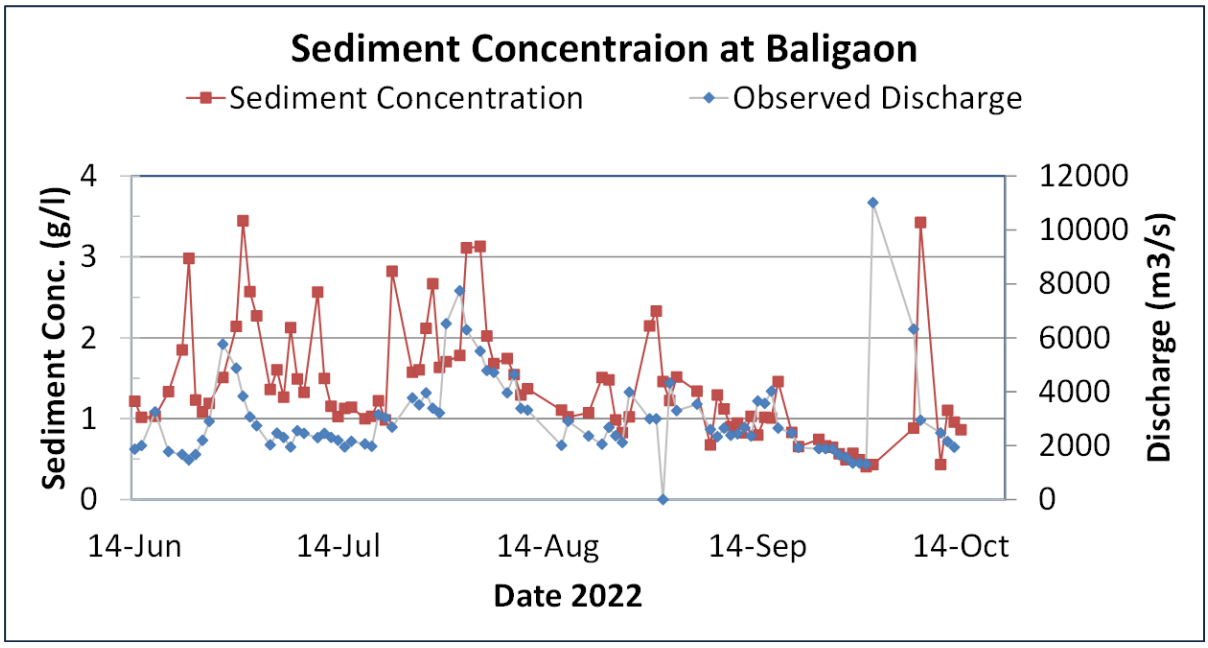

Figure 3.11: Hydrological data collected by NIH at Baligaon

The sediment samples (suspended sediments and the bed materials) are also analysed for grain size distribution. The grain size distribution charts for suspended and sediment and bed material are shown in Figure 3.12 and Figure 3.13, respectively. The d_{50} for suspended sediments and bed materials are computed as 0.102 mm and 0.152 mm, respectively.

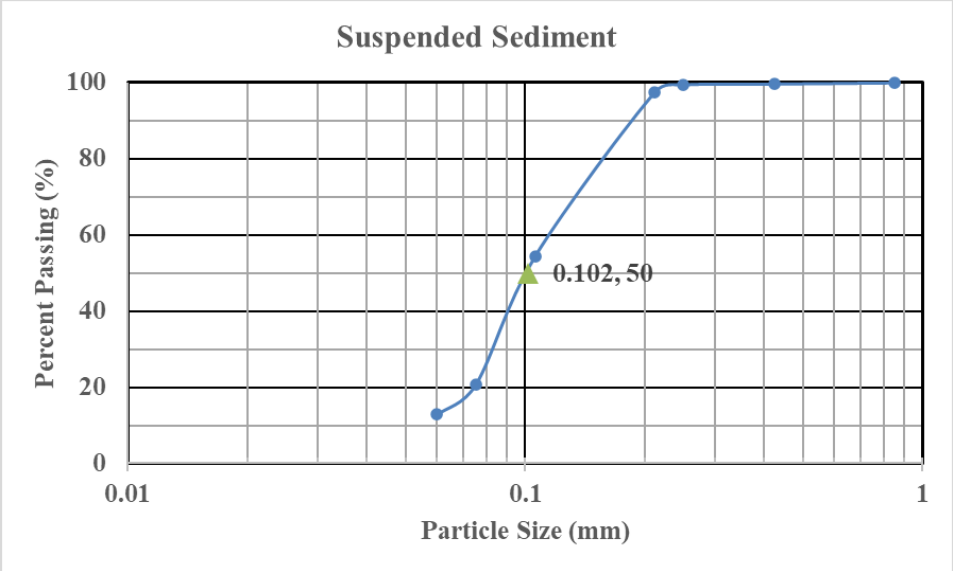

Figure 3.12: Grain size distribution chart for suspended sediment.

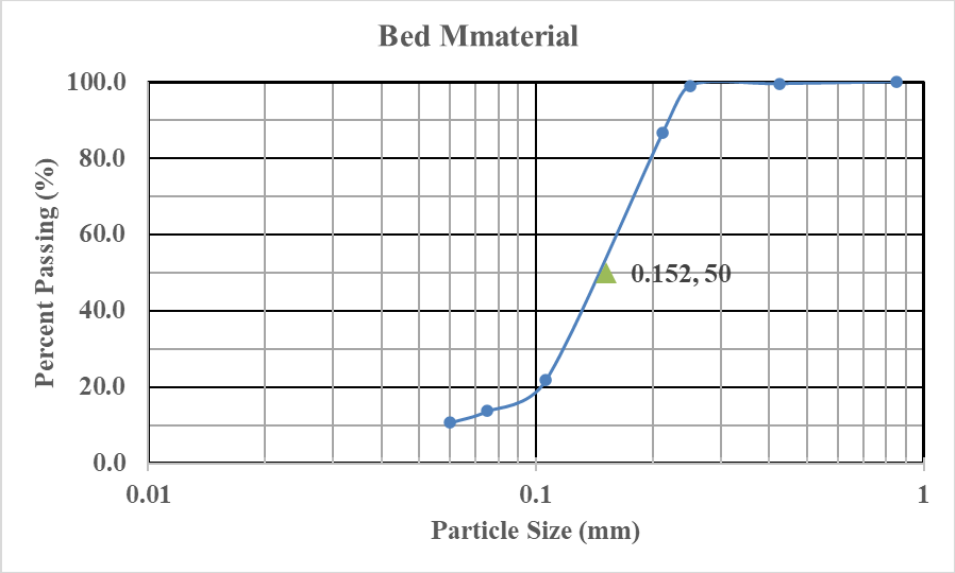

Figure 3.13: Grainsize distribution chart for bed sediment.

3.3 River Geometry

The river cross section survey data is collected through outsourcing. In the 98 km stretch of Gandak river from Dumarighat to Hajipur GD site of CWC, 78 river cross sections are surveyed from embankment to embankment. The river cross section at every 500 m is surveyed in the river stretch from Kunwari village to Baligaon. At other locations, the river section at every 2 km is surveyed. The survey is carried out using DGPS and echo sounder. The temporary benchmark is transferred at the pillars on both the embankment river section is to be surveyed. Some ground elevations on the country side are also surveyed. The datum available at CWC sites have been used for transfer of benchmark to pillars. Some field photographs taken during the survey work are shown in Figure 3.14.

The river cross section data is available from embankment to embankment and few meters on the country side. However, for flood inundation modeling, the DEM data for the flood plain is also required. ALOS PALSAR data (spatial resolution of 12.5 m) is used for floodplain geometry. The online DEM is corrected with the elevation data of land masses captured through field survey of river cross section. The two data sets are merged and DEM of the river stretch at 20 m grid is developed as shown in Figure 3.15.

CWC Benchmark at Dumarighat

DGPS Base station for datum transfer

Pillar (TBM) at cross section locations

Figure 3.14: Field photographs during the river cross section survey

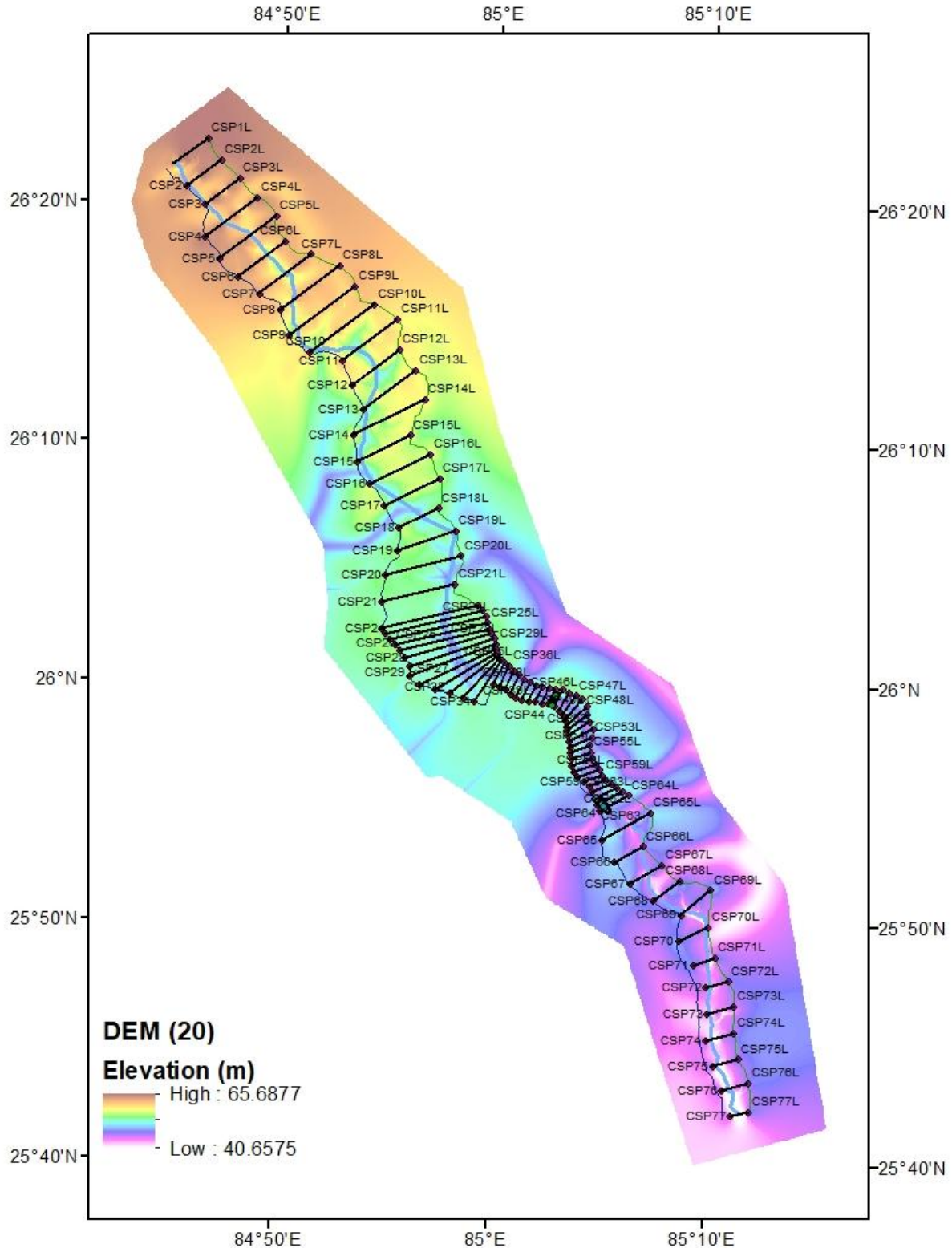

Figure 3.15: The surveyed cross sections and the DEM of the river reach.

4 METHODOLOGY

In the study, multiple data analysis are carried out to achieve the various objectives. The major analysis include the remote sensing satellite data processing to carry out river morphological study, L-moment based flood frequency analysis to estimate the design flood in the study reach and development of 1D and 2D curvilinear flow model to study river hydrodynamics and morphology, sediment transport etc. In this section, the methodology for each activities are discussed in details.

4.1 Remote sensing based river shifting and morphological analysis

River shifting and meandering analysis has been carried out using satellite images downloaded from USGS website and processed further using image process techniques and GIS analysis. The river courses in various years are extracted and using overlay analysis, the extent of river shifting is estimated. The satellite image of year 2020 is used to estimate the morphological characteristics of the river in the study stretch. The study reach is very extensive and therefore multiple of images are used to cover the entire stretch in a specific year (various images in nearby dates). The digital analysis was carried out in the image processing software, 'ERDAS Imagine' and GIS analysis is carried out in ArcGIS. The following steps are adopted for delineation of the river course using satellite remote sensing data :

(a) Download and visualization,
(b) Separation of area of interest (AOI),
(c) Delineation of river course from remote sensing data, and
(d) GIS analysis

The downloaded images are visualized for cloud cover, data distortion and projection systems. In the temporal images, if there are some projection errors, the images are rectified so that permanent features overlay perfectly in various images. Some clearly identifiable features like crossing of roads, railways, canals, bridges etc. were located on all images and are selected as control points. Further, the separation of area of interest (AOI) was performed to optimize processing time and data storage. The AOI is developed with sufficient buffer around the study stretch. Further, the image is analysed to determine the water spread area

and river sand which together represents the river course. The digital classification technique of feature classification of image is used for the river bank line extraction. Supervised classification of satellite images for identifying water pixel and sand pixel is carried out and two individual classes are identified. Later on, these two class (Water pixel and river sand) are merged together to represent, the river course. Entire image processing exercise is carried out in "ERDAS Imagine" software. In the visible region of the spectrum (0.4 – 0.7 μm), the transmittance of water is significant and the reflectance is low. The absorption of water rises rapidly in the near-IR where both, the reflectance and transmittance are low. At near-IR wavelengths, water apparently acts as a black body absorber. Deep water bodies have quite distinct and clear representation as compared to shallow water. Shallow water can be mistaken for soil while saturated soil can be mistaken for water, especially along the periphery of the surface water features. To differentiate water pixels from the adjacent wetland pixels, comparative analysis of the digital numbers in different band is usually carried out.

The various layers of river course for different years prepared using supervised classification of multi-spectral image are analysed in GIS (ArcGIS). As all the images are geo-referenced in same projection system, the overlay are ready for shifting analysis. Through over analysis, the critical locations where significant shifting has taken place were identified. The details of the shifting characteristics of river Gandak at the critical locations are first identified. Further, detailed studies were carried out for estimating the shifting pattern of the river at these critical locations using the temporal satellite data.

4.2 Estimation of Floods of Various Return Periods Using L-Moments Based Frequency Analysis

For design of hydraulic structures and flood management measures, estimation of flood of a specified return period is an important input. These are computed either using flood frequency analysis (FFA) over the observed annual peak flood at the specified gauging site. The procedure of identification of best fit frequency distribution function includes (i) selection of frequency distribution function (say Exponential, Generalised Extreme Value, Normal, Logistic etc.), (ii) method of estimation of their parameters (like method of moments, MOM or L-moments, LMO), (iii) Carrying out diagnostic test for Goodness of Fit (GoF) and (iv) estimating flood frequency values (FFVs) (Vivekanandan, 2015).

In method of moments technique, parameters of distribution functions are estimated by matching the moments of sample data set with the selected distribution (Ghorbani et al., 2010). The r^{th} central moment (μ_r) about the mean $\bar{R}$ of a random variable R is defined by:

$$\mu_r = E\left(R-\bar{R}\right)^r = \int \left(R-\bar{R}\right)^r f(R)dR, \text{ if } R \text{ is continuous variable} \qquad \textbf{Eq. 4.1}$$

where, f(R) is the probability distribution function (PDF) of a random variable R. The second moment (μ_2) about $\bar{R}$ is called variance. Similarly, third and fourth moments (μ_3 and μ_4) about $\bar{R}$ are used to define skewness (C_S) and kurtosis (C_K), which are as follows:

$$C_s = \left(\frac{\mu_3}{\mu_2^{3/2}}\right), \text{ and } C_k = \left(\frac{\mu_4}{\mu_2^2}\right) - 3 \qquad \textbf{Eq. 4.2}$$

Method of moments (MOM) is in use since long, for computing the parameters of the probability distributions. But due to its limitation of defining the shape of distribution, particularly by the moments of third and higher order, the estimated parameters are comparatively less accurate than those estimated by other procedures of parameter estimation like maximum likelihood method, method of least squares and probability weighted moments (PWMs). L-moment (LMO) approach was introduced by Hosking (1990) and later on, Hosking and Wallis (1997) presented it as an alternative system for computing the parameters of probability distributions. LMO is more accurate in parameter estimation, more robust to the presence of outliers in data and less subjected to bias in estimation (Hosking 1990). LMO is defined as linear combination of Probability Weighted Moments (PWMs) defined as:

$$\beta_r = E\lfloor x\{F(x)\}^r \rceil \qquad \textbf{Eq. 4.3}$$

and, can also be written as

$$\beta_r = \int_0^1 x(F)F^r dF \qquad \textbf{Eq. 4.4}$$

where, F=F(x) is the Cumulative Distribution Function (CDF) for x and x(F) is the inverse CDF of x evaluated at the probability F, and r ≥0. For r=0, β_0 is the mean of the distribution defined by μ=E[x].

For any distribution the r^{th} L-moment λ_r is related to the r^{th} PWM through

$$\lambda_{r+1}=\sum_{k=0}^{r}\beta_k(-1)^{r-k}\binom{r}{k}\binom{r+k}{k} \quad \textbf{Eq. 4.5}$$

The first four L-moments are related to PWM as follows:

$$\lambda_1=\beta_0 \quad \textbf{Eq. 4.6}$$

$$\lambda_2=2\beta_1-\beta_0 \quad \textbf{Eq. 4.7}$$

$$\lambda_3=6\beta_2-6\beta_1+\beta_0 \quad \textbf{Eq. 4.8}$$

$$\lambda_4=20\beta_3-30\beta_2+12\beta_1-\beta_0 \quad \textbf{Eq. 4.9}$$

Though the procedure of PWMs and L-moments are similar, L-moments are more convenient for their ability to interpret and measure the scale and shape of PDF. Here λ_1, the mean, is a measure of location and λ_2 is a measure of scale or dispersion of random variable. The higher order moments λ_3 and λ_4 are standardised to make them independent of units of measurement of variable.

$$\tau_r=\frac{\lambda_r}{\lambda_2} \text{ for } r=3, 4 \quad \textbf{Eq. 4.10}$$

Corresponding to coefficient of variation, skewness and kurtosis of conventional moment ratios, τ, τ_3 and τ_4 are L-coefficient of variation, L-skewness and L-kurtosis in LMO. Here, τ_3 and τ_4 reflects the degree of symmetry of a sample and measure of peakedness respectively. These are defined as:

$$\tau, \text{ L-coefficient of variation (L-CV)} = \frac{\lambda_2}{\lambda_1} \quad \textbf{Eq. 4.11}$$

$$\tau_3, \text{ L-coefficient of skewness (L-skew)} = \frac{\lambda_3}{\lambda_2} \quad \textbf{Eq. 4.12}$$

$$\tau_4, \text{ L-coefficient of kurtosis (L-kutosis)} = \frac{\lambda_4}{\lambda_2} \quad \textbf{Eq. 4.13}$$

The upper and lower bound limits for λ_2, τ_3 and τ_4 are,

$$0 < \lambda_2, \qquad -1 < \tau_3 < 1, \qquad \frac{1}{4}\left(5\tau_3^2-1\right) \leq \tau_4 < 1. \qquad \textbf{Eq. 4.14}$$

L-moments are similar to conventional moments in summarising the basic properties: location, scale, skewness and kurtosis of the sample data set and can be used in estimating the parameters for underlying distribution. The parameter estimation through L-moments approach, performed through linear combination are less sensitive to sampling variability and measurement errors in extreme data values and thus produces more accurate and robust estimates (Kumar et al., 2003; Kumar and Chatterjee, 2005).

Frequency Distributions

In this study, twelve frequency distributions have been used for FFA. These are; (i) Extreme value (EV1)/Gumbel distribution, (ii) Generalised extreme-value (GEV), (iii) Logistic (LOS), (iv) Generalised logistic (GLO), (v) Normal (NOR), (vi) Generalised Pareto (GPA), (vii) Generalised normal (GNO), (viii) Uniform (UNF), (ix) Pearson type-III (PT3), (x) Kappa (KAP), (xi) Wakeby (WAK) and (xii) Exponential (EXP).

Goodness of fit measures

Assessment of validity of the candidate distribution may be made on the basis of how well a distribution fits the observed data. The goodness of fit (GoF) measure evaluates the comparative performance of several distributions selected for assessment and help in identifying the most appropriate, i.e., robust distribution. A number of methods are available for testing goodness of fit of the proposed frequency analysis models like Chi-square test, Kolmogorov-Smirnov test, descriptive ability tests and the predictive ability tests. In this study, statistic Z_i^{dist} based on L-moment ratio diagram are also used to identify the suitable frequency distribution. The L-moment statistics of the sample is plotted on the L-moment ratio diagram and the distribution nearest to the plotted point is identified as the underlying frequency distribution. One big advantage of L-moment ratio diagram is that one can compare fit of several distributions using a single graphical instrument (Vogel and Wilson, 1996). The GoF decides how well the L-Skewness and L-Kurtosis of the fitted distribution and of observed data matches. The goodness-of-fit measure for a distribution is given by statistic Z_i^{dist}.

$$Z_i^{dist} = \frac{\bar{\tau}_i^R - \tau_i^{dist}}{\sigma_i^{dist}} \qquad \textbf{Eq. 4.15}$$

where $\bar{\tau}_i^R$ is the weighted average of L-moment statistic i, τ_i^{dist} and σ_i^{dist} are the simulated average and standard deviation of L-moment statistics i for a given distribution. The distribution giving the minimum $\left|Z^{dist}\right|$ value is considered as the best fit distribution. When all the three L-moment ratios are considered in the goodness-of-fit test, the distribution that gives the best overall fit is selected as the underlying frequency distribution. According to Hosking (1990), distribution is considered to give good fit if $\left|Z^{dist}\right|$ is sufficiently close to zero, a reasonable criteria being $\left|Z^{dist}\right| \leq 1.64$. Thus, once the robust frequency distribution for the observed annual peak data set is identified, the floods for various return period are estimated.

4.3 Study of Morphological Process

The physical processes in rivers (and therefore their morphology) depend on the following factors (Church, 1992):

i) The volume and temporal distribution of the inflow (supply from the upstream reach).
ii) The characteristics, volume and temporal distribution of the sediment
iii) The characteristics of alluvium through which river flows, and
iv) The geometrical characterises of the river channel (cross section and longitudinal profile etc.).

The flow at a given point along a drainage basin depends on the size of the catchment area. As the catchment area increases, the flow discharge also increases. However, with the increase in catchment area, the size of the sediment usually decreases. Further, a systematic variation in channel properties and a sharp increase in sediment storage (floodplain area) is observed (e.g. floodplain area) once drainage basins reach a 'critical' size (Figure 4.1). The decrease in channel gradient, decrease in particle size, increase in channel size, increase in sediment storage, and gradual but slow increase in average flow velocity represent the overall representation of complex interactions among numerous variables (Church, 1992; Knighton, 1998).

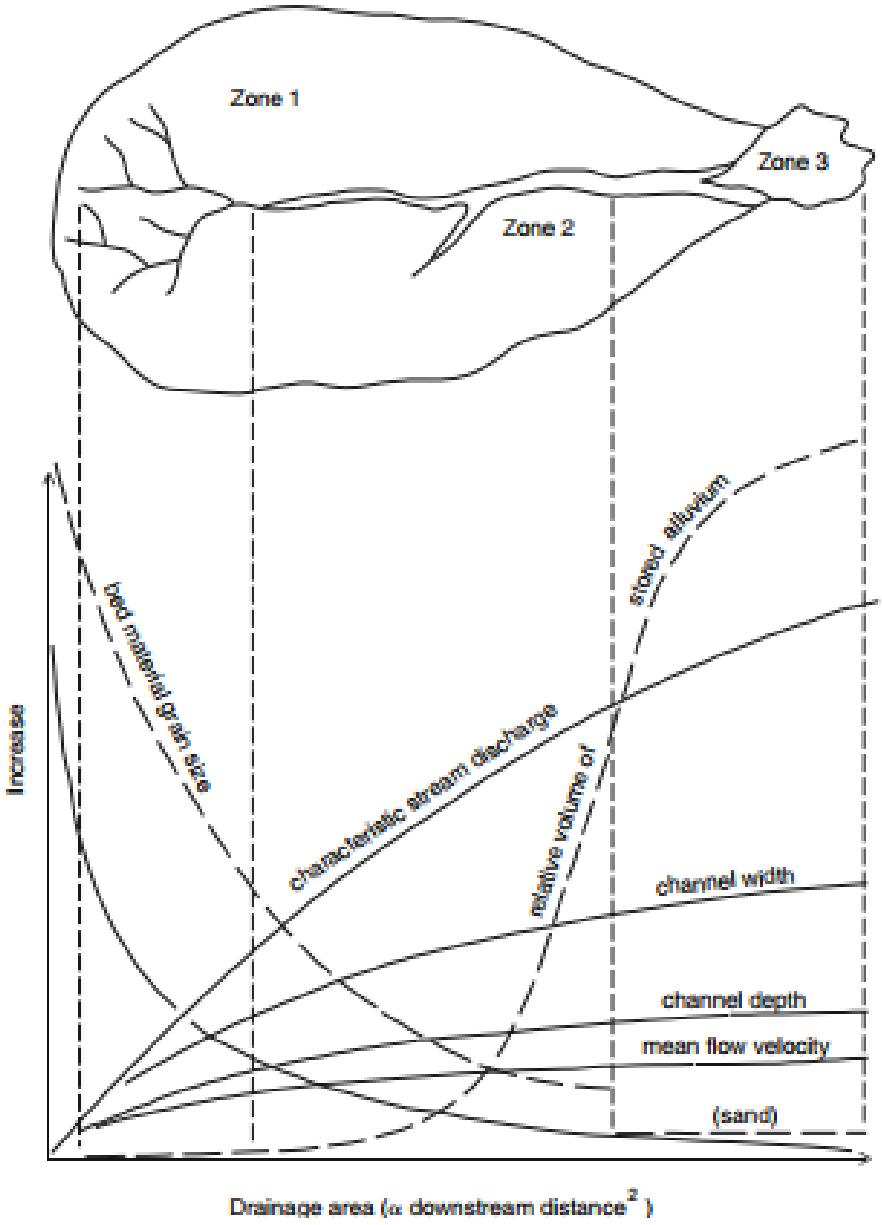

Figure 4.1: Schematic representation of the variation in channel properties within a drainage basin

(Source: Robert 2003)

The river morphology is affected by the volume and the character of the sediment delivered to the channel from upstream. Changes in the calibre of the sediment supplied to a given river reach and changes in the bed material size along the river channel are important factors controlling many physical processes occurring within alluvial channels (Powell, 1998). The very fine material tends to be transported in the flow itself, i.e. in suspension, and will be deposited during floods when overbank flows occur (i.e. floodplain deposition). Coarse

sediment, because of its greater weight, will be transported near the bed of the river and locally deposited onto the channel in the form of 'bars'. These bar accumulations in turn affect the river flow characteristics, with local deflection and lateral activity (Church, 1992). The nature of the sediment over which the river flows is therefore influenced by the sediment supply conditions and, in turn, the characteristics of the river bed sediment will significantly influence the mean and turbulent properties of the water flow. Moreover, the organization of sediment movement down channel tends to vary significantly as a function of particle size. The type of bedform observed along a given river reach is directly a function of the bed material size and the flow strength. A clear distinction is usually made between features observed along sand-bed channels and bed undulations frequently observed in coarse-grained or sand-bed mixtures (Best, 1996). The transition between fine- and coarse-grained channels depends to some extent on the energy of the stream, and can be placed within the range 0.3–1 mm (Church, 1992).

Based on sediment supply conditions and the capacity of streams to transport the supplied load, different channel types are formed.

4.4 Principles of Water Flow in alluvial River

Motion occurs when a fluid is subjected to a gradient of mechanical potential energy (MPE) which is due to the forces of gravity and hydrostatic pressure. In open channel flows this is expressed as

$$H_p = z + y\cos\theta + \frac{1}{2g}v^2 \qquad \textbf{Eq. 4.16}$$

As the flows moves downstream, the total mechanical energy decreases, consequently;

$$z_1 + y_1\cos\theta + \frac{1}{2g}{v_1}^2 = z_2 + y_2\cos\theta + \frac{1}{2g}{v_2}^2 + h_\Delta \qquad \textbf{Eq. 4.17}$$

Where the subscript 1 and 2 refers to upstream and downstream sections, respectively. h_Δ is the head loss between the two sections.

The property of viscosity leads to a distinction between laminar and turbulent flows. This distinction between turbulent and laminar flows is important to establish as it provides the conceptual framework needed to better understand flow and bedform dynamics. For viscous

laminar fluid, the relationship between the applied force, the shear rate, and the resistance to deformation (or molecular viscosity) can be summarized by the following relationship:

$$\tau = \mu \frac{du}{dy} \qquad \textbf{Eq. 4.18}$$

Where τ is shear stress, μ is dynamic viscosity; *du* and *dy* are change in velocity and height; respectively. Thus the shear stress can be regarded as the force that produces a change in velocity relative to height above the boundary. Kinematic viscosity (ν) is defined as the ratio of molecular viscosity (μ) to the fluid density (ρ),

$$\nu = \frac{\mu}{\rho} \qquad \textbf{Eq. 4.19}$$

In turbulent flows, however, the relationship between the shearing force and the velocity gradient is defined by:

$$\tau = (\mu + \varepsilon) \frac{du}{dy} \qquad \textbf{Eq. 4.20}$$

Where, ε is the coefficient of eddy viscosity. Eddy viscosity is a friction within the flow that results from the vertical circulation of turbulent eddies (rather than from the sliding of layers). Reynolds numbers (R_e) are used to differentiate between laminar and turbulent flows. Reynolds numbers are defined as:

$$R_e = \frac{ud}{\nu} = \rho \frac{ud}{\mu} \qquad \textbf{Eq. 4.21}$$

With R_e < 500, the flow is laminar while for R_e > 2000, the flow is turbulent. For 2000> R_e > 500, the flow is in transition stage. Most of the natural flows in fluvial studies, the flow is generally turbulent in nature.

The separated flows are also significant in fluvial dynamics. These occur when there is a sudden change in the boundary condition or orientation when the flow cannot remain attached to the boundary. There are numerous flow and bedform dynamics phenomena that are directly related to flow separation in alluvial channels. The flow characteristics in these zones (average flow properties and turbulent flow characteristics) are important, because they control many sediment transport processes (erosion–deposition). Within a separation zone,

there is basically no downstream flow. The separation zone is usually separated from the much faster external flow by a zone of rapid velocity change called a shear layer, in which there is normally intense mixing in the water column. Perhaps the best examples of flow separation in rivers are those schematically illustrated in Figure 4.2, i.e. at river confluences, downstream from the junction 'corner' and immediately downstream from transverse steps (e.g. bedform crests or obstacles). These phenomena will be described and explained in detail later. Finally, secondary flows, as the name implies, are flow components that are superimposed upon the main downstream flow component. Secondary flows are commonly observed, for instance, in river meanders and at channel confluences (as summarized for instance in Allen (1994) and Powell (1998)).

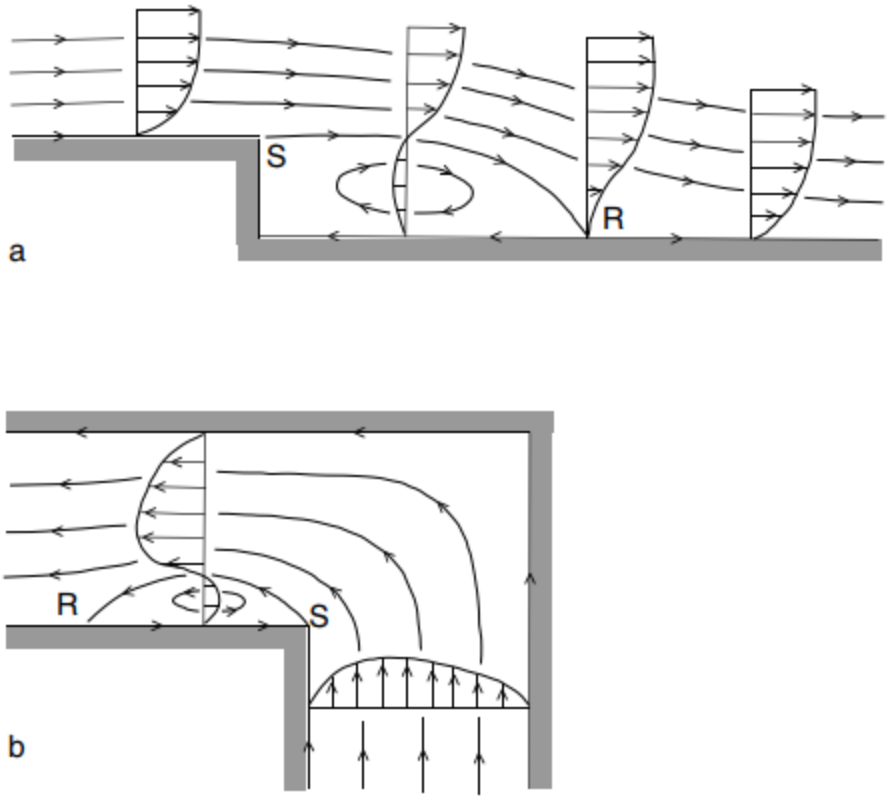

Figure 4.2: Examples of flow separation (S: separation point; R: reattachment point), illustrated by time-averaged streamline patterns at (a) a downward transverse step and (b) a sharp bend in an open channel.

(Source: Robert, 2003).

The boundary layer is the zone within which there is a velocity gradient due to the friction exerted by the solid boundary on the moving fluid. The velocity characteristics of the boundary layer are of great interest in fluvial studies. The shape of the velocity profiles,

especially in the near-bed region, the rate of increase in velocity with height above the bed surface, the turbulent flow characteristics within this layer, and their links with sediment movement and bed surface features are inter related.

The water flowing in river channels is retarded by the resistance exerted by the bed. At free surface end, the friction exerted by the bed becomes less effective and retardation diminishes. External boundary conditions (especially the range of particle sizes and the shape and size of bedforms) control the magnitude of the resistance exerted by the bed on flow. Resistance is also affected by other types of obstruction, such as aquatic vegetation (Hickin, 1984) and abrupt changes in cross-section geometry.

The average velocity at a given vertical (within 20% of the flow) is affected by the magnitude of the resistance exerted by the bed on the flow. The average velocity at vertical 'y' is given by *law of the wall* and expressed as:

$$U_y = \left(\frac{1}{\kappa}\right) U_* \ln\left(\frac{y}{y_0}\right) \qquad \textbf{Eq. 4.22}$$

Where κ is the von Karman's constant and = to 0.41 (in clear water flows), U_y is the mean velocity at a given height y, U_* is the shear velocity and y_0 represents the (projected) height above the bed at which the velocity is zero. For average velocity at a vertical with flow depth, *d*, the expression is

$$\frac{U}{U_*} = 2.5 \ln\left({}^{d}/_{\kappa_s}\right) + 6.0 \qquad \textbf{Eq. 4.23}$$

κ_s is called equivalent sand height and is equal to $30.1y_0$, (Robert, 2003). This equation constitutes the basic theoretical equation used to estimate the flow resistance in straight uniform open channels (two-dimensional flow).

The value of κ_s under natural conditions in coarse-grained channels estimated as 3.5 D_{84} (where D_{84} is the size for which 84 per cent of the bed material is finer) or 6.8 D_{50} (e.g. Robert, 1990; Clifford et al., 1992b).

At the reach scale, $U_* = \sqrt{{}^{\tau_0}/_{\rho}} = (gds)^{1/2}$ and Eq. 4.23 can be rewritten as:

$${}^{U}/_{\sqrt{gds}} = 6.0 + 2.5ln\left({}^{d}/_{\kappa_s}\right) \qquad \textbf{Eq. 4.24}$$

This equation is used to compute the average velocity (and therefore discharge) for a known or assumed flow depth (d) and channel slope (S), and by setting ks equal to a given multiplier grain size index that corresponds with widely observed empirical observations (e.g. 6.8 D_{50} for coarse-grained channels).

$$U/\sqrt{gds} = 6.0 + 2.5ln\left(d/\kappa_s\right) \qquad \textbf{Eq. 4.25}$$

Hence, Reynolds numbers can be calculated based on the shear velocity and particle size (orκs). These values are referred to as the boundary, grain or shear Reynolds number (Re*) and are defined as:

$$Re_* = \frac{U_*\kappa_s}{\nu}, = U_*D/\nu \qquad \textbf{Eq. 4.26}$$

where U_* is shear velocity, D is particle size, ν is kinematic viscosity and k_s is the equivalent sand roughness as described above. Fully turbulent flows (which characterize most open-channel flows) have boundary Reynolds numbers (Re_*) in excess of 100.

In addition to the ratio U/U*, there are two other commonly used flow resistance coefficients in alluvial channels. These are the Darcy–Weisbach and the Manning friction factors. The empirical coefficient that is defined as follows:

$$n = (d^{2/3}S^{1/2})/\,U \qquad \textbf{Eq. 4.27}$$

The Darcy–Weisbach friction factor (f) is defined as:

$$f = 8gdS/U^2 \qquad \textbf{Eq. 4.28}$$

4.4.1 Flow resistance (and shear stress) components

Generally, the natural alluvial channels are characterized by heterogeneous bed material and with the presence of bedforms. The total flow resistance measured from the mean flow properties is a function of both the friction created by the grains on the flow and the additional roughness introduced by the bed undulations. The former component is usually referred to as grain roughness (or skin or grain friction) and the latter as form roughness or form resistance. Thus the total flow resistance can be divided into two components:

$$f = f' + f'' \qquad \textbf{Eq. 4.29}$$

f' is estimated using equations:

$$1/\sqrt{f} = 2.11 + 2.03 \log_{10}(d/\kappa_s) \quad \textbf{Eq. 4.30}$$

Hence, the total mean boundary shear stress τ_0 ($=\rho U_*^2$) in uniform flow can also be divided into two components, and;

$$\tau_0 = \tau_0' + \tau_0'' \quad \textbf{Eq. 4.31}$$

τ_0' is an 'effective' shear stress acting on a river bed i.e. only the grain stress is responsible for bedload transport (i.e. moving sediment particles in contact with the bed surface). The form roughness or the form drag component (f'' or τ_0') can then be estimated by simply subtracting the grain component from the total value of f or τ_0.

4.4.2 Flow turbulence

Turbulence is generated when a fluid flows past a solid surface or past an adjacent stream of the same fluid with a different velocity (Middleton and Southard, 1984; Clifford and French, 1993a,b). In turbulent flows, the fluid particles move in irregular paths, causing an exchange of momentum from one portion of the fluid to another (Bradshaw, 1985; Chanson, 1999). Two terms are very commonly used in the analysis of turbulent flows and turbulent boundary layers in rivers: turbulent eddies and vortices. Eddies can be defined as swirls of fluid with highly irregular shapes and a wide range of sizes, that are in a continual state of development and decay. While vorticity, can be loosely defined as the property of solid-body-like rotation of fluid at a given point in the flow.

The quantitative analysis of turbulent flows is based on measurements of velocity fluctuations at a single point in the flow (or a multitude of points from which flow fields can be inferred). Velocity fluctuations can be defined as:

$u' = U - u$

where u' is the deviation (the fluctuation) from the mean velocity U, and u is the 'instantaneous' velocity. Fluctuations for the vertical (v) and lateral (w) flow components can similarly be defined from:

$v' = V - v$, and $w' = W - w$

Root-mean-square values are considered measures of turbulence intensity. For the downstream flow component, RMS is defined as:

$$RMS_u = \sqrt{\sum (u'^2)/N} \quad \textbf{Eq. 4.32}$$

Where N is the total number of observations in a given series. Similarly, the turbulence in vertical and lateral direction may be computed using *v* and *w* (velocity components in respective direction).

The total turbulent kinetic energy (TKE) of the flow (per unit volume) is defined by Clifford and French, 1993a as below:

$$TKE = 0.5\rho(RMS_u^2 + RMS_v^2 + RMS_w^2 \quad \textbf{Eq. 4.33}$$

Where ρ is water density.

Turbulent kinetic energy represents the energy extracted from the mean flow by turbulent eddies. When the turbulence intensity is the same for each velocity component (i.e. in all directions), the turbulence is said to be isotropic. Otherwise, the turbulence flow field is anisotropic. Measurements in alluvial channels show turbulent fields that are usually strongly anisotropic (with RMS_u being dominant).

4.4.3 Vortices

Turbulent boundary layers are dominated by the presence of various types of vortices. A first category of vortices correspond to features that have been observed over smooth surfaces originating from alternate zones of low and high fluid speeds in the very near-bed region. Low-speed streaks represent a key component of turbulent boundary layers. They are known to be persistent features of the near-bed flow above smooth surfaces in fully developed turbulent flows. A second major group of vortices and coherent flow structures has been observed over coarse-grained surfaces. Coherent flow structures above coarse surfaces in natural rivers may be dominated by vortices induced by the presence of large particles on the bed and/or the presence of bedforms

4.5 Sediment transport Modeling

Sediment transport is a natural dynamic process causing gradual change in the earth surface landform. In shallow water, sediment transport is caused mainly by the combined action of surface gravity waves and currents. With continuous development of computational facilities, sediment transport modeling has become a popular tool for addressing many environmental and engineering problems. Using computational hydrodynamic/sediment transport models, in

general, involves the numerical solution of one or more of the governing differential equations of continuity, momentum, and energy of fluid, along with the differential equation for sediment continuity. An advantage of computational models is that they can be adapted to different physical domains more easily compared to physical models.

Physical processes, including those of sediment production, transport, and storage, are increasingly seen as vital for the ecological functioning of fluvial systems. Among these, sediment transport is certainly one of the most important in natural river channels, and its measurement and prediction continue to receive considerable attention. Progress in understanding and modeling sediment transport has been facilitated by the collection of extensive field data over recent decades under a relatively wide range of flow, bed load transport, and channel slope conditions, which has supported the development of new bed load formulae and/or the testing of older, well-known equations (Diplas and Shaheen, 2008). In some cases, these data have also provided the opportunity to investigate the behavior of gravel streams and the structure of channel beds in the context of watershed processes and characteristics (i.e., Hassan et al., 2008). Collection of new field data has certainly received a boost from recent technological progress, with traditional methods and sampling being combined with innovative techniques such as the use of piezoelectric sensors (Rickenmann and McArdell, 2008) or the magnetic bedload movement detector (Hassan et al., 2009).

The channel conveys the water and sediment from the catchment to the sea or outfall of the river. Makkaveyev (1955) represented the channel processes as interaction of flows in river channels with its bed and bank material. He defined a three level fluvial sediment transport cascade system which includes sheet and rill erosion or slope wash; linear or gully erosion and finally the concentrated flows in rivers. Thus the sediment particles transported by a river flow can originate either from the drainage basin (basin-sourced sediment) or from particle detachment within a channel itself from its bed and banks (channel-sourced sediment). On any river one can find intensively eroded channel banks and recently formed accumulative within-channel bars. Transport of relatively coarser sediment particles (bedload, sediment transported in drag or saltation mode) is most often associated with downstream movement of alluvial channel bedforms (bars, dunes) with erosion dominated gradual upstream slope and deposition-dominated steep downstream slope. According Makkaveyev (1955), “channel morphological patterns can be considered as one of the forms of sediment transport by the flowing water”, while “alluvial depositional bodies composing such river channel forms as

meander bends, riffles and dunes commonly move downstream and therefore represent certain type of river sediment yield" (Alekseevskiy, 2008)

In alluvial river, there is usually no distinctive zones of continuous erosion, transport and deposition along its length, the entire length of an alluvial river is characterized by interchanging erosion, sediment transit and re-deposition. Part of transported sediment is re-deposited in channel itself or on floodplain surface. Certain proportion of that material becomes incorporated into longer-term geological storage in form of alluvial deposits. Continuous alluvial deposition typically takes place in lower river reaches where regressive aggradation is caused by river mouth seaward expansion, sea level (erosion basis) fluctuation or tectonic depression. Under most circumstances the flow of water forms both the river channel and the plan form of the river. As a result, all natural rivers are subject to change, either through erosion, deposition or plan form change.

4.6 Limitation of Sediment transport models

Although our understanding and numerical modeling of waves and currents have improved greatly in recent decades, sediment transport by water motions remains poorly understood. The difficulty in matching theoretical results to observations is due to the sensitivity of sediment particle mobility to many environmental factors and processes at different temporal and spatial scales. By now there exist no mathematical formulas which can accurately predict the motion of a large number of sediment particles in natural environment. Most existing formulas are derived empirically and their applicability is restricted to a narrow range of environmental settings. Results obtained from different models often differ drastically from each other even though they are based on the same initial conditions (Yang, 1996).

Three major obstacles hinder precise modeling of sediment transport in marine environment. The first is the genetic diversity of sediment particles. Their different physical and biochemical properties lead to various dynamic responses to ambient water motions. For example, grains of granular, noncohesive sediment like sands and gravels normally migrate as individual particles, possibly interacting with each other by direct collisions, through which momentum and energy is transferred. Fine sediment particles with a diameter <0.063 mm show quite different behaviors due to the existence of a cohesive force. They rarely exist as individual particles but rather tend to aggregate together, forming much larger structures

which may consist of tens of thousands of particles. During the transport, these flocculated structures may further attract more fine particles or break down to smaller ones, depending on a bunch of parameters (e.g., turbulence strength, particle concentration, ion concentration, temperature, organic matters) in the ambient water. Such dynamics are still poorly understood.

Another major obstacle is the stochastic nature of sediment particle movement in fluids. A primary source of randomness of particle movements is turbulence, which remains still one of the most challenging problems in fluid dynamics. Another important source contributing to this uncertainty is the fundamental ambiguity of pickup process of particles from the seabed. It is commonly recognized that sediment particles only start to move when the moments of the driving forces (exerted by the ambient water motion) exceed those of the stabilizing forces. Although the physics behind this phenomenon is clear, mathematical description of the pickup threshold is still ambiguous. Most sediment transport models treat the pickup threshold by the use of a critical shear stress following Shields (1936). Some other studies (e.g., Einstein, 1942; van Rijn, 1984; Nelson et al., 1995) suggest that such critical shear stress is not a deterministic value but rather lies in a range of values characterized by certain probability distributions (e.g., a Gaussian or Gamma distribution). The usual presence of a mixture of different-sized sediment particles on the seabed further complicates the problem to define a reliable pickup threshold.

The third major obstacle is the presence of greatly different scales in the process of sediment transport. Coastal and ocean sediment transport models are normally developed at a scale (both spatially and temporally) that is much larger than the one on which turbulence, sediment particle–particle interactions and particle–fluid interactions occur. These small-scale processes have to be either parameterized by subgrid modeling techniques or simplified by empirical formulae. In either case errors are inevitably induced and different formulations may produce significant differences in the results (Amoudry and Souza, 2011). Despite great efforts in recent decades to reduce errors of medium to large scale sediment transport models, such as data assimilation and improvement of numerical schemes, even the most advanced model to date can only predict sediment transport within an accuracy of ±50 % at best and higher uncertainties are common (Amoudry and Souza, 2011). According to the strategy in treating the uncertainty of sediment motion in fluids, existing sediment transport models can

be divided into deterministic and probabilistic models. Deterministic models treat sediment transport in a time- and space-averaged manner. Usually the entire system is divided into smaller (grid) cells and a single value for each physical parameter is evaluated as representing its properties in the entire cell at each time step. Probabilistic models specify a possible range of the parameters and provide a collection of values characterized by different possibilities. Microscale (particle-based) sediment transport models such as discrete element models are not discussed here as they are not applied to open environments due to an intrinsic restriction of computational capacity and memory space. Nevertheless, outcomes of microscale particle-based models that are further validated by laboratory observations may help to improve numerical models for sediment transport in natural environments.

According to the strategy in treating the uncertainty of sediment motion in fluids, existing sediment transport models can be divided into deterministic and probabilistic models. Deterministic models treat sediment transport in a time- and space-averaged manner. Usually the entire system is divided into smaller (grid) cells and a single value for each physical parameter is evaluated as representing its properties in the entire cell at each time step. Probabilistic models specify a possible range of the parameters and provide a collection of values characterized by different possibilities. Microscale (particle-based) sediment transport models such as discrete element models are not discussed here as they are not applied to open environments due to an intrinsic restriction of computational capacity and memory space. Nevertheless, outcomes of microscale particle-based models that are further validated by laboratory observations may help to improve numerical models for sediment transport in natural environments.

4.7 Fluvial Sediment Process

The processes of erosion (entrainment), transport, and deposition of sediment particles by water are controlled essentially by the characteristics of those particles and the moving fluid. The particle size is directly proportional to its mass, which in turn controls mode of sediment movement and rates of transport. The density of natural sediments in rivers is usually assumed to be constant at 2650 kg m^3. The other bulk sediment properties are:

Grain size distribution: The median grain size of a sample of bed sediments is commonly identified by D50, where the subscript 50 simply refers to the size for which 50 per cent of the sampled material is finer. Sorting refers to the range of particle sizes observed in a

distribution. the ratio D_{84}/D_{16} (or its square root) can be conveniently used as a sorting index (e.g. Robert, 1990). The degree of sorting increases with a decrease in the ratio D_{84}/D_{16}.
Packing arrangements and friction angle: It refers to the organization of the particles on the stream bed. In addition to inertia, the forces opposing the motion of dry, cohesionless material are frictional. Loosely defined, frictional forces can be described as a measure of the ability of a grain to resist failure. In the context of sediment transport, it refers to the contact angle between superimposed particles and, again, the 'rollability' of a given grain or how easily it can be moved from its resting position.

Porosity, moisture content, and cohesion are also important bulk sediment characteristics to consider in alluvial channels. The shear strength of a given soil volume is essentially what controls the resistance to erosion of river banks or their stability with respect to mass failure. Shear strength depends on cohesion, friction angle and the normal stress exerted on a given planar surface covered by unconsolidated soil material. Under saturated conditions, shear strength is therefore reduced, and material is more susceptible to instabilities and mass failure.

Grain density affects the settling or fall velocity of a sediment particle together with other factors such as grain shape and fluid viscosity. The specific gravity of of a solid or fluid is its density relative to that of water, i.e. 2.65. Further, grain shape also affects sediment movement. Shape here refers to both the actual form of the grain and the surface texture. Shape affects fall velocity; the greater the departure from a spherical shape, the smaller the settling velocity.

The fall velocity for smaller particles, silt and clays is affected by viscosity and expressed by Stoke's Law as:

$$V_0 = \left({}^{1}/_{18}\right) D^2 (\rho_s - \rho) g/\mu \qquad \text{Eq. 4.34}$$

The coarser particle (>2 mm) will experience resistance from water and the fall velocity for coarse material, sand, can be determined from:

$$V_0 = \sqrt{\frac{2}{3} D g (\rho_s - \rho)/\rho} \qquad \text{Eq. 4.35}$$

For sand particles of intermediate size (0.063–2 mm), the fall velocity depends on combination of viscous and inertial forces.

4.7.1 Bank erosion

Bank erosion varies significantly along river channels. This spatial variability in erosion rates is in turn controlled by the longitudinal and/or vertical variation in grain size, moisture content, organic content, bank vegetation, channel curvature, bank angle, and related variations in shear stress applied on a given bank. There are two broad categories of bank erosion processes: flow erosion and mass failure. Water flowing in the channel exerts a drag force on the river banks, which may lead to detachment and entrainment of surface particles. This in turn is balanced by the shear strength of the bank material or the internally derived force capable of resisting the shear force applied by the flow. Bank materials are often stratified, becoming gradually finer upwards (because they are formed primarily by fluvial deposition). The bank material properties may also vary significantly along river channels.

Most river banks contain fine grains (significant amounts of silt and clay). They possess some degree of cohesion and they resist erosion essentially through inter-particle, electrochemical bonding. When erosion does take place, it is often aggregates of grains that are detached. The strength of such soil characteristics is highly dependent upon recent antecedent conditions of wetting and drying. For all these reasons, the critical conditions for erosion of cohesive banks are complex and difficult to define accurately, and are usually higher than for non-cohesive banks.

The second major category of bank erosion processes is referred to as mass failure. The susceptibility of the banks to erosion, or their susceptibility to mass failure, depends on the processes of weathering and weakening. In poorly drained soils, the pore-water pressure is usually positive, and positive pore-water pressures act to reduce bank stability. Soil moisture conditions at and beneath the bank surface can therefore be very significant in controlling bank stability (as are previous flow and precipitation conditions). Rapid immersion of dry banks and repeated wetting and drying cycles can contribute to cracking which will in turn reduce the shear strength of the bank materials and increase its susceptibility to erosion. Intense drying and shrinkage of the bank in particular may lead to ‘desiccation’ cracking. Mass failure is also related to flow erosion, in the sense that the flow scours the bed and the bottom portion of the bank. This may increase the bank height and the bank angle (by undercutting). It is the cause of bank retreat, which may also trigger instability and mass failure.

4.7.2 Bed Erosion

Most river beds are composed of cohesionless sediment particles. The bed shear stress estimate is used in analyses of the thresholds of initial motion can be derived from the average flow conditions at the reach scale, from the local flow conditions (as determined for instance from the law of the wall), or from the turbulent stresses. The critical shear stress (τ_c) is usually approximated by:

$$\tau_c = k(\rho_s - \rho)gD \qquad \text{Eq. 4.36}$$

Where, k is a constant (0.045) depending upon soil packing density and pivoting angle. Considering that water density and sediment density can be considered as constant), it follows Eq. 20 that:

$$\tau_c = 0.73\ D \qquad \text{Eq. 4.37}$$

τ_c is expressed in Nm^{-2} and D is in mm.

A dimensionless approach can also be used for the determination of critical shear stress. The dimensionless shear stress is usually represented by theta (θ), and it is simply defined from the ratio of critical dimensional shear stress to submerged weight:

$$\theta_c = \tau_c/(\rho_s - \rho)gD \qquad \text{Eq. 4.38}$$

where θ_c is known as the Shields parameter (Buffington, 1999).

Dimensionless critical shear stresses for heterogeneous sediments can be summarized by

$$\theta_{ci} = a(D_i/D_{50})^{-b} \qquad \text{Eq. 4.39}$$

where θ_{ci} is the dimensionless critical shear stress needed to move a particle of size D_i, D_{50} is the median bed particle size, and a and b are empirically derived coefficients.

4.7.3 Sediment Transport

Once the threshold of initial motion has been reached, particles are displaced downstream, and the mode of transport varies with sediment size and flow intensity. Modes of movement are usually summarized in three categories: in contact with the bed surface, i.e. particles rolling or sliding on or along the bed, in saltation (intermittent contacts with bed surface), or in suspension within the flow. Coarse particles such as gravels (or grains coarser than gravels) generally move as bedload, fine and medium sands usually move predominantly in suspension, and coarse sands either as bedload or suspended load, depending on the flow

conditions (Middleton and Southard, 1984). For most river systems, particles within the medium size range (i.e. between 0.1 and 1 mm) appear to correspond with the largest fraction generally transported in suspension. Particles smaller than 0.1–0.2 mm goes directly into suspension when disturbed. Saltation may be viewed as an intermediate step between rolling and suspension.

Suspended sediment concentrations and load are highly variable both spatially and over time. Suspended sediment concentration (SSC) at a given point in a stream channel is highly variable over time. Water discharge (Q) is clearly a dominant factor. Further, the time elapsed since the last storm event is important, as it affects the supply of sediment. The following type of relation is frequently observed

$$SSC = a(Q)^b \qquad \text{Eq. 4.40}$$

where a and b are constants. The value of b usually varies between 1 and 2. Plots of SSC and Q appear roughly linear on log–log diagrams.

Two criteria can be used to distinguish between modes of movement and to establish suspension stages. These are the ratio of shear velocity (U_*) to settling velocity (V_0) and the ratio of RMS_v to V_0 (i.e. the ratio of the root-mean-square of the vertical velocity fluctuations to the settling velocity of the particles). Using the former criterion, a conservative estimate suggests that suspension occurs when U_*/V_0 is greater than 1. When the ratio of U_* to V_0 is roughly equal to unity, grains are travelling at speeds that are almost equal to that of the fluid, in which case suspension is likely to be the dominant transport mechanism. Based on the assumption that suspension occurs when the particles can be maintained in the flow by the upward component of turbulent velocity fluctuations.

The bedload transport processes are confined to a thin layer in the immediate vicinity of the stream bed. The particles that composed the bedload move at speeds that are less than the transporting flow, A range of empirical results based on laboratory / field measurements are available for sand, bimodal sediments (sand–gravel mixtures), and coarse-grained channels. The bedload transport rates are usually expressed in units of mass (dry mass) per unit width per unit time. The rate of bedload transport is almost entirely a function of the transporting capacity of the flow. Two variables are commonly used to estimate or predict bedload transport rates: the bed shear stress (τ_0) and the stream power (ω) per unit bed area (defined

as the product of bed shear stress and average velocity. One of the most widely used bedload transport equation has been that of Meyer-Peter and Mueller (1948).

4.8 Sediment transport Formula used in MIKE 21

Several empirical formulas are available to estimate the sediment transport (Vanoni, 1984). Some formulas predict total load (bed load + suspended load). However, information about both bed load and suspended load is required. The total load formulas can still be applied by using the calibration factors k_b (bed load calibration factor) and k_s (suspended load calibration factor) for bed load and suspended load, respectively.

Due to the non-uniform vertical distribution of the suspended sediment concentration, the effective fall height of grains will be different from the mean fall height $h/2$ (where h is water depth). For a uniform vertical concentration profile, the time scale for settling is defined as h/w_s (w_s is the settling velocity). With information about the Rouse number Z, the actual concentration profile can be predicted and therefore a better estimate for the settling time scale t_s can be obtained if using the height of the centroid. However, the time scale effect on the settling has already been included in the modelling using the described profile functions, and the $\Phi(\eta_0)$ factor on the sink/source term in the advectiondispersion equation for the concentration of the suspended sediment.

The Shields parameter θ is defined as:

$$\theta = \frac{\tau}{\rho g(s-1)d_{50}} \qquad \text{Eq. 4.41}$$

Where, τ is the flow shear stress, ρ is density of water, approx. 1000 kg/m^3, g is acceleration of gravity, 9.81 m/s^2, s is relative density of the sediment = ρ/ρ_s, ρ_s is density of sediment, for quartz sand = 2650 kg/m^3.

Flow shear stress is divided into form drag τ" and skin friction τ'. The total shear stress τ = τ' + τ" is estimated from the local flow velocity u and the local Chezy number C:

$$\tau = \rho g \frac{u^2}{C^2} \qquad \text{Eq. 4.42}$$

For skin friction the following approximate friction formula (Engelund & Hansen, 1967) is applied unless otherwise calculated (i.e. in the model of van Rijn or the model of Engelund and Fredsøe, where more sophisticated models are used to describe the physical processes):

$$\theta' = 0.06 + 0.4\,\theta^2 \qquad \text{Eq. 4.43}$$

The non-dimensional sediment rate is defined as:

$$\phi = \frac{S}{\sqrt{(s-1)gd^2}} \qquad \text{Eq. 4.44}$$

Where, S is sediment transport (bed load, total or suspended load), d is characteristic grain size and ϕ is non-dimensional sediment transport.

4.8.1 Engelund and Hansen model

The model by Engelund and Hansen (1967) is a total load model that needs user specified information in order to divide the sediment transport into bed load and suspended load. The total sediment load S_{tl} is estimated using following relations

$$S_{sl} = 0.05\frac{C^2}{g}\theta^{5/2}\sqrt{(s-1)gd_{50}^3} \qquad \text{Eq. 4.45}$$

$$\begin{aligned} S_{bl} &= k_b S_{tl} \\ S_{sl} &= k_s S_{tl} \end{aligned} \qquad \text{Eq. 4.46}$$

The equilibrium concentration is simply specified as the suspended load divided by the water flux and converted from volumetric concentration to mass concentration:

$$c_e = \frac{S_{sl}}{V.h}.s.10^6 \qquad \text{Eq. 4.47}$$

Where c_e is equilibrium mass concentration, V is velocity. Other symbols as defined earlier.

4.8.2 Van-Rijn model

Van-Rijn (1984) proposed the following models for sediment transport of bed load and suspended load:

$$S_{bl} = 0.053\frac{T^{2.1}}{D_*^{0.3}}.\sqrt{(s-1)gd_{50}^3} \qquad \text{Eq. 4.48}$$

Where T is the non-dimensional transport stage parameter and given by:

$$T = \left(\frac{u'_f}{u_{f,c}}\right)^2 - 1 \qquad \text{Eq. 4.49}$$

$u_{f,c}$ is the critical friction velocity and defined as:

$$u_{f,c} = \sqrt{\theta_c (s-1) g d_{50}} \quad \text{Eq. 4.50}$$

The effective friction velocity u'_f is estimated from

$$u'_f = V \frac{\sqrt{g}}{C'} \quad \text{Eq. 4.51}$$

Where, C' is the resistance from skin friction and is based on logarithmic velocity profile assuming a certain bed roughness and is defined as

$$C' = 18 log\left(\frac{4h}{d_{90}}\right) \quad \text{Eq. 4.52}$$

The non-dimensional particle parameter D* in the van Rijn bed load transport formula is defined as:

$$D_* = d_{50}\left(\frac{(s-1)g}{v^2}\right)^{1/3} \quad \text{Eq. 4.53}$$

Where ν, is the kinematic viscosity and approximately equal to 10^{-6} m^2/s for water. Instead of using a constant critical Shields parameter θ_c (approximately equal to 0.06), van Rijn assumes the following variation as a function of D_*:

Range of D_*	**θ^c**
$D_* < 4$	$0.24/ D_*$
$4 < D_* < 10$	$0.14/ D_*^{-0.64}$
$10 < D_* < 20$	$0.04/ D_*^{-0.1}$
$20 < D_* < 150$	$0.013/ D_*^{-0.29}$
$D_* > 150$	0.055

Suspended sediment transport occurs only if one of the following criteria is satisfied:

$u_f >= \frac{4w_s}{D_*}$ $for\ D_* < 10$ and

$u_f >= 0.4 w_s$ $for\ D_* > 10$ and

Eq. 4.54

The reference level, at which the bed concentration is determined, is expressed as:

$$a = max\begin{pmatrix} 0.01\,h \\ 2d_{50} \end{pmatrix} \quad \text{Eq. 4.55}$$

The volumetric bed concentration is obtained from the relation:

$$c_a = 0.015\left(\frac{d_{50}T^{1.5}}{aD^{0.3}}\right) \quad \text{Eq. 4.56}$$

A correction coefficient, denoted β is applied to the hydrodynamic diffusion coefficient in order to transform the coefficient into a diffusion coefficient for the suspended sediment:

$$\beta = 1 + 2\left(\frac{w_s}{u_f}\right)^2 \quad \text{Eq. 4.57}$$

Van Rijn defines a correction factor φ for the concentration profile, which is determined by:

$$\varphi = \frac{8}{2}\left(\frac{w_s}{u_f}\right)^{0.8}\left(\frac{c_a}{c_o}\right) \quad \text{Eq. 4.58}$$

Where c_o (if expressed as volumetric concentration) is the concentration corresponding to firm packing of the sediment, i.e.: $c_o = 0.65$ (m^3/m^3)

When applying the correction coefficients defined above, a Rouse suspension parameter Z can be obtained by

$$Z = \frac{w_s}{\beta kuf} + \varphi \quad \text{Eq. 4.59}$$

Finally, the depth-integrated transport of suspended load is computed as:

$$S_{sl} = f.c_a.V.h \quad \text{Eq. 4.60}$$

Where the correction factor for suspended load is obtained from:

$$f = \frac{\left(\frac{a}{h}\right)^z - \left(\frac{a}{h}\right)^{1.2}}{\left(1-\frac{a}{h}\right)^z (1.2 - z)} \quad \text{Eq. 4.61}$$

The equilibrium concentration c_e is calculated by another approximation formulas given in table below:

Condition	**Corresponding value of Ce and h***
Z ≤ 1	c_e = *ca*[[(2.21Z - 6.41)Z + 7.21)Z - 3.95]Z + 0.97]
1 ≤ Z ≤ 3	c_e = *ca* [[(0.007Z – 0.06)Z + 0.220)Z - 0.347]Z + 0.22]
Z > 3	c_e = *ca* [[(4·10-6 Z - 1.2·10-4)Z + 1.4·10-3)Z - 7.67·10-3]Z + 0.018]

4.8.3 Engelund and Fredsøe model

The probability of a moving sediment grain can, according to Engelund and Fredsøe (1976), be determined by the expression:

$$p = \left[1 + \left(\frac{\frac{\pi}{6}\mu_d}{\theta' - \theta_c}\right)^4\right]^{-\frac{1}{4}}, \theta' > \theta_c \qquad \text{Eq. 4.62}$$

The dynamic friction coefficient μ_d is equal = 0.51 = tan27°. The non-dimensional skin shear stress is defined by:

$$\theta' = \frac{{u_f'}^2}{(s-1)gd_{50}} \qquad \text{Eq. 4.63}$$

Where the friction velocity related to skin friction is calculated from the assumption of a logarithmic velocity profile:

$$u_f' = \frac{V}{6 + 2.5ln\left(\frac{h}{2.5d_{50}}\right)} \qquad \text{Eq. 4.64}$$

The bed load transport rate is estimated from:

$$S_{bl} = 5p.(\sqrt{\theta'} - 0.7\sqrt{\theta_c}\sqrt{(s-1)gd_{50}^3}. \qquad \text{Eq. 4.65}$$

The reference concentration near the bed is calculated from an empirical relation obtained by Zyserman and Fredsøe (1994):

$$c_b = \frac{0.331(\theta-\theta_c)^{1.75}}{1+\frac{0.331(\theta-\theta_c)^{1.75}}{0.46}}. \qquad \text{Eq. 4.66}$$

The empirical relation was established from analysis of the experimental data sets of Guy et al. (1966) and covers a range from pure bed load to dominant suspended transport. The influence of lateral bed slope is included in the relation through a reduced critical Shields stress for onset of motion.

Numerical integration is performed along a logarithmic vertical scale, because a greater density of computational points is required close to the bottom, where the largest velocity gradients occur.

The Rouse suspension parameter Z, is defined as:

$$Z = \frac{w_s}{\kappa u_f} \qquad \text{Eq. 4.67}$$

The suspended load transport rate S_{sl}, is obtained from

$$S_{sl} = c_b V h \int_{\eta_0}^{1} u(\eta) \, . \, c(\eta) d\eta \qquad \text{Eq. 4.68}$$

Where, η is the dimensionless vertical coordinate.

The equilibrium mass concentration c_e, is determined from:

$$c_e = \frac{S_{sl}}{Vh} s . 10^6 \qquad \text{Eq. 4.69}$$

4.8.4 Meyer-Peter and Müller model

The Meyer-Peter and Müller model (1948) relates the non-dimensional bed load transport Φ to the dimensionless shear stress acting on the grains through the relation:

$$\Phi_{bl} = 8(\theta' - \theta_c)^{1.5} \qquad \text{Eq. 4.70}$$

or expressed as a transport rate:

$$S_{bl} = 8(\theta' - \theta_c)^{1.5} \sqrt{(s-1) g d_{50}^3} \qquad \text{Eq. 4.71}$$

Where θ' is the part of the Shields stress related to skin friction. The relation is only valid for fluvial systems with dominating bed load and slopes ranging from 0.0004 to 0.02.

5 ANALYSIS AND RESULTS

The river bank erosion, sediment deposition and shifting characteristics of the Gandak river from Dumariaghat to Hajipur is studied using temporal satellite images. The river bank line is delineated for 1975, 1980, 1991, 1995, 2000, 2005, 2010, 2015 and 2020. The Landsat image of 1975 is used as reference to compute the bank erosion and river shifting.

5.1 Geomorphological Characteristics and River Shifting Analysis

5.1.1 Geomorphological Characteristics

The sinuosity index parameter indicates if the river is straight, sinuous or meanders. This it measures the spatial spread/ pattern of the alluvial river. Sinuosity is the ratio of stream length to valley length. It can also be described as the ratio of valley slope to channel slope. Meander geometry characteristics are directly related to sinuosity, consistent with the principle of minimum expenditure of energy.

However, the term ‘entrenchment ratio’ defines the vertical containment of the river. The entrenchment ratio is the ratio of the width of the flood-prone area to the surface width of the bankfull channel. Using the satellite images the bank full width and flood prone area can be identified easily at any of the river section. The study stretch of Gandak River in which river the morphological characteristics is estimated is shown in Figure 5.1. The study stretch, from Dumariaghat to Hajipur, is divided into 9 sections; 1 to 9 and 8 reaches (A to H). The sinuosity and entrenchment ratio of each stretch is estimated as discussed above. The sinuosity and entrenchment ratio of the river in various stretches have been computed and shown in Table 5.1.

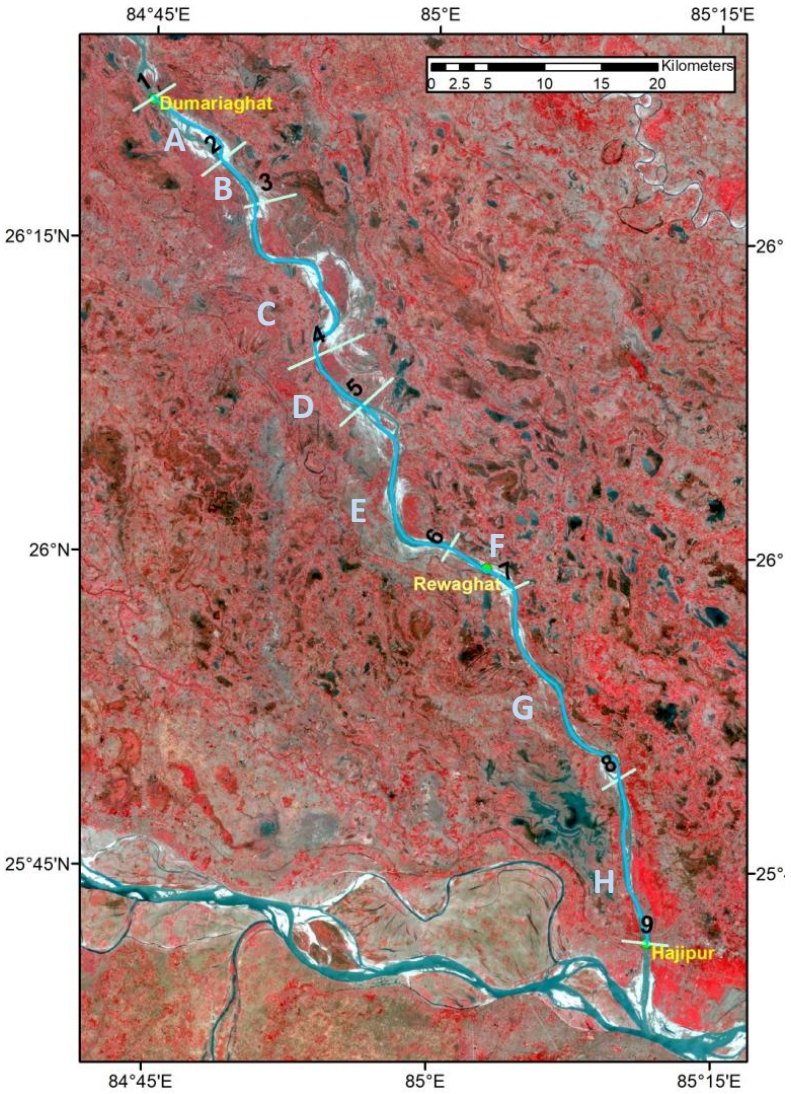

Figure 5.1: Gandak river stretch for morphological analysis.

Table 5.1: Morphological parameters computed for different river stretches.

River Stretch Name	Length (m)	Sinuosity	Entrenchment ratio
A	8723	1.08	1.58
B	4967	1.02	1.74
C	18644	1.29	1.68
D	6147	1.03	1.77
E	18168	1.23	2.15
F	6741	1.01	1.21
G	20699	1.08	2.68
H	14930	1.01	1.30

5.1.2 Satellite based river shifting analysis

Temporal satellite image for 45 years, at an average interval of about 5 years, downloaded from USGS website are used for river shifting study. The progressive shifting of the river is estimated by overlaying the river bank line extracted for different years, as shown in Figure 5.2. The figure shows the position of the river bank line from 1975 to 2020. The figure shows that the river bank line has shifted significantly at three locations. The entire stretch is further split into three scenes for detailed visualization and analysis (Figure 5.3).

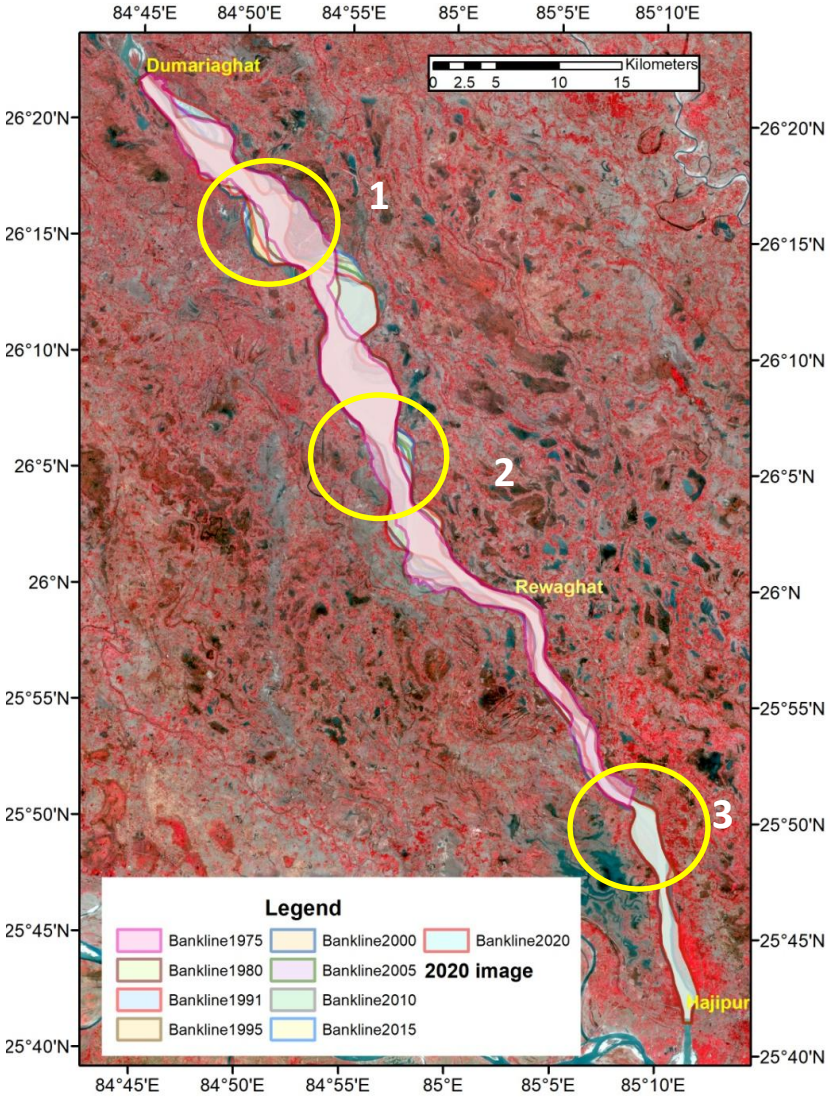

Figure 5.2: Overlay of the river bank line during 1975 to 2020 extracted from temporal images.

5.1.2.1 Shifting at Location-1

The shifting of river bank with respect to current position (2020 image) has been estimated by overlaying the bank line extracted from two images. At location 1, the left bank of the river was about 2 km east in the year 1975 compared to 2020 position. The shifting is observed to be reducing gradually; 1.7 km in 1980, 0.8 km in 1991, 0.6 km in 1995, 0.3 km in 2000, respectively. Since 2005, the Gandak river at this locations appears to be tamed and no appreciable change in its bank line has been observed. In fact, construction of embankments on both the banks, anti-erosion works and other engineering interventions have resulted into the confinement of the river. In this stretch, the river shifting at critical locations of major habitats is restricted using human intervention (anti-erosion works etc). At locations namely Munja village on right bank and Chak Alhdad on left bank, shifting has been restricted through construction of spurs as shown in Figure 5.5. However, the intermittent shifting (within intermediate period of satellite images) could not be captured through such analysis.

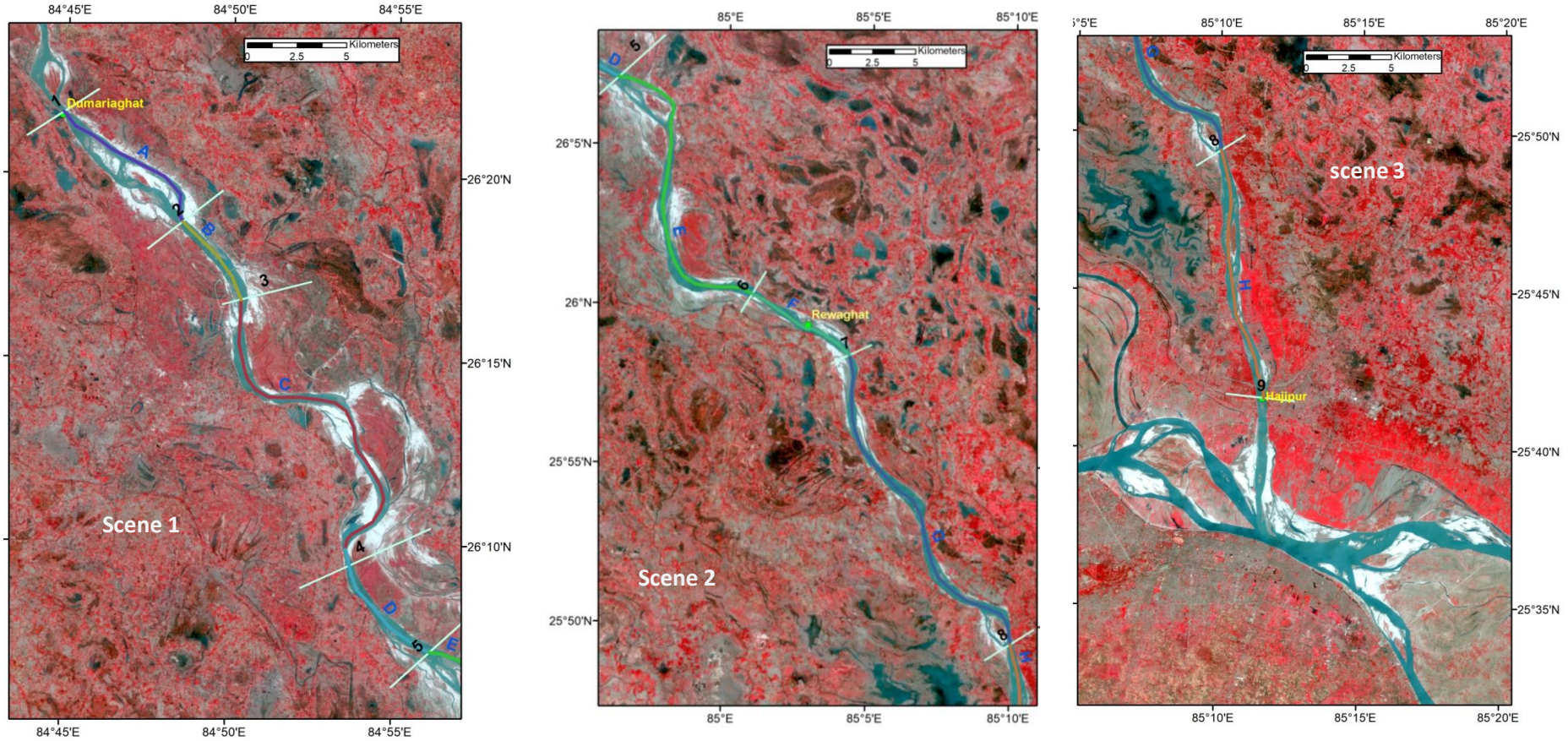

Figure 5.3: The study stretch is split into three divisions (scenes) for detailed visualization.

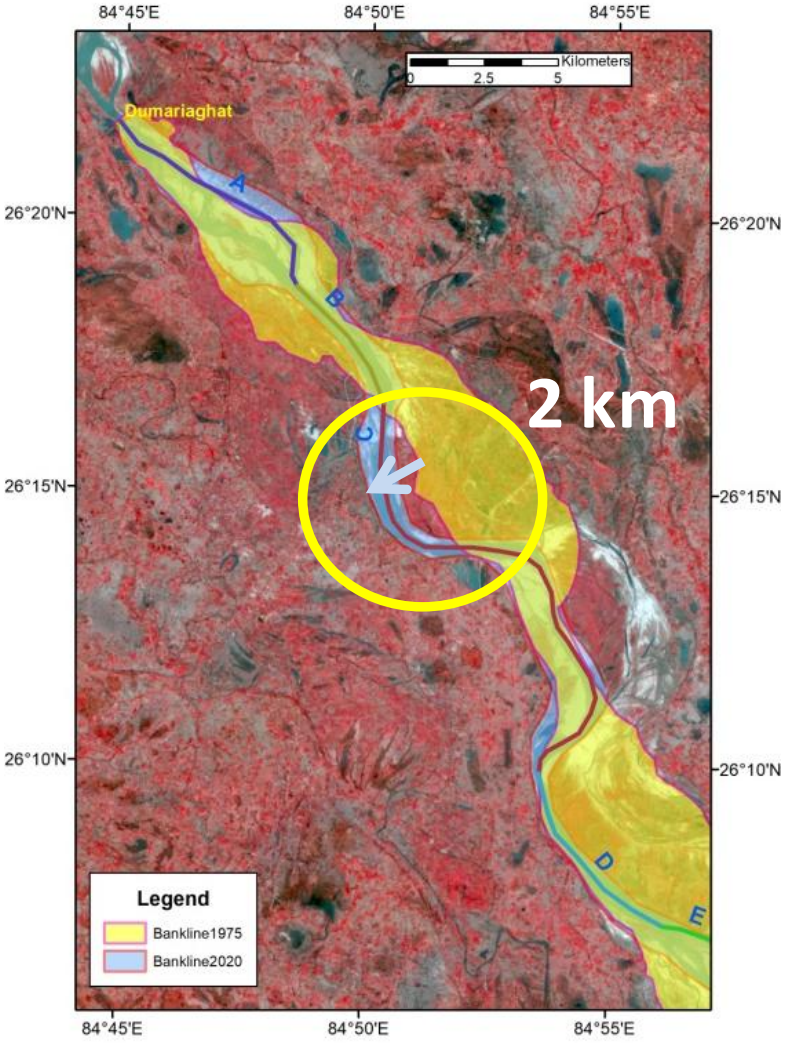
84°45'E
84°50'E
84°55'E
Kilometers
0 2.5 5
Dumariaghat
A
B
C
D
E
2 km
26°20'N
26°15'N
26°10'N
Legend
Bankline1975
Bankline2020

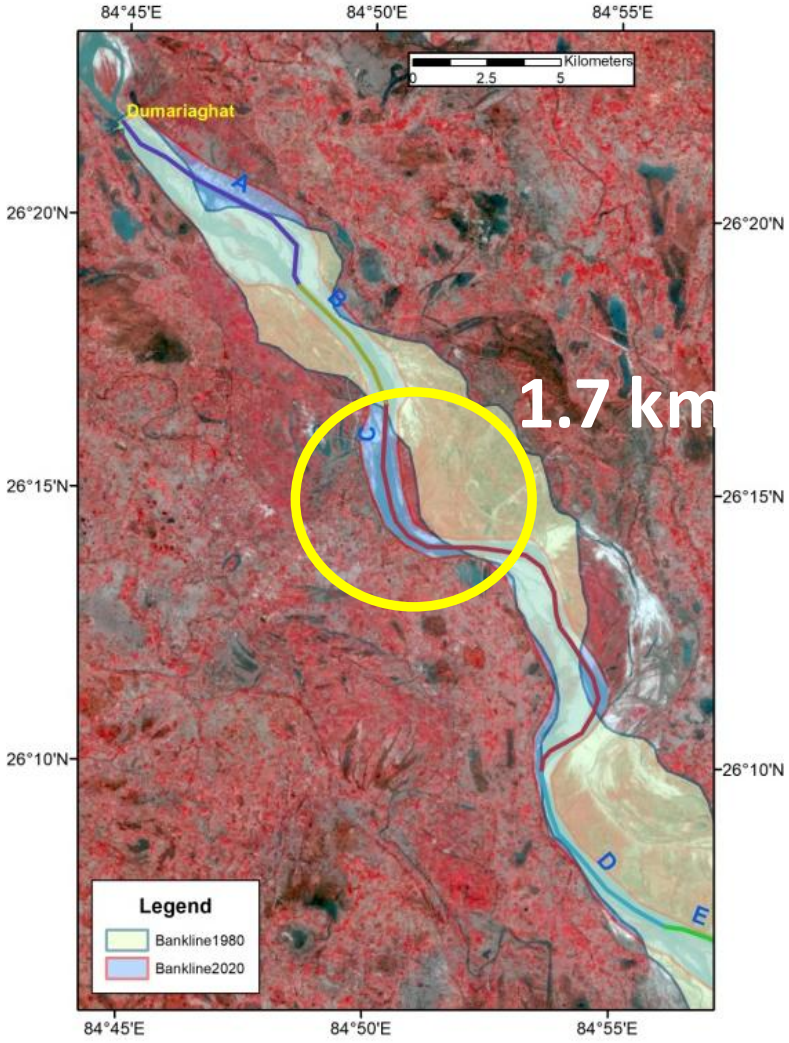
84°45'E
84°50'E
84°55'E
Kilometers
0 2.5 5
Dumariaghat
A
B
C
D
E
1.7 km
26°20'N
26°15'N
26°10'N
Legend
Bankline1980
Bankline2020

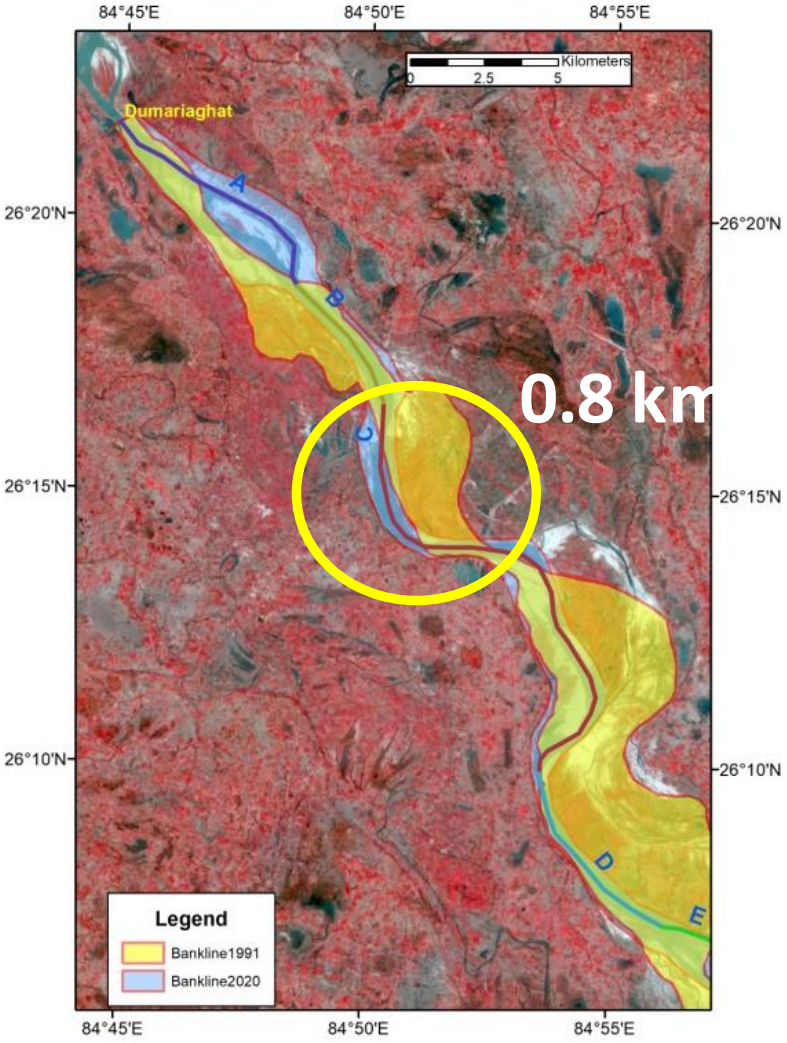
84°45'E
84°50'E
84°55'E
Kilometers
0 2.5 5
Dumariaghat
A
B
C
D
E
0.8 km
26°20'N
26°15'N
26°10'N
Legend
Bankline1991
Bankline2020

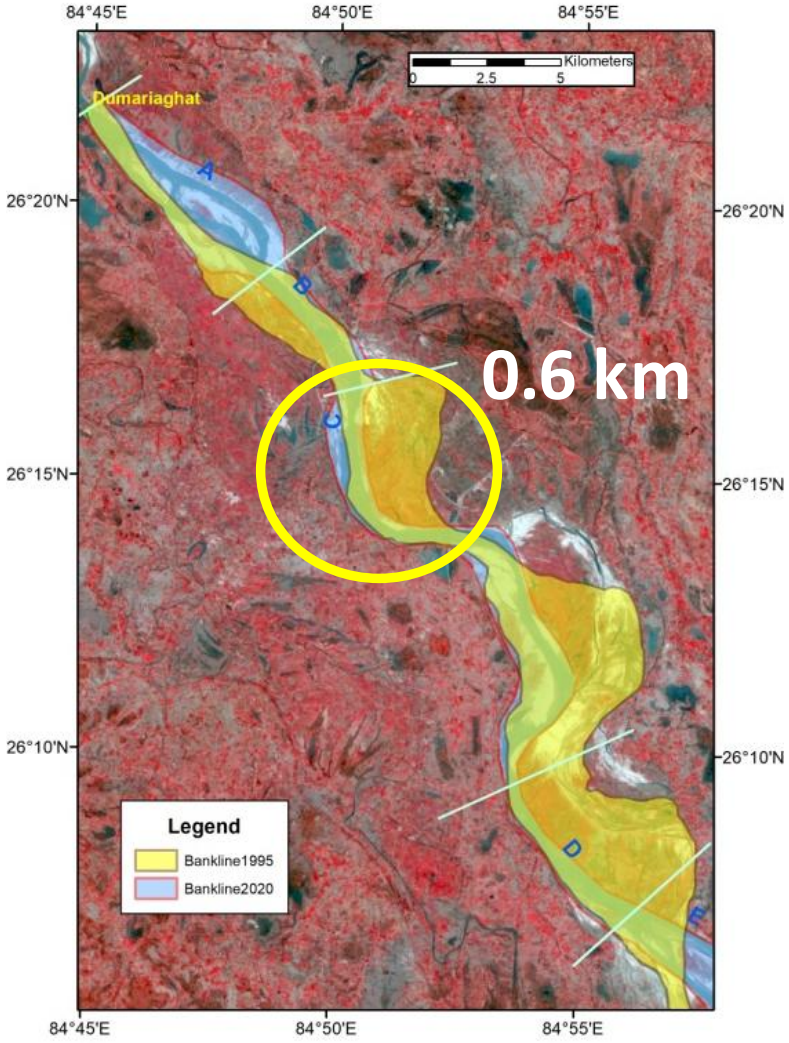
84°45'E
84°50'E
84°55'E
Kilometers
0 2.5 5
Dumariaghat
A
B
C
D
E
0.6 km
26°20'N
26°15'N
26°10'N
Legend
Bankline1995
Bankline2020

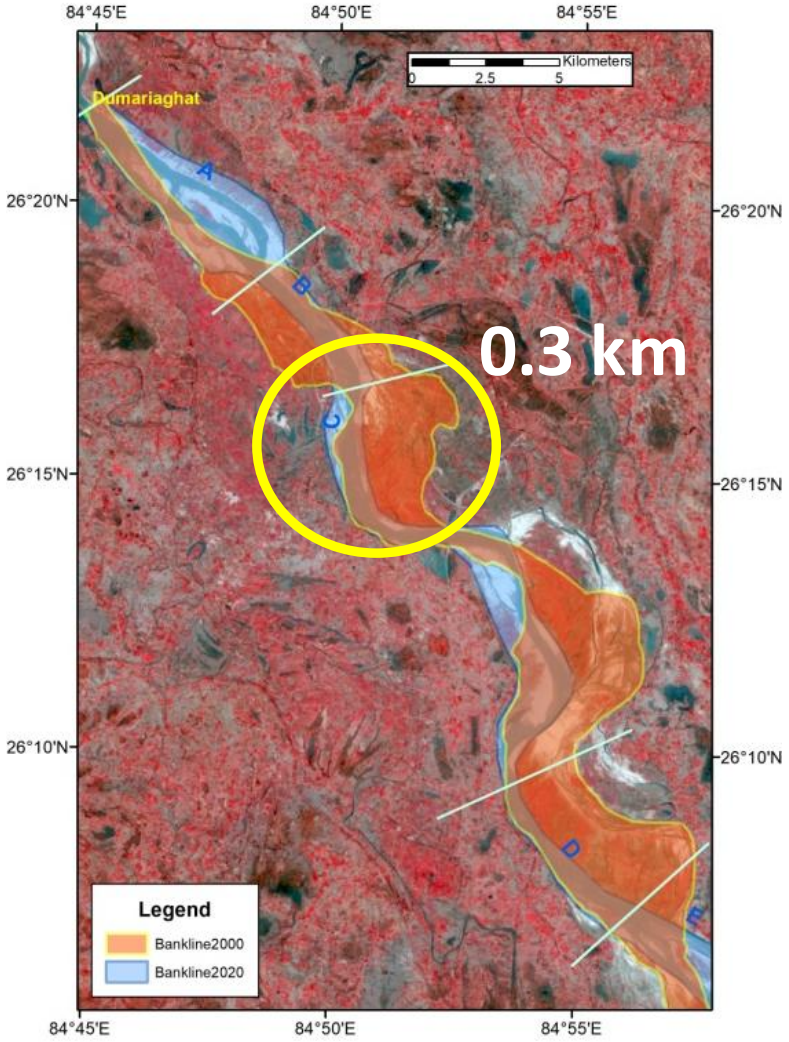
84°45'E
84°50'E
84°55'E
26°20'N
26°15'N
26°10'N
Kilometers
0 2.5 5
Domariaghat
A
B
C
D
E
0.3 km
Legend
Bankline2000
Bankline2020

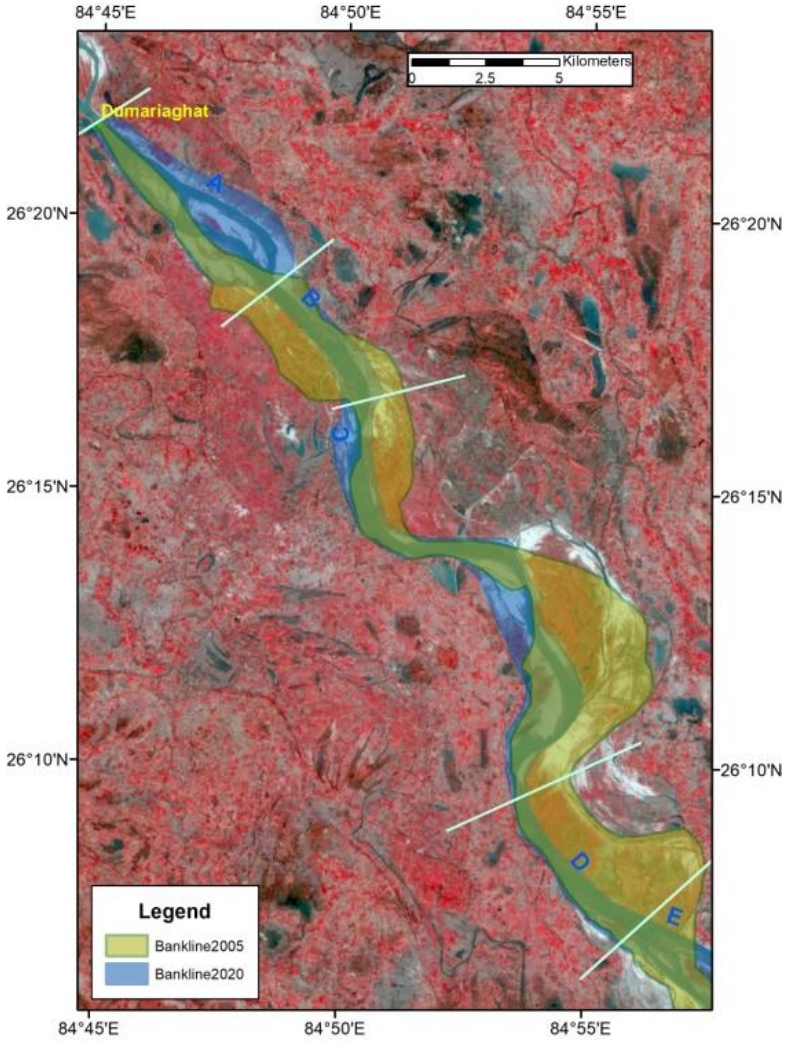
84°45'E
84°50'E
84°55'E
26°20'N
26°15'N
26°10'N
Kilometers
0 2.5 5
Domariaghat
A
B
C
D
E
Legend
Bankline2005
Bankline2020

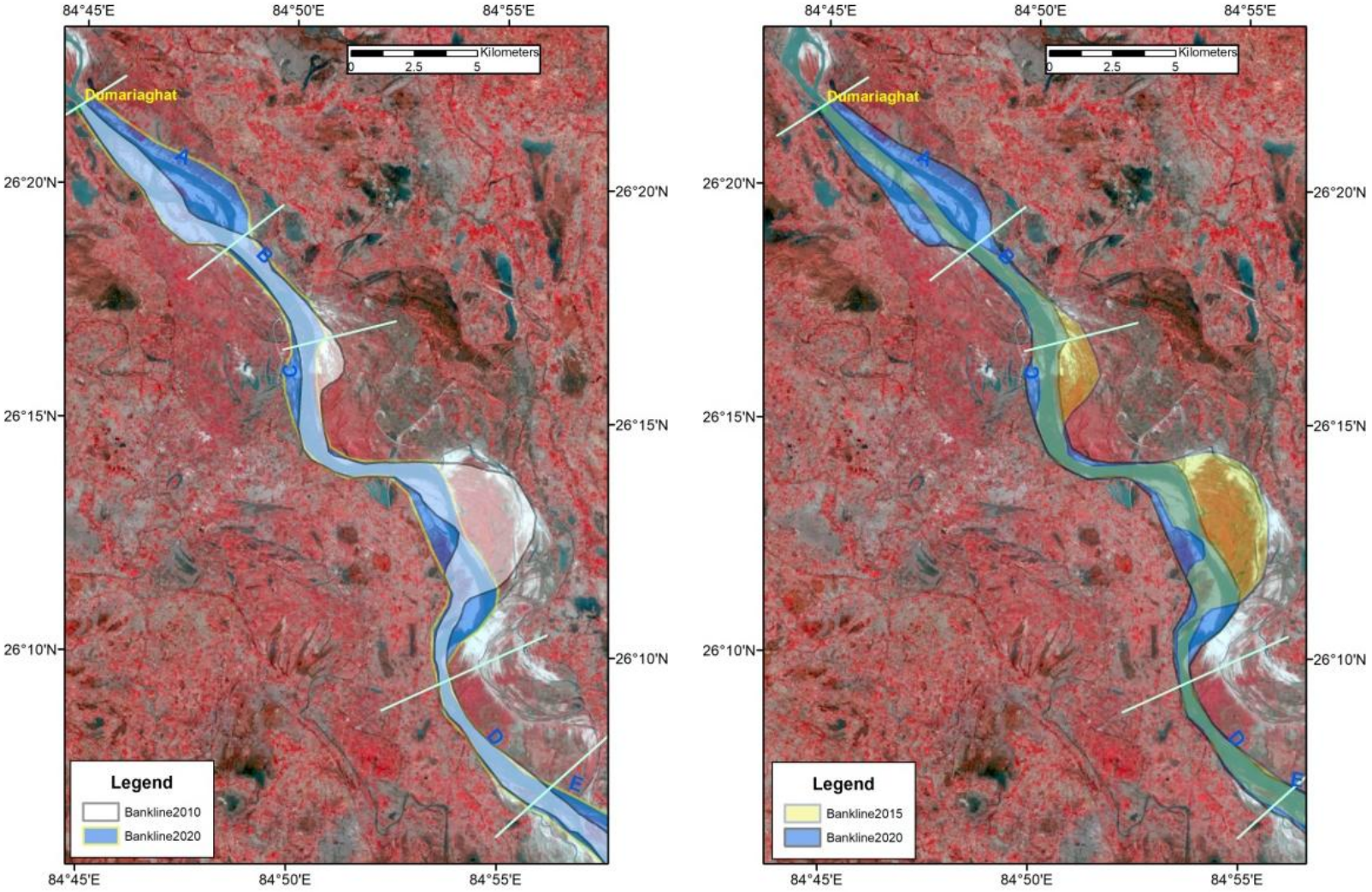

Figure 5.4: River shifting trend at Location 1 (Munja village).

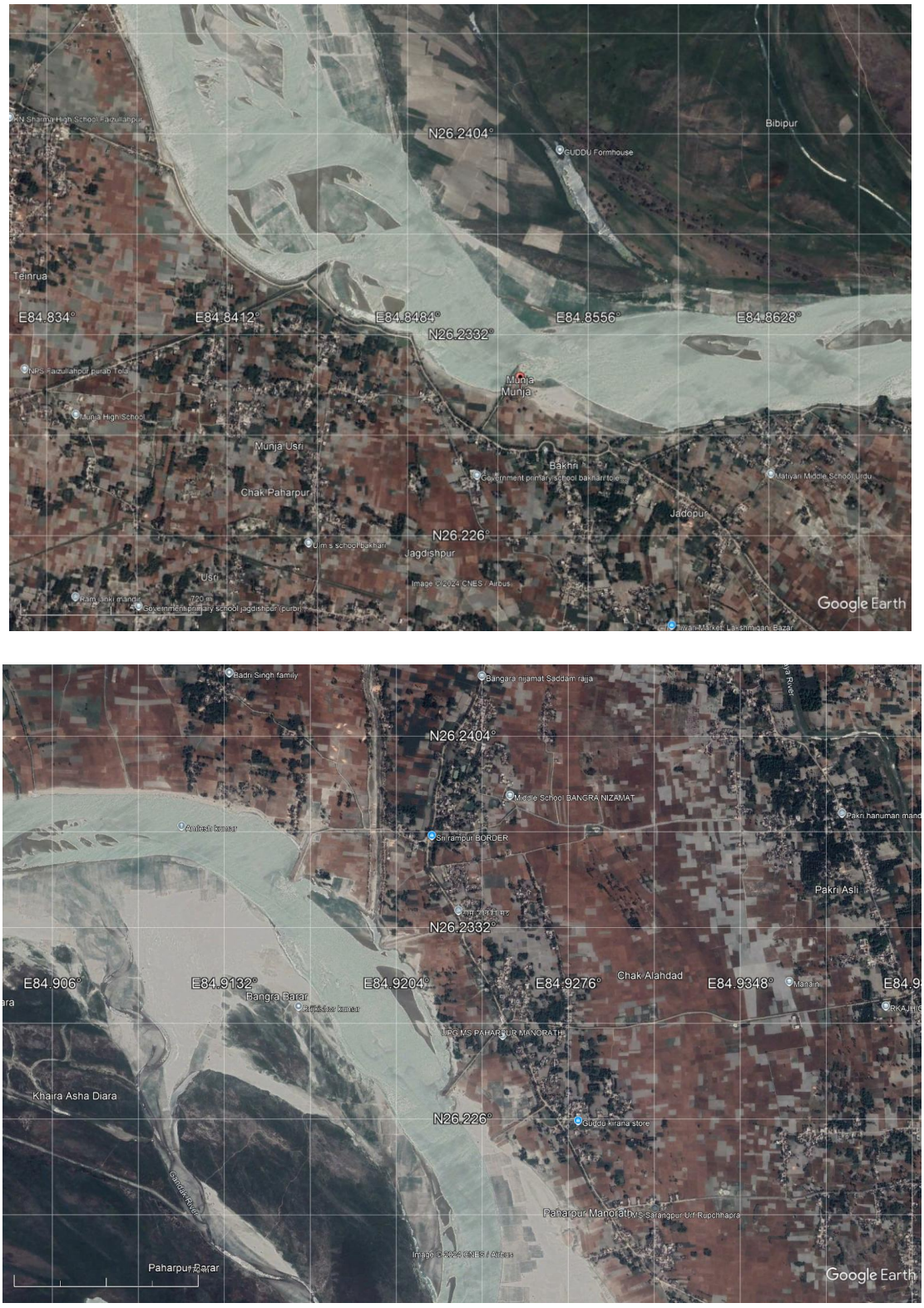

Figure 5.5: The shifting is controlled due to anti-erosion works and construction of embankments at village Munja and Chak Alahdad appearing in 2013 images in Google Earth Images.

5.1.2.2 Shifting at Location-2

Another critical location where major shifting has been observed is located between village Jadopur to village Gokhula Rupali (Figure 5.6). At this location, the river has shifted significantly, as high as 1.5 km since 1975 and increased to 1.8 km in 1995, as shown in Figure 5.7.

Afterwards the river bank at this location appears to be stable. In fact the river has touched the left embankment and the shifting has been restricted due to this man made flood protection measure. In this stretch, the river is shifting and sometimes braiding between left and right embankments. Near Gokhula Rupali it has touched the left bank in 2017 and since then flowing along the embankment.

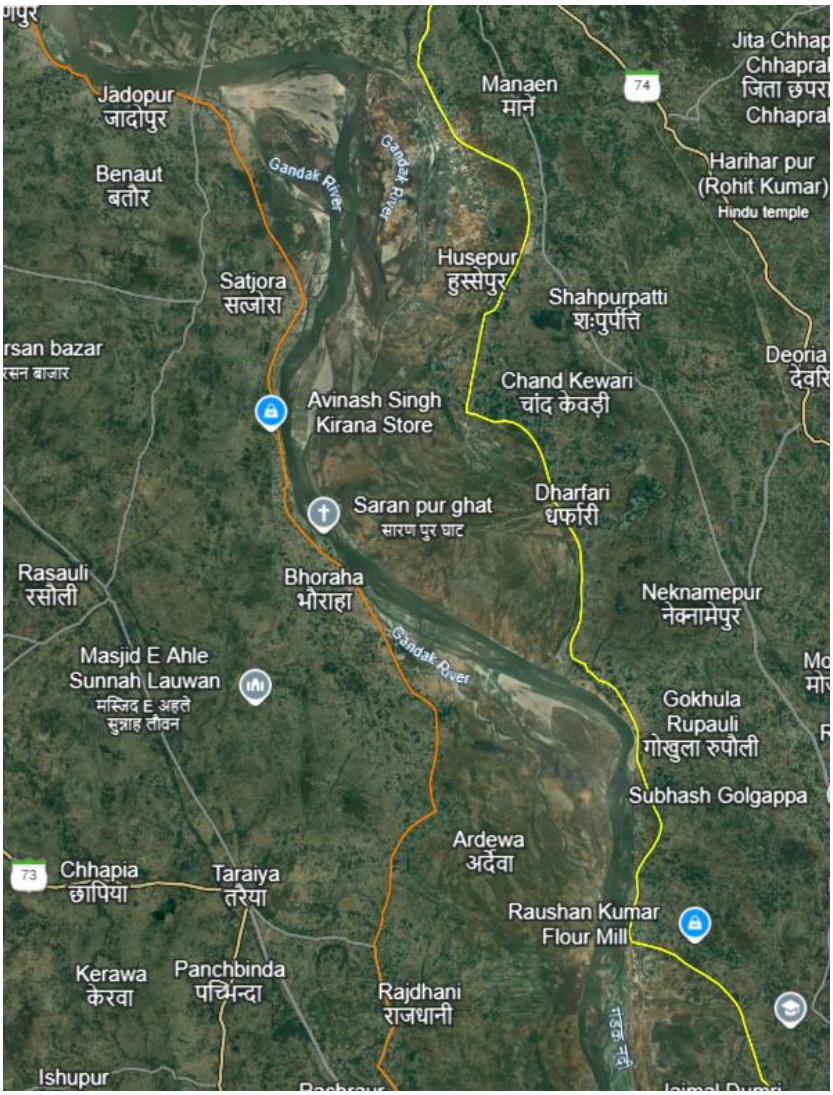

Figure 5.6: Location 2 where major shifting was observed during 1975-2020.

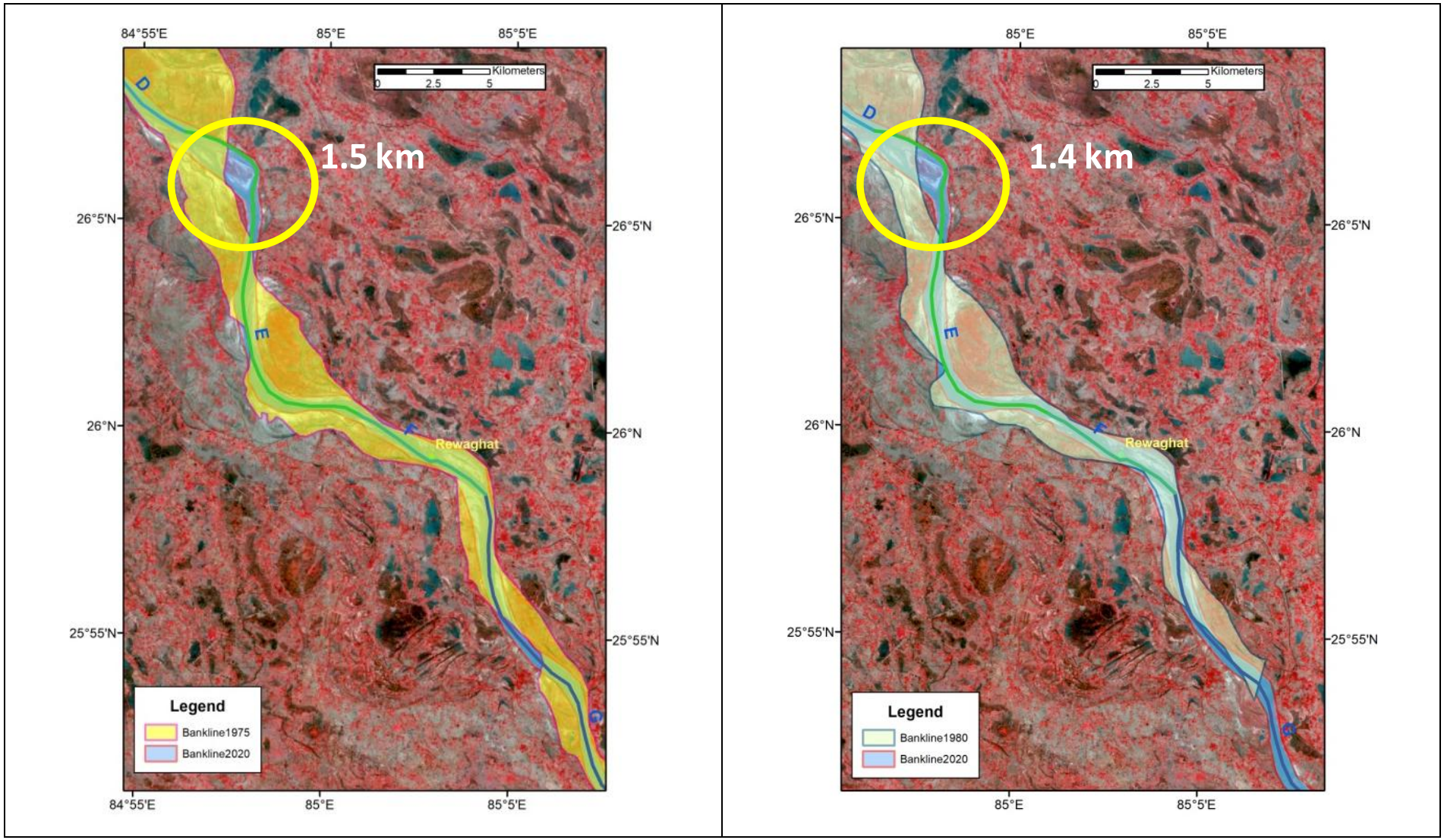
84°55'E
85°E
85°5'E
26°5'N
26°N
25°55'N
Kilometers
0 2.5 5
1.5 km
D
E
F
G
Rewaghat
Legend
Bankline1975
Bankline2020
1.4 km
Legend
Bankline1980
Bankline2020

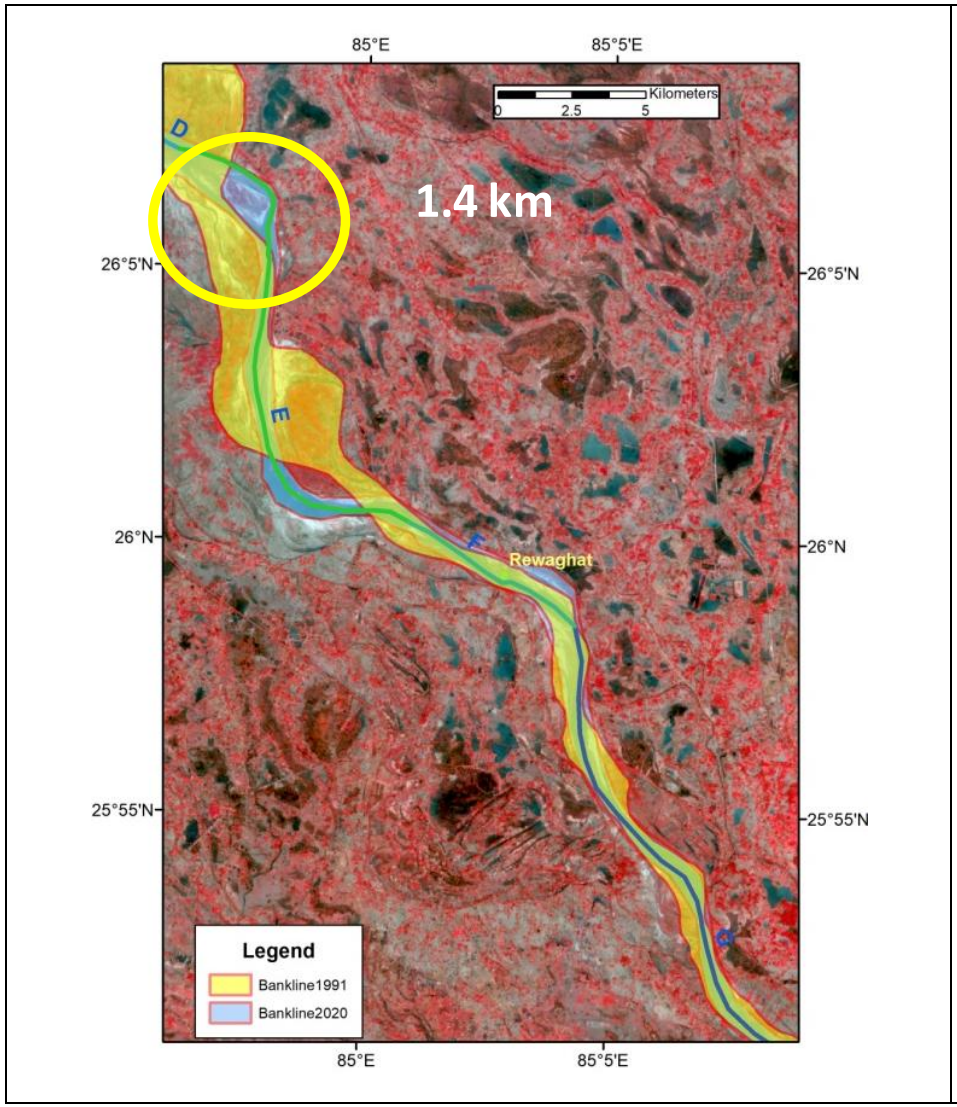
85°E
85°5'E
Kilometers
0 2.5 5
1.4 km
26°5'N
26°N
25°55'N
D
E
F
G
Rewaghat
Legend
Bankline1991
Bankline2020

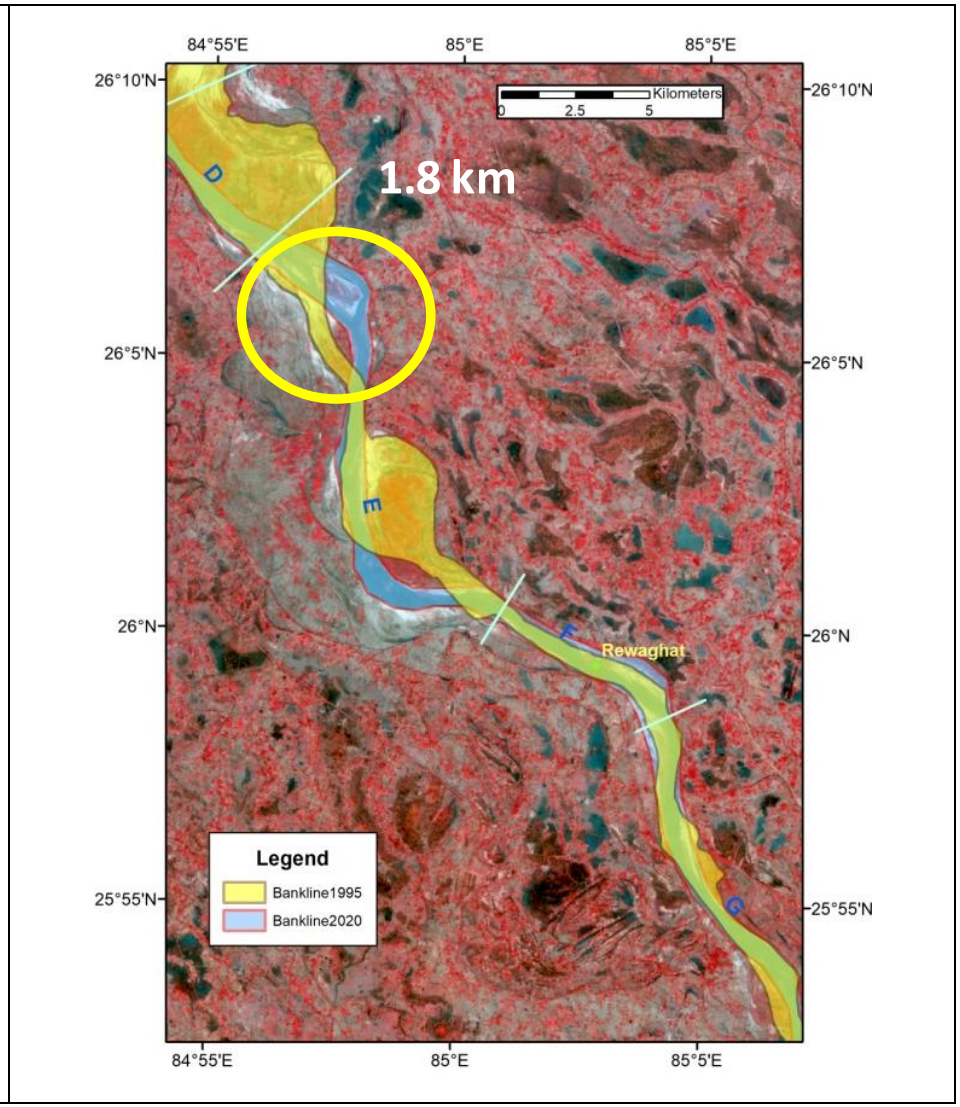
84°55'E
85°E
85°5'E
Kilometers
0 2.5 5
1.8 km
26°10'N
26°5'N
26°N
25°55'N
D
E
F
G
Rewaghat
Legend
Bankline1995
Bankline2020

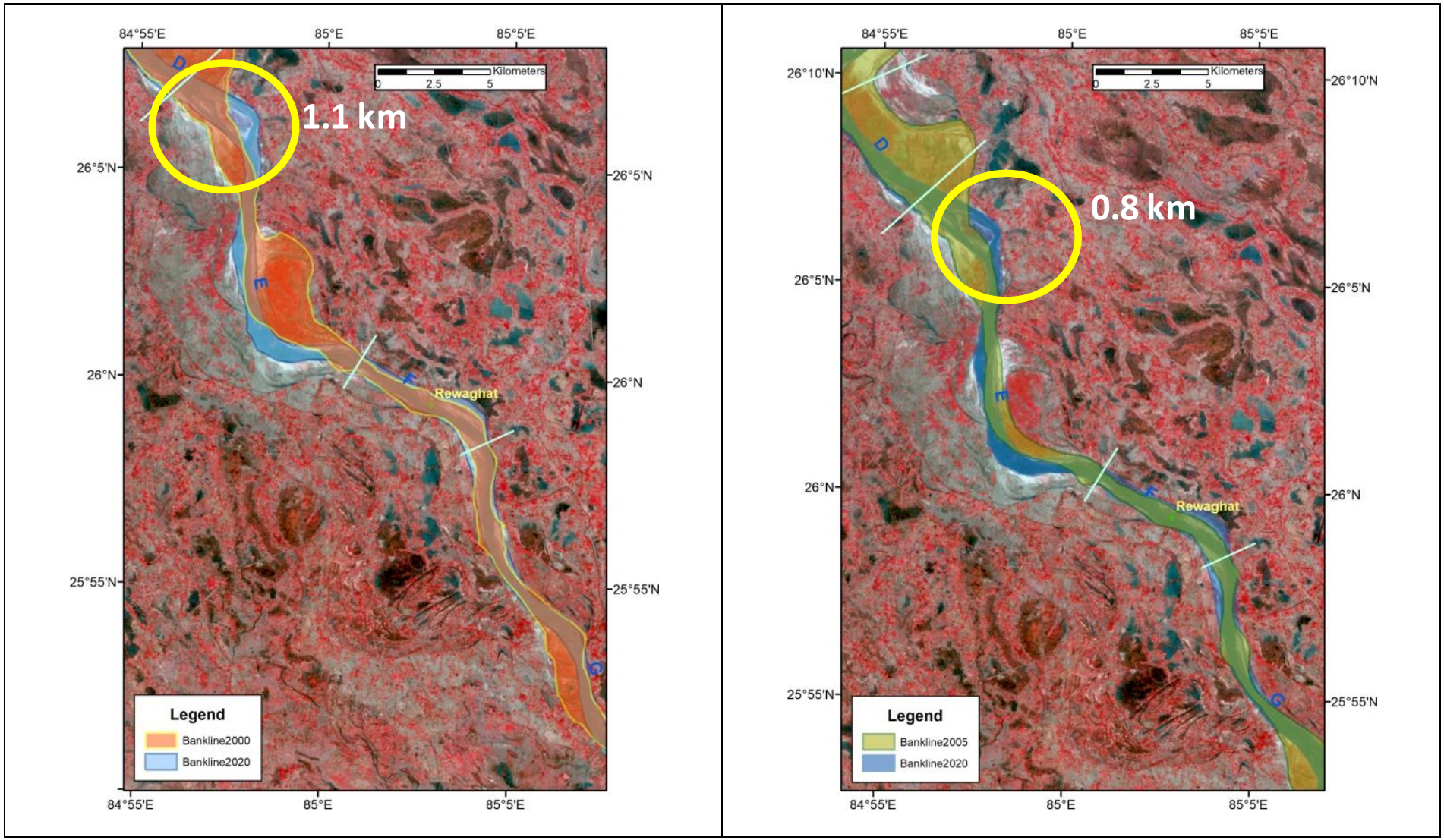
84°55'E
85°E
85°5'E
26°5'N
26°N
25°55'N
Kilometers
0 2.5 5
1.1 km
D
E
F
G
Rewaghat
Legend
Bankline2000
Bankline2020
26°10'N
0.8 km
Legend
Bankline2005
Bankline2020

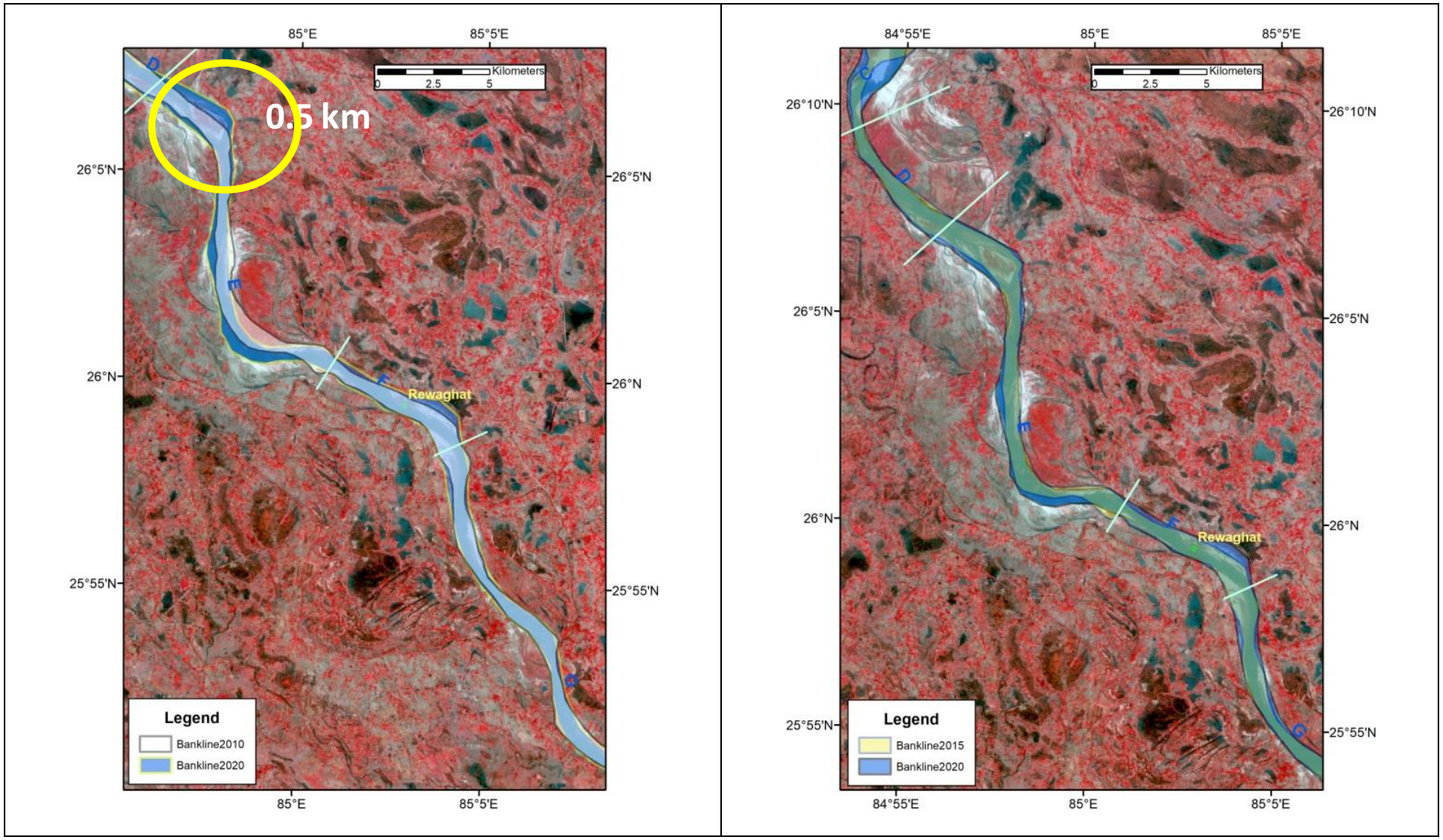

Figure 5.7: river shifting during various years at specified location (2) (Gokhula Rupali) with reference to river position as on 2020.

Figure 5.8: River is shifting between Village Jadopur and Gokhula Rupali in bwteen the embankment since 2000.

Shifting at Location-3

Third location where major shifting has been observed is at village Dharahara. At this location 1.8 km shift has been noticed at the right bank during 1985-2000 as shown in Figure 5.9. However, on closer look, it is observed that the river is highly braiding in this stretch and its braiding patter is changing since 2000. Before 1985, two branches of the river are clearly appearing. After 2000, right branch of the river starts disappearing (having very low flow) and the flow is mainly confined in the left branch. Figure 5.9 shows the braiding of the river after 2000. The image for 2020 shows the single branch river flowing adjacent to the right embankment. However, the re-development of braiding near Darahara is again appearing in this image. Thus, after the construction of embankments on both the banks, river is swinging between the embankment, sometimes, the main flow is towards left embankment or right embankment. The braiding also disappears and after some period, again starts developing.

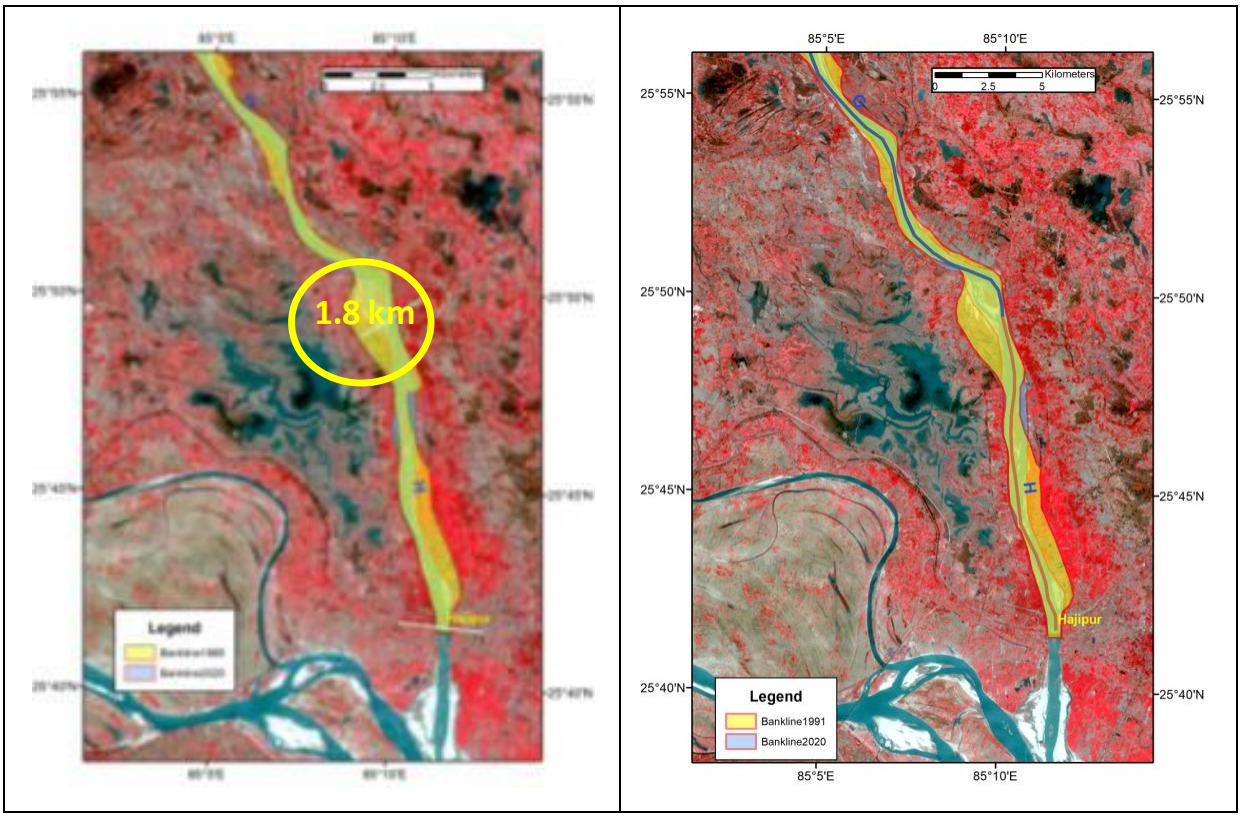

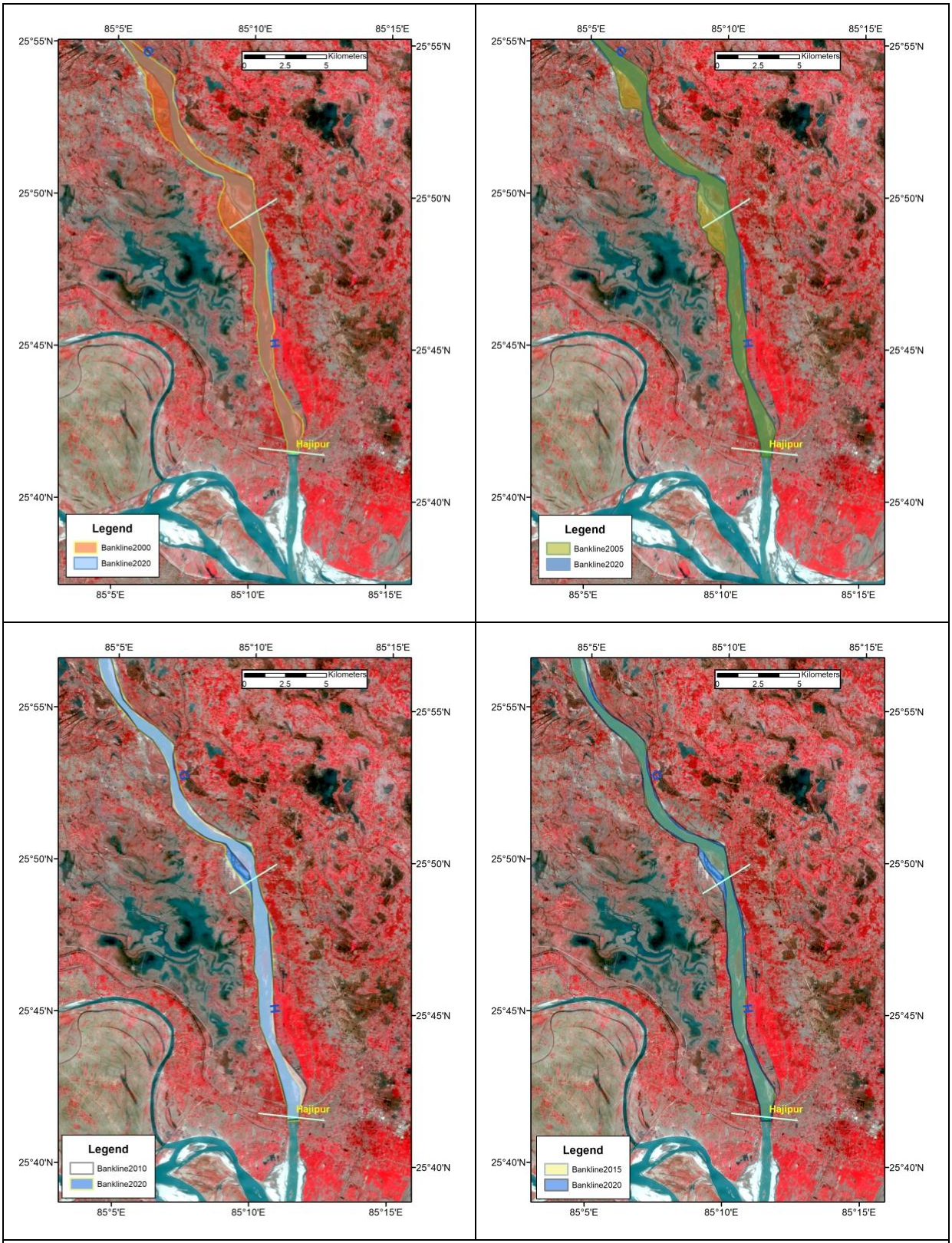

Figure 5.9: river shifting at various periods at specified location (3) with reference to river position as on 2020.

Figure 5.10: Braiding of Gandak river near village Darhara from images in GE.

5.2 Estimation of Design Flood

The box plot of annual peak flood series for Dumariaghat and Lalganj GD sites are given in Figure 5.11. The maximum, minimum and average peak floods at Dumariaghat site are estimated as 17886 m^3/s, 3560 m^3/s, and 9227 m^3/s, respectively. Similarly, the maximum, minimum and average peak floods at Lalganj sites are estimated as 18000 m^3/s, 5400 m^3/s, and 9819 m^3/s, respectively. The median flood value calculated at Dumariaghat and Lalganj sites are 8550 m^3/s and 9035 m^3/s, respectively.

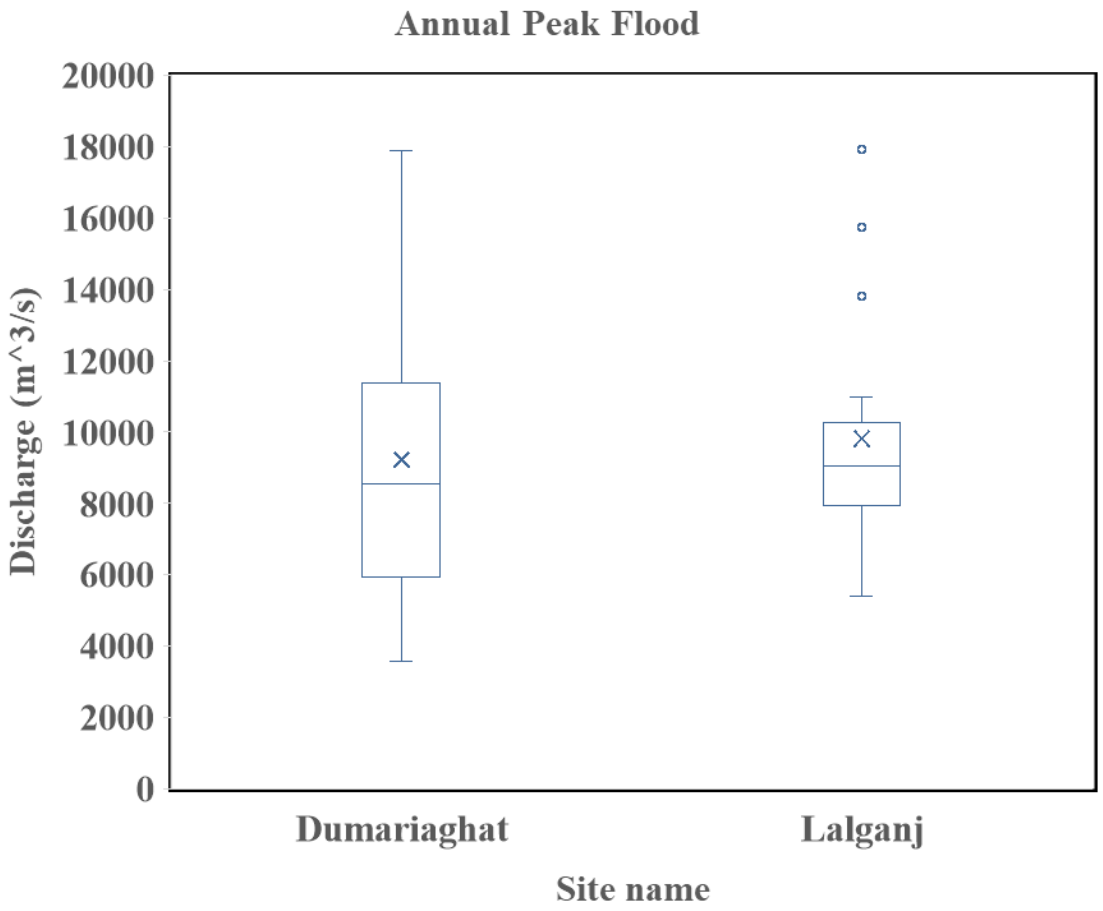

Figure 5.11: Box plot for annual peak flood data at Dumariaghat and Lalganj site.

5.2.1 Estimation of floods of various return periods using L-Moments based Frequency Analysis

In flood frequency analysis has been carried out using 30 years annual peak discharge data at Dumariaghat and Lalganj GD sites. The robust frequency distribution has been identified based on Z_i^{dist} Statistic and L-moment ratio diagram. The five lowest Z_i^{dist} Statistic among

various frequency distributions are given in Table 5.2 and the selected lowest value row is in bold font. Based on the Z_i^{dist} Statistic (Table 5.2), the parameters for various distributions are given in Table 5.3. The first row of the parameter values (Table 5.3) shows the robust identified frequency distribution. The flood values of various return periods are estimated by multiplying the growth factor with the mean annual peak flood value. The values of the growth factors or site-specific scale factors ($Q_T/\overline{Q}$) along with estimated flood values of various return periods are given in Table 5.4 and Table 5.5.

Table 5.2: Z_i^{dist} –statistic for various distributions

S. No.	Distribution	Z_i^{dist} –statistic
A: Dumariaghat		
1	**Pearson Type III (PE3)**	**0.16**
2	Generalized Normal (GNO)	0.34
3	Generalized Extreme Value (GEV)	0.40
4	Generalized Pareto (GPA)	-0.94
5	Generalized logistic (GLO)	1.01
B : Lalganj		
1	**Generalized logistic (GLO)**	**-0.76**
2	Generalized Extreme Value (GEV)	-1.03
3	Generalized Normal (GNO)	-1.20
4	Pearson Type III (PE3)	-1.5
5	Generalized Pareto (GPA)	-1.72

Table 5.3: Parameters for various distributions

Distribution	Parameters of the Distribution				
A: Dumarighat					
PE3	**ξ =1.000**	**α = 0.464**	**K=0.982**		
GNO	ξ =0.926	α = 0.430	K=-0.333		
GEV	ξ =0.791	α = 0.371	K= 0.013		
GPA	ξ =0.379	α = 0.896	K= 0.444		
GLO	ξ =0.933	α = 0.243	K= -0.162		
WAK	ξ =-0.308	α = 1.123	β= 3.278	γ= 0.473	δ = -0.102
B: Lalganj					
GLO	**ξ =0.923**	**α = 0.154**	**K=-0.279**		
GEV	ξ =0.837	α = 0.213	K=-0.162		
GNO	ξ =0.915	α = 0.270	K=-0.581		
PE3	ξ =1.000	α = 0.339	K= 1.673		

WAK	ξ =0.218	α = 13.878	β= 27.604	γ=0.256	δ = 0.136

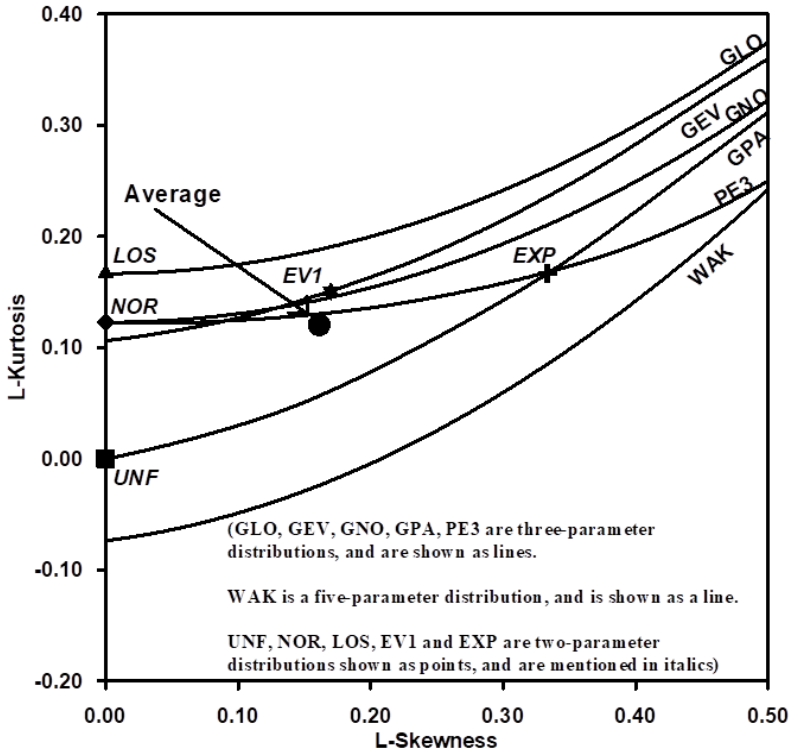

Figure 5.12: L-moments diagram for annual maximum discharge data for Dumarighat GD site.

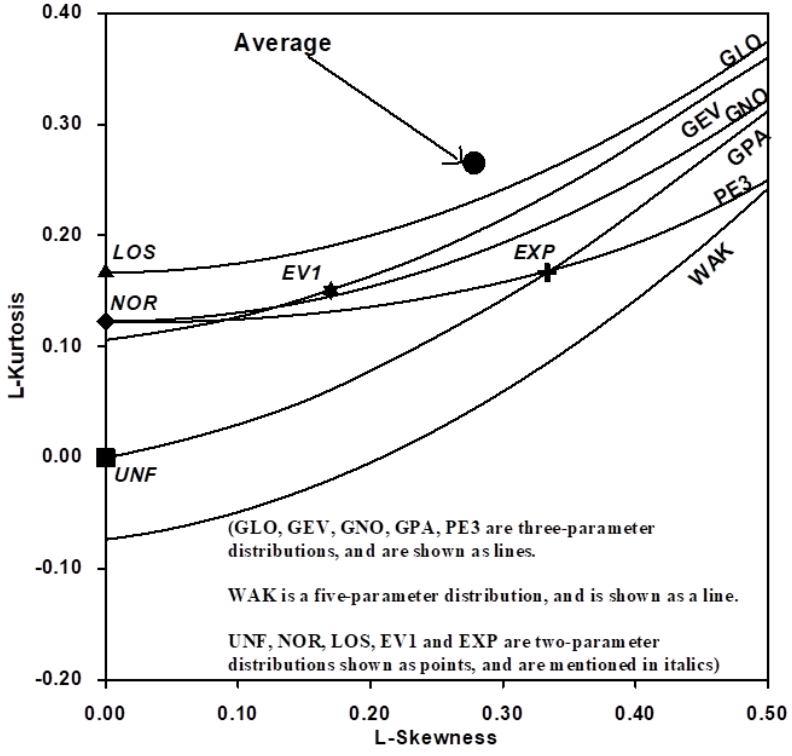

Figure 5.13: L-moments diagram for annual maximum discharge data for Lalganj GD site.

Table 5.4: Values of growth factors ($Q_T/\overline{Q}$) and flood estimates for various return periods at Dumariaghat site.

S. No.	Return period (Years)	Growth factors (GF)	Flood GF*(Mean=9227) (m^3/s)
		PE3	PE3
1	2	0.925	8535
2	10	1.622	14966
3	20	1.869	17245
4	25	1.946	17956
5	50	2.176	20078
6	100	2.397	22117

Table 5.5: Values of growth factors ($Q_T/\overline{Q}$) and flood estimates for various return periods at Lalganj site.

S. No.	Return period (Years)	Growth factors (GF)	Flood GF*(Mean=9819) (m^3/s)
		GLO	GLO
1	2	0.923	9063
2	10	1.389	13639
3	20	1.625	15956
4	25	1.709	16781
5	50	2.003	19667
6	100	2.357	23143

5.2.2 Estimation of flood hydrographs for Dumarighat site

Later in the study, the flow model simulations have been carried out for estimation of design parameters corresponding to 25-, and 100- year return period flood. The observed peak flood at Lalganj site during 2019 is 9140 m^3/s, which is near to the 2 year return period flood as estimated in Table 5.5. This time series of Lalganj for the year 2019 is used as the base line to compute the flood series for entire monsoon corresponding to 25- and 100- year return period. The estimated 25- and 100- year return period time series is shown in Figure 5.14.

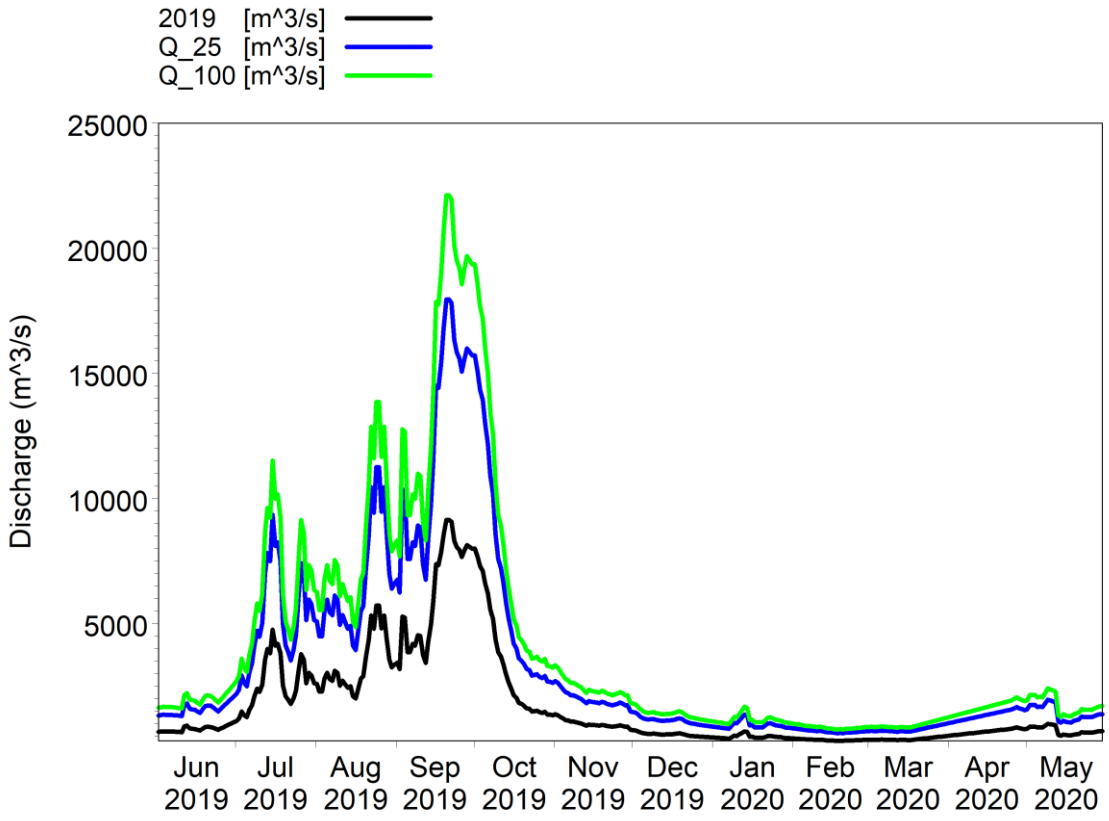

Figure 5.14: Observed flood hydrograph for 2019-2020 and the scaled hydrograph for 25- and 100- year return period at Dumariaghat GD site.

5.3 Development of 1D flow model

As stated above, for Gandak river from Dumariaghat GD site to Hajipur GD site, one dimensional (1D) flow model has been developed The details of flow model and their performance are discussed in the flowing sections:

5.3.1 Flow model for Gandak river between Dumariaghat to Hajipur

The Gandak river stretch from Dumariaghat to Hajipur is shown in Figure 5.15. The length of the Gandak river is about 98 km, the chainage of Dumariaghat is 0.000 km while that of Hajipur is 98.112 km. Rewaghat gauging site is located at Chainage 60.056 km while Lalganj GD site is located at Chainage 81.223 km. Altogether 77 rive cross-sections are available in this reach, at the interval of 2 km. However, between Kunwari village to Baligaon, river cross sections at every 0.5 km is available. MIKE 11 model is used to develop the one dimensional river flow model.

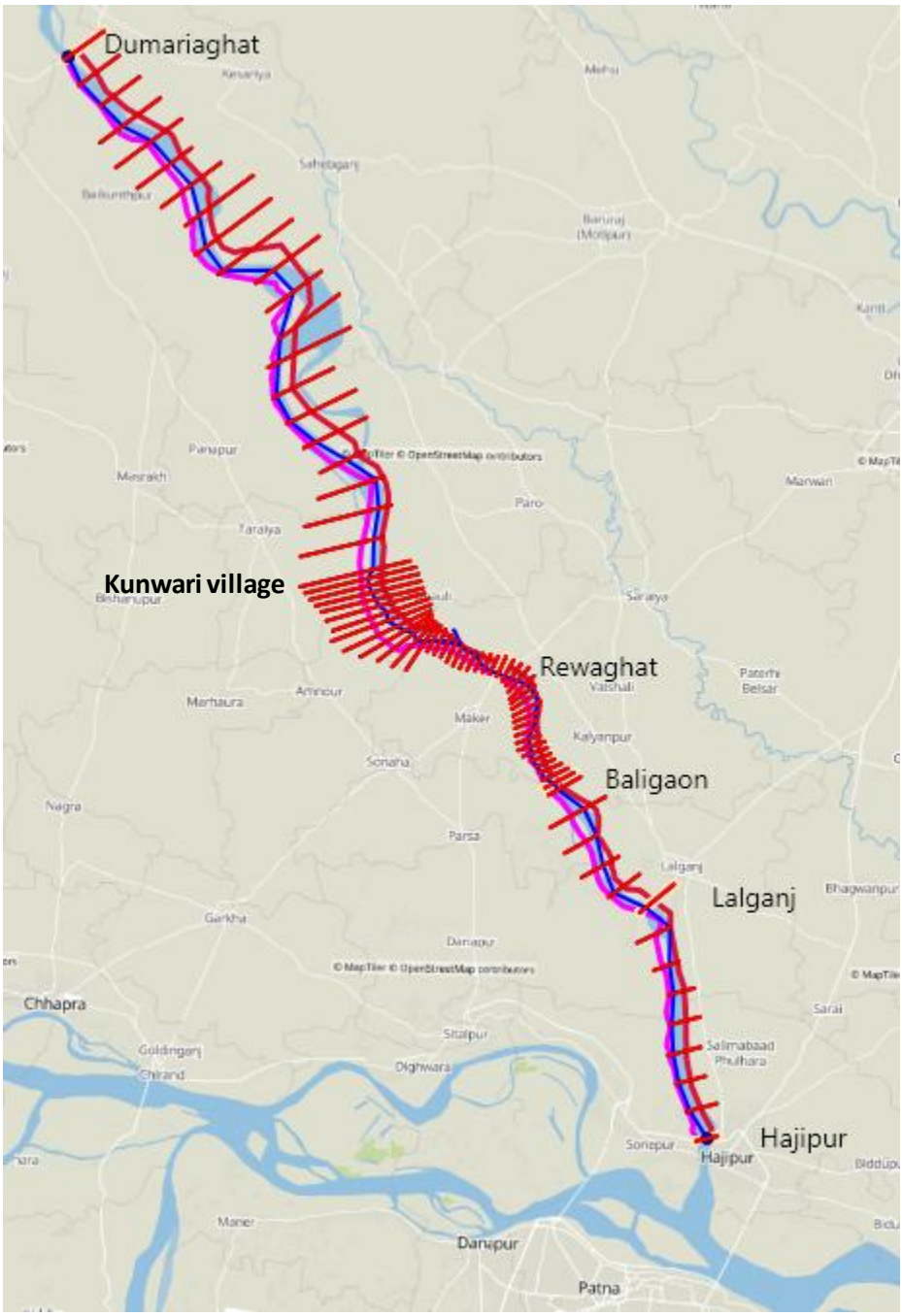

Figure 5.15: Extent of 1D flow model.

The observed discharge at Dumariaghat is used as the upstream inflow boundary condition while the observed water level at Hajipur is used as the downstream boundary condition. The computed and simulated water levels at Rewaghat gauging site is used for calibration and validation of flow model. The hydrological data for 2015 and 2016 are used to calibrate the model. The simulated and observed water levels for the calibration period are shown in

Figure 5.16 and Figure 5.17. The Manning's roughness (n) estimated through model calibration is 0.023 ($s/m^{1/3}$).

It is to mention that the flow model is developed for the inflow at Dumarighat. However a significant intermediate catchment (from Dumarighat to Hajipur) also contributes the flow in the river that has not been considered. Gandak river in the study reach is embanked and the flood contribution of the intermediate catchment is regulated through several sluice gates in the reach on both the banks. As the data for these sluice gates operations are not available, the corresponding flood contribution could not be considered in the model. Further, there is no information available regarding the embankment breach or faulty operation of sluice gates if any, that might lead to spill of river flood to the country side.

The model is further validated with hydrological data for the year 2017, 2018, 2019 and 2020. The simulated and observed water levels for the validation period are shown in Figure 5.18, Figure 5.19, Figure 5.20 and Figure 5.21. The performance of the developed flow model is shown in Table 5.6.

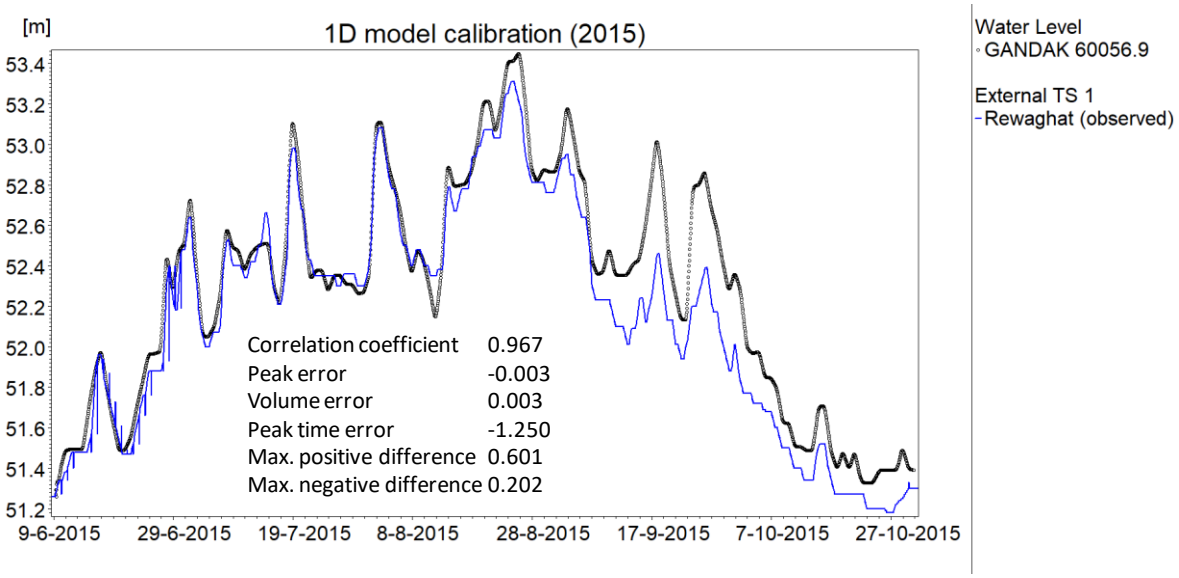

Figure 5.16: Calibration of 1D flow model for 2015 flow data.

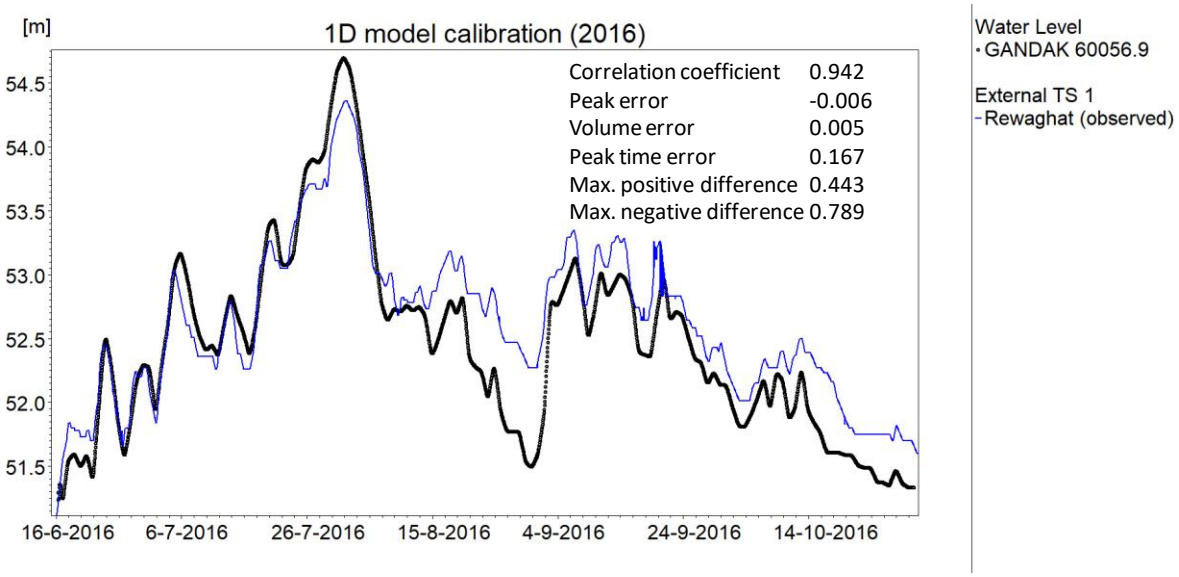

Figure 5.17: Calibration of 1D flow model for 2016 flow data.

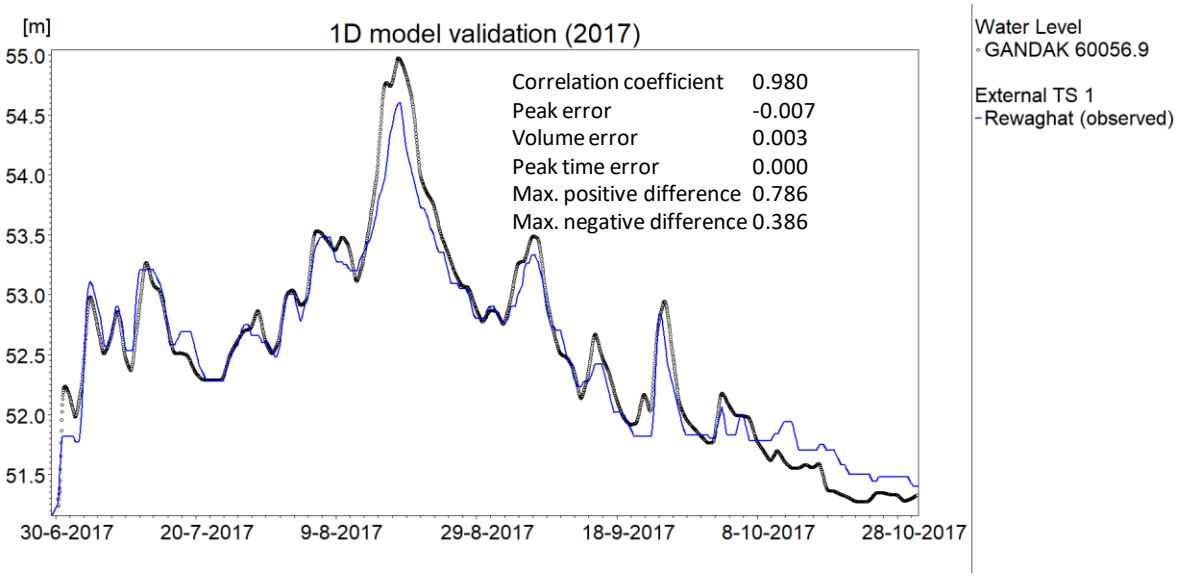

Figure 5.18: Validation of 1D flow model for 2017 flow data.

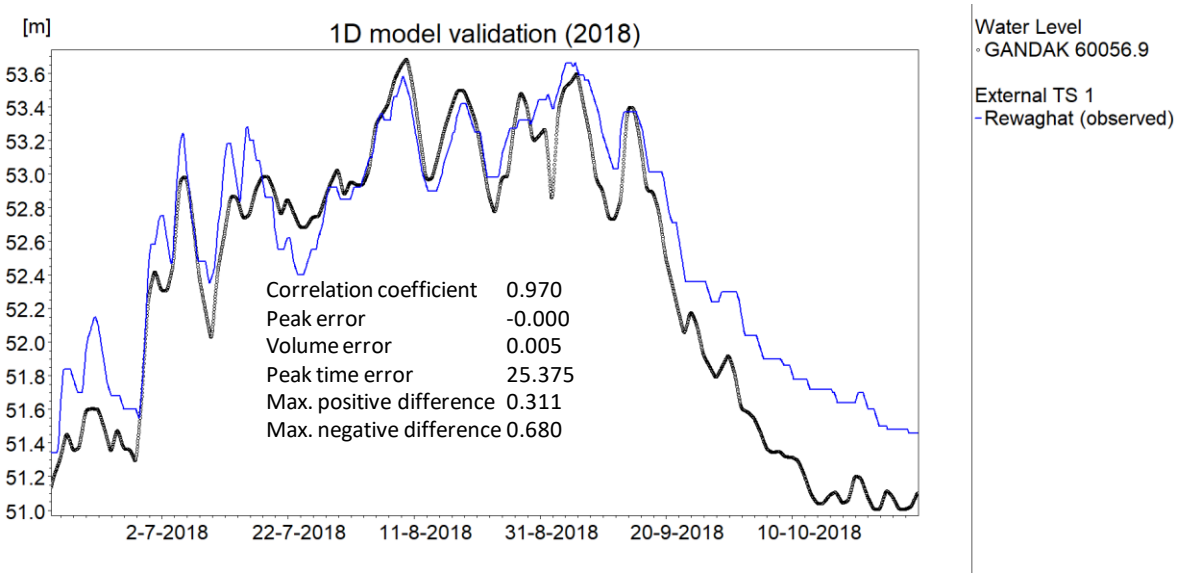

Figure 5.19: Validation of 1D flow model for 2018 flow data.

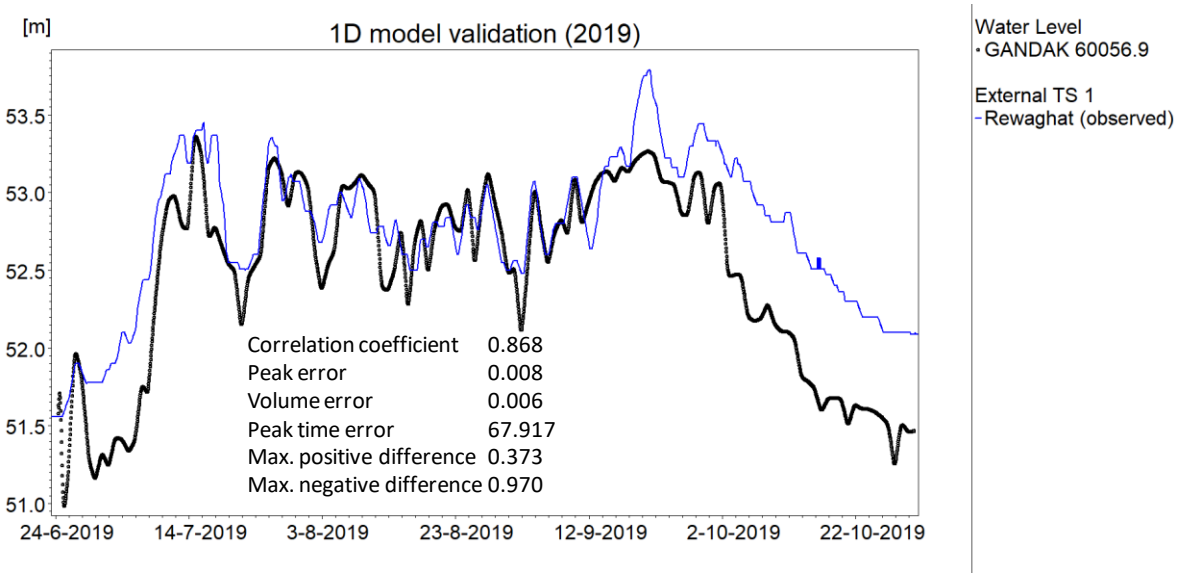

Figure 5.20: Validation of 1D flow model for 2019 flow data.

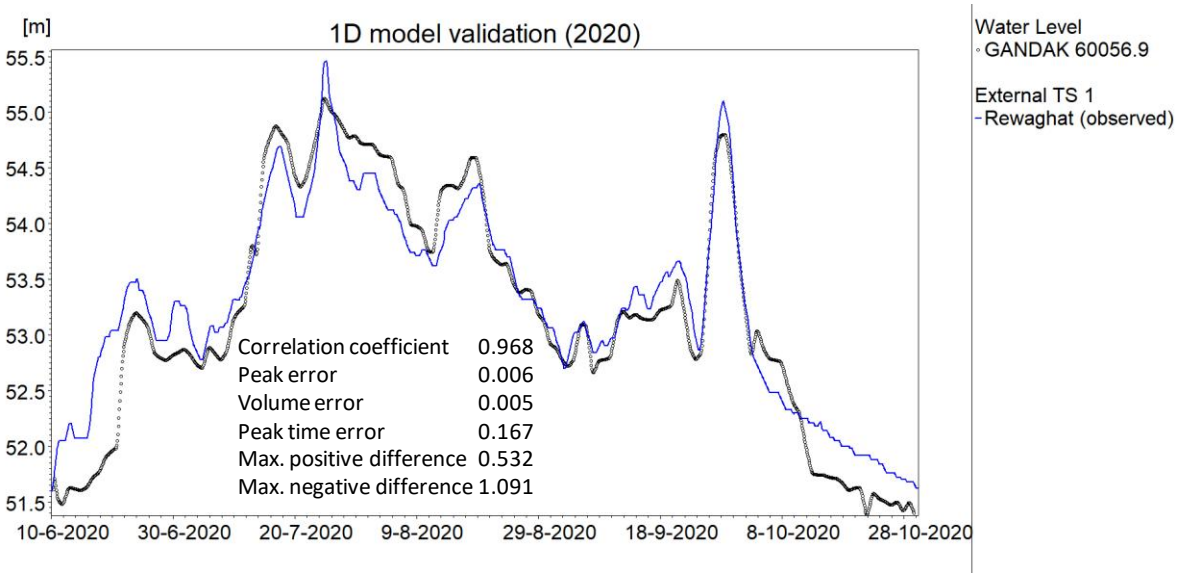

Figure 5.21: Validation of 1D flow model for 2020 flow data.

Table 5.6: Performance of 1D flow model

	Calibration		Validation			
Model Performance	**2015**	**2016**	**2017**	**2018**	**2019**	**2020**
Correlation coefficient	0.967	0.942	0.980	0.970	0.868	0.968

5.3.2 Simulation of 1D flow model for design flood.

The flow model is simulated for 25-year and 100 year flood and the flood attributes are estimated at the pre defined locations. Two locations namely Kunwari and Baligaon village are identified where the flood attributes are computed for various design flood estimates. The maximum flood levels at Kunwari village and Baligaon village are shown in Figure 5.22 and Figure 5.23, respectively. The figure shows that the maximum flood levels estimated at Kunwari village for 25- Yr and 100- Yr flood are 56.58 and 57.07 m, respectively. Similarly, the maximum flood levels estimated at Baligaon village for 25- Yr and 100- Yr flood are 54.01 and 54.58 m, respectively.

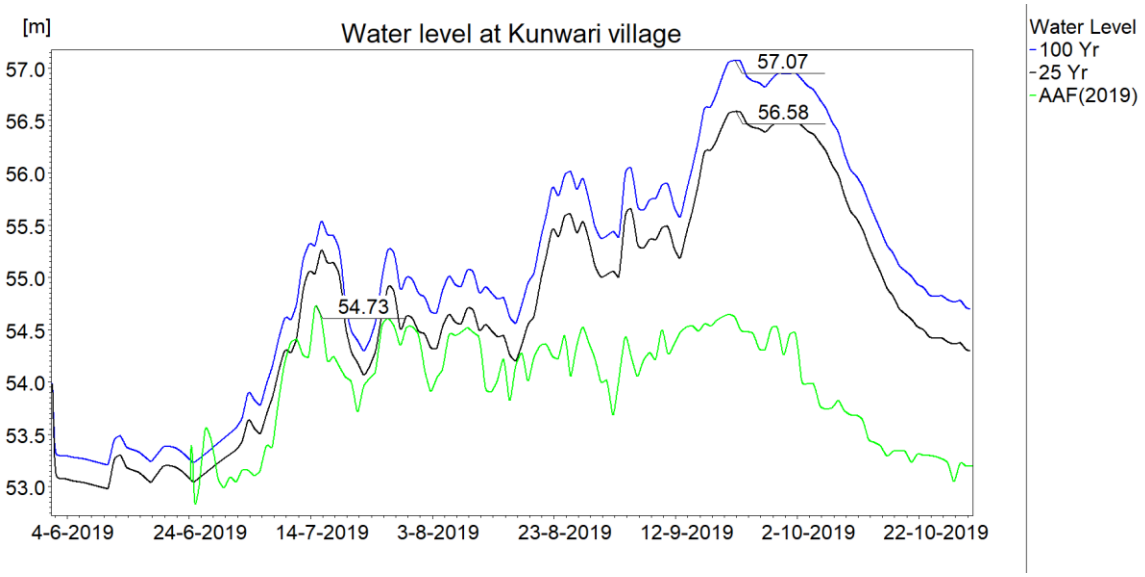

Figure 5.22: Maximum flood levels computed at Kunwari village for various flood estimates.

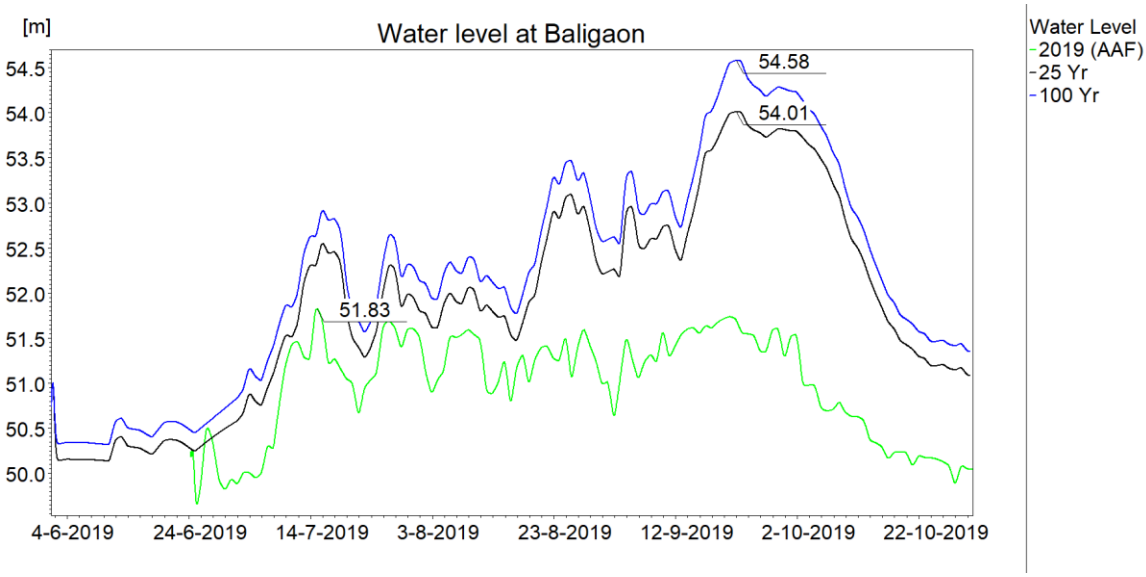

Figure 5.23: Maximum flood levels computed at Baligaon village for various flood estimates.

Further, the maximum flow velocities at Kunwari village and Baligaon village are shown in Figure 5.24 and Figure 5.25, respectively. The figure shows that the maximum flow velocities estimated at Kunwari village for 25- Yr and 100- Yr flood are 1.33 and 1.31 m/s, respectively. Lokewise, the maximum flow velocities estimated at Baligaon village for 25- Yr and 100- Yr flood are 1.43 and 1.49 m/s, respectively.

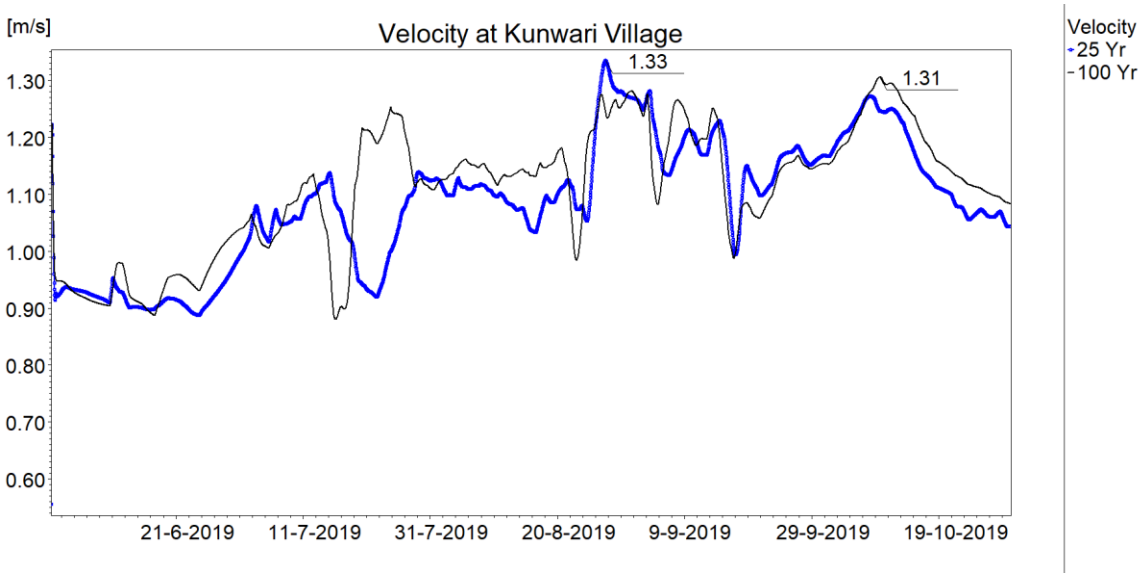

Figure 5.24: Maximum flow velocities computed at Kunwari village for various flood estimates.

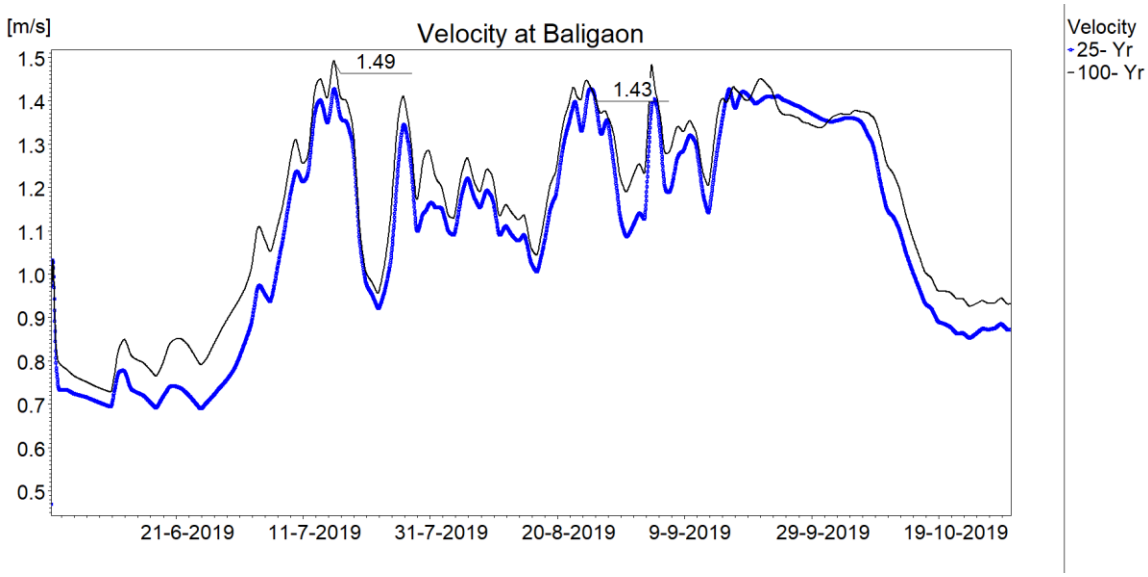

Figure 5.25: Maximum flow velocities computed at Baligaon village for various flood estimates.

5.3.2.1 1D sediment transport modelling.

The sediment transport model of Gandak river from Dumariaghat to Hajipur GD site is developed in MIKE 11. The silt data for Dumarighat is available for 2020 while the same for Lalganj site is available for 2019 only. For Dumariaghat site, even for 2020, data for many dates are missing. Based on the observed suspended silt load and discharge data, Silt-Discharge relationships have been developed for Dumarighat and Lalganj site. A power

function is fitted between suspended silt and discharge. Figure 5.26 and Figure 5.27 shows the silt-discharge curve for the Dumarighat and Lalganj sites, respectively. The discharge at Dumarighat ranges from 350-7500 m^3/s while the suspended silt load ranges from 0.01 to 7.5 m^3/s. At Lalganj, (downstream site), the discharge ranges from 300-7600 m^3/s while the silt load ranges from 0.01 to 1.8 m^3/s. Thus, the observed data shows that the silt load is reducing in the downstream reach. The R^2 values for this relations are computed as 0.8761 and 0.986 for Dumarighat and Lalganj sites, respectively.

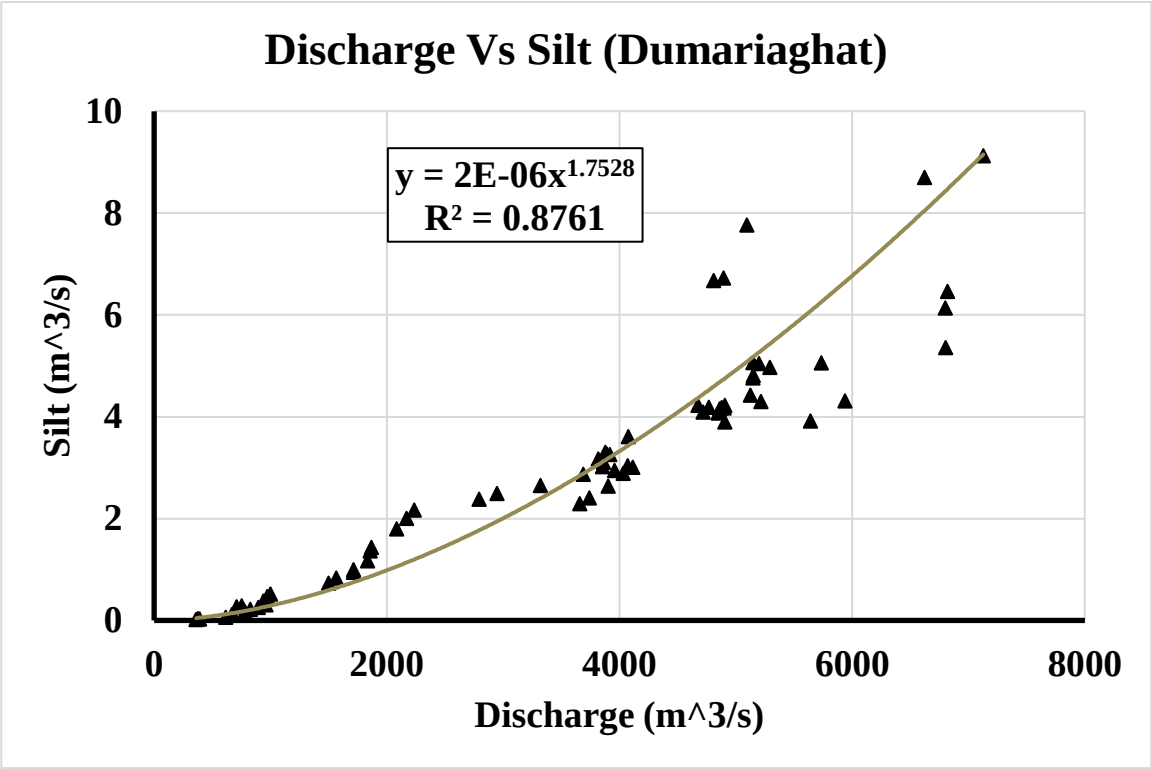

Figure 5.26: Silt discharge relationship for Dumarighat site based on 2020 observed data.

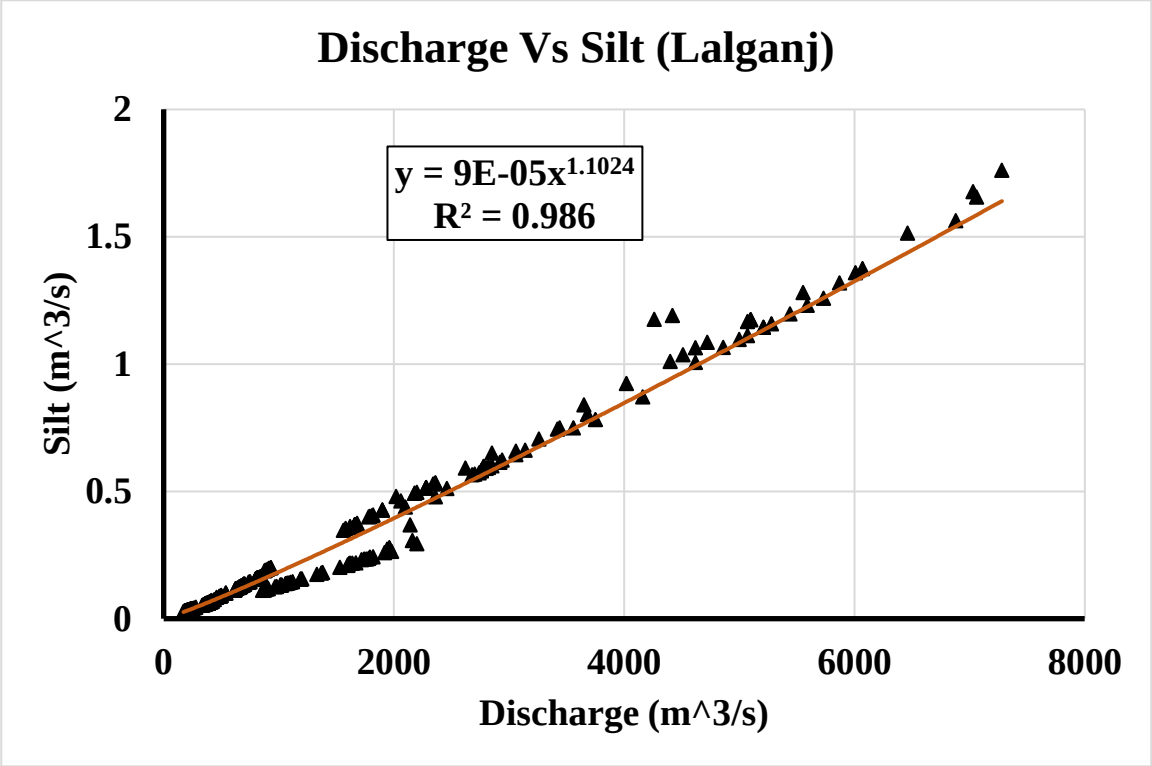

Figure 5.27: Silt discharge relationship for Lalganj site based on 2019 observed data.

The sediment transport formula proposed by Engelund and Fredsoe is used for suspended sediment and bed load. The grain size (d_{50}) of 0.000152 m has been used. The observed sediment data for Lalganj site is available for the monsoon of 2019 and the same has been used as the upstream sediment flux inflow. The downstream boundary condition for sediment transport model is assumed as no change in bed level at Hajipur site. Further, the sediment transport model is simulated for 25-Yr and 100-Yr flood in the Gandak river. The bed level change along the river for 25- and 100- Yr floods are shown in Figure 5.28 and Figure 5.29, respectively. The Figure shows the initial river bed by dark maroon colour line, the blue line shows the maximum river bed due to sedimentation while the dashed line shows the minimum river bed line during the simulation of design floods of 25- and 100- Yr. During the simulation, the river bed lines remains in between these two bounds. For 25-Yr flood, the average variations of bed level are 1.08 m, with maximum and minimum variation computed as 6.15 m and 0.35 m, respectively. Similarly, for 100- yr flood, the average variations of bed level are 1.14 m, with maximum and minimum variation computed as 5.52 m and 0.44 m, respectively.

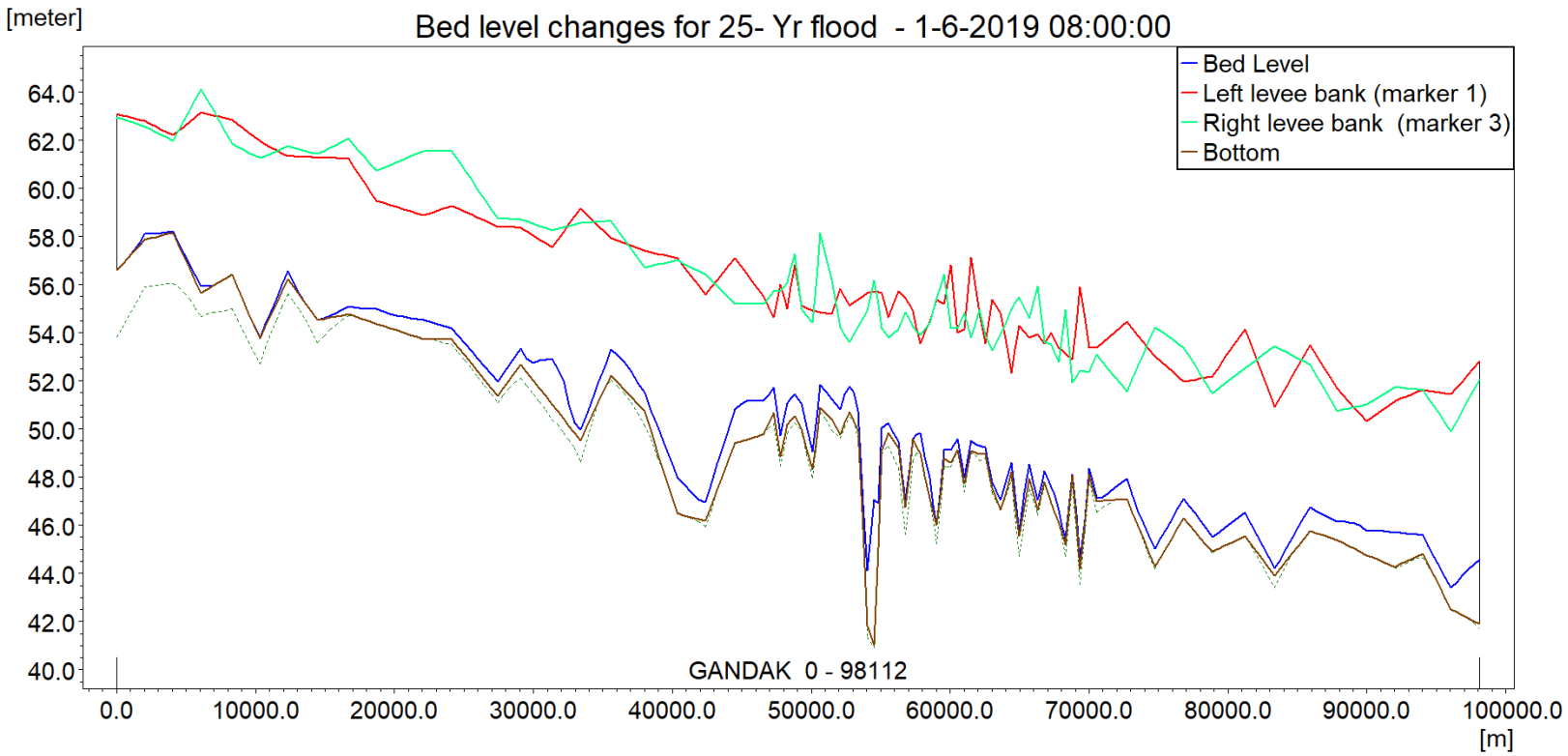

Figure 5.28: Bed level change along Gandak river for 25-year flood.

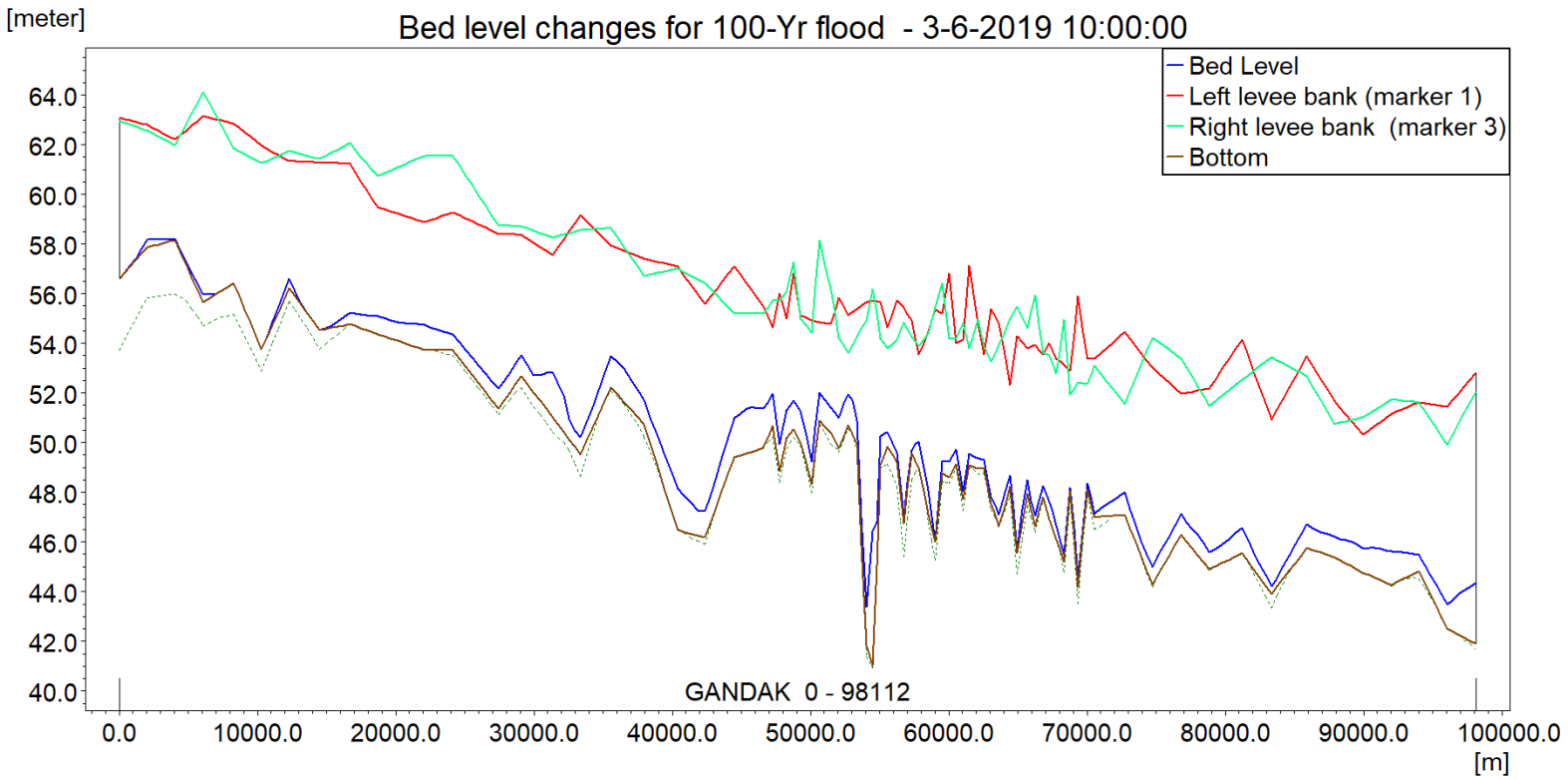

Figure 5.29: Bed level change along Gandak river for 25-year flood.

5.4 2D curvilinear grid flow model

5.4.1 Development of curvilinear grid

The 2D curvilinear grid model is generated in MIKE 21C Grid generator for the Gandak river stretch from Kumari village to Baligaon village. The river is about 20 km long while the river width varies from 1.5 km to 7 km. In this study, the bank line of Gandak river in the study stretch is extracted from the satellite image of 2020 in ArcGIS. UTM 45N projected coordinate systems have been used for bank line extraction and further processing in MIKE 21C. The plyline shape file of the bank line are further converted to .xyz format which is the required input of MIKE 21 C Grid generator. The curvilinear grid follows the curvilinear coordinate system, as shown in the Figure 5.30. In the curvilinear grid co-ordinate system ‘s’ represents direction along the river flow and ‘n’ direction represents the direction transverse to flow. The generation of orthogonal curvilinear grid is an iterative process which consists of solving a set of elliptical partial differential equation by using an implicit finite difference approximation.

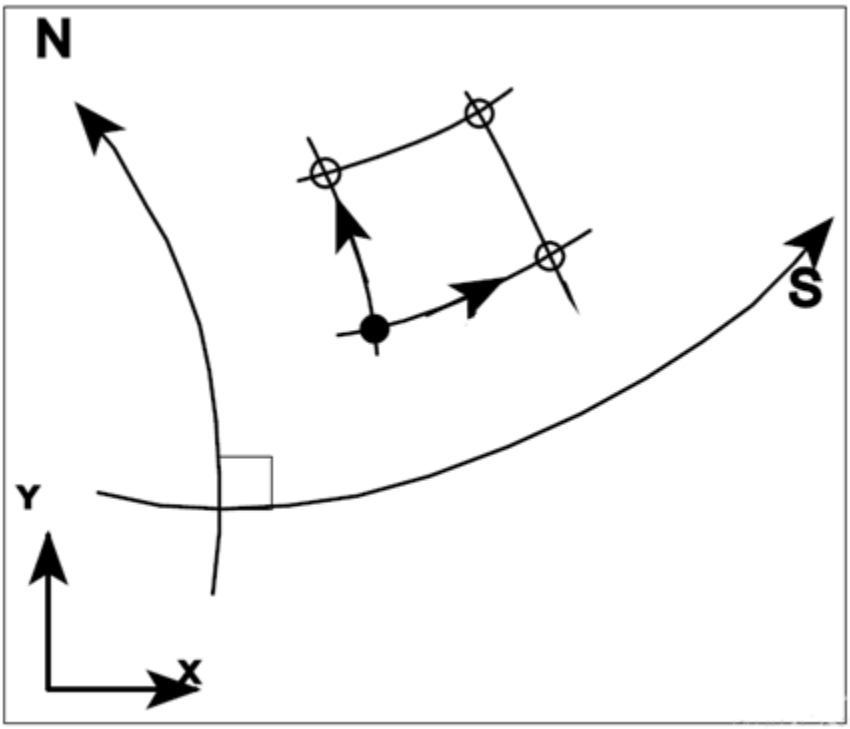

Figure 5.30: Curvilinear Grid Co-ordinate System

The study stretch is covered with the orthogonal curvilinear gird of 481x133 cells. The grid map is shown in Figure 5.31. The grid covers the larger area and therefore appears too small

to visualize. Therefore part of the study area is zoomed over and shown in this figure. The grid size along the flow varies from 20 to 100 m while the grid size along the cross section varies in the range of 15-80 m.

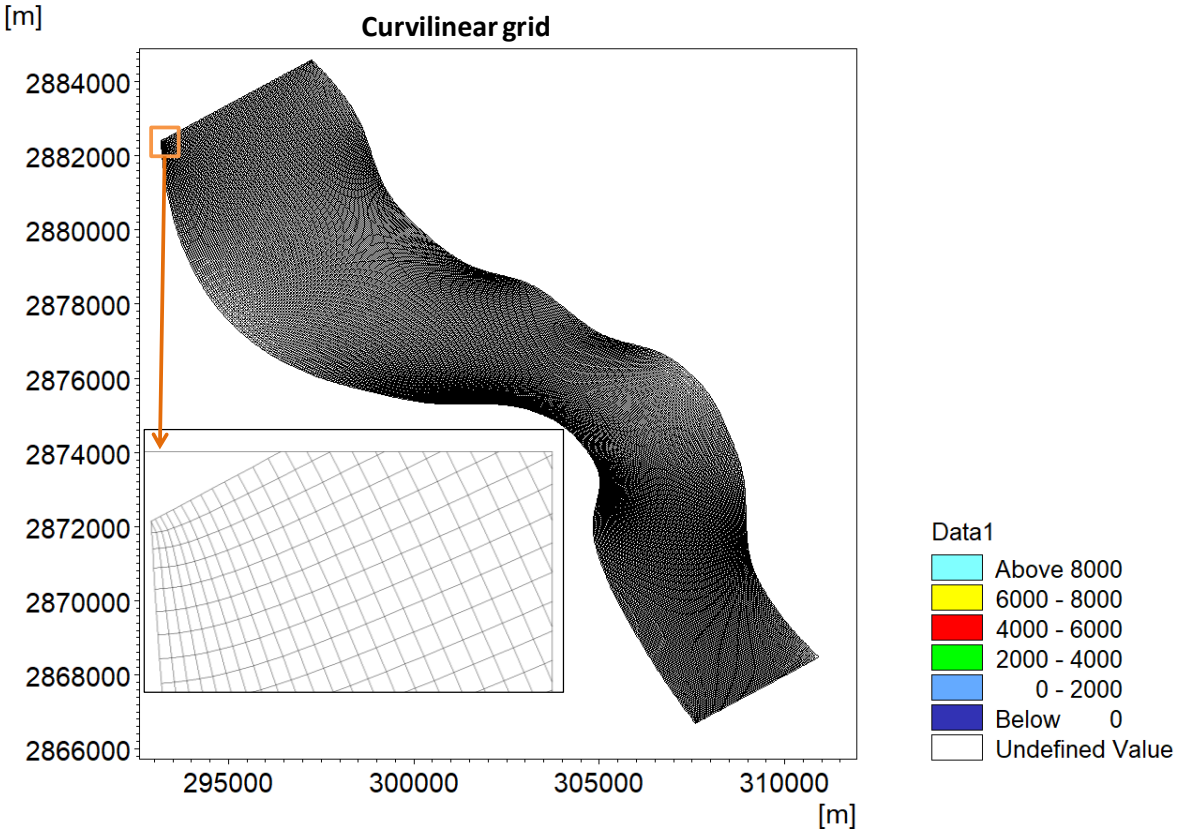

Figure 5.31: Curvilinear grid generated for the study reach.

The number of grids in 'n' and 's' directions are adjusted to fulfil the requirement of grid orthogonality and aspect ratio. For optimal curvilinear grid, the aspect ratio in the range of 2-8 is recommended while the orthogonality should ideally be 0 or in the range of -0.05 to 0.05 for all practical applications. The aspect ratio for the developed grid is shown in Figure 5.32 which shows that the aspects of grids are in the specified range (range 2-17.65, mean 2.1).

The orthogonality check for the developed curvilinear grids are also carried out and the orthogonality map is shown in Figure 5.33. The orthogonality of the developed grid is within the specified range (range -0.04-0.04 and mean 0.016).

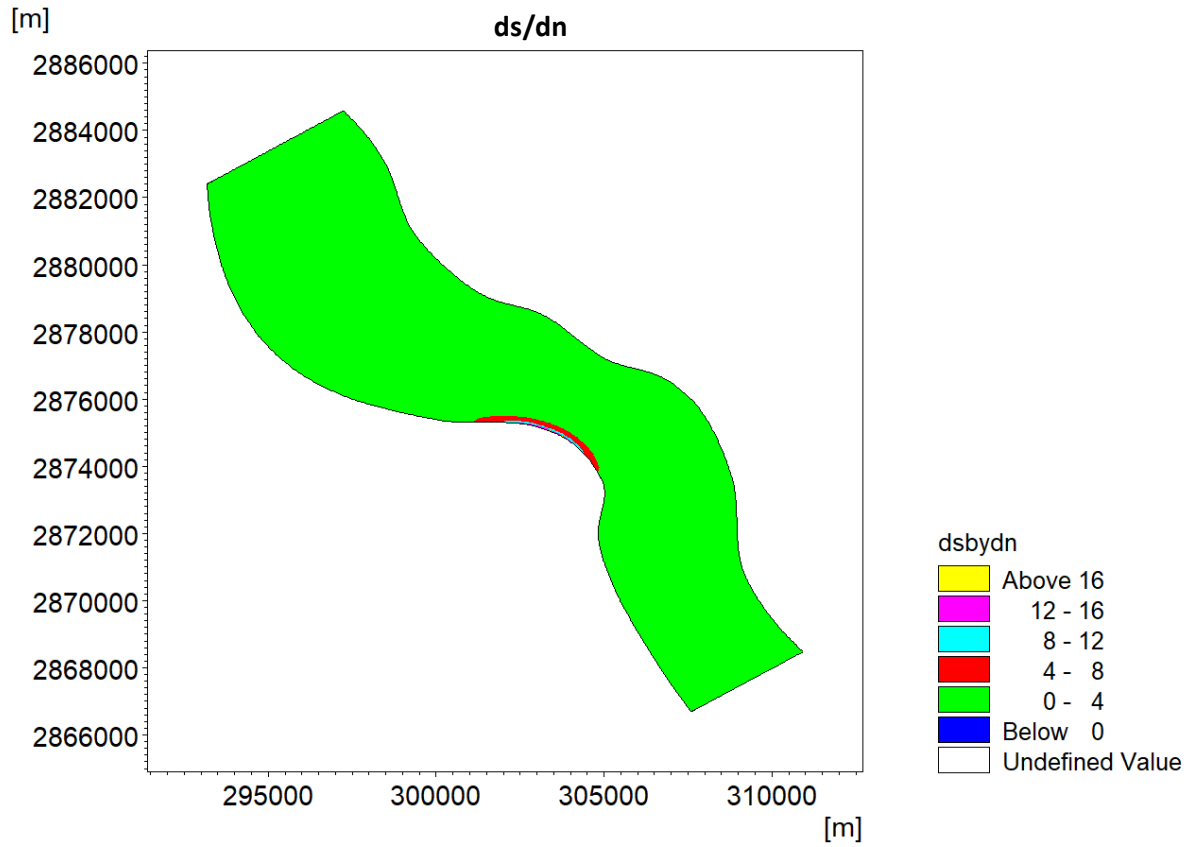

Figure 5.32: Aspect ratio of curvilinear grid.

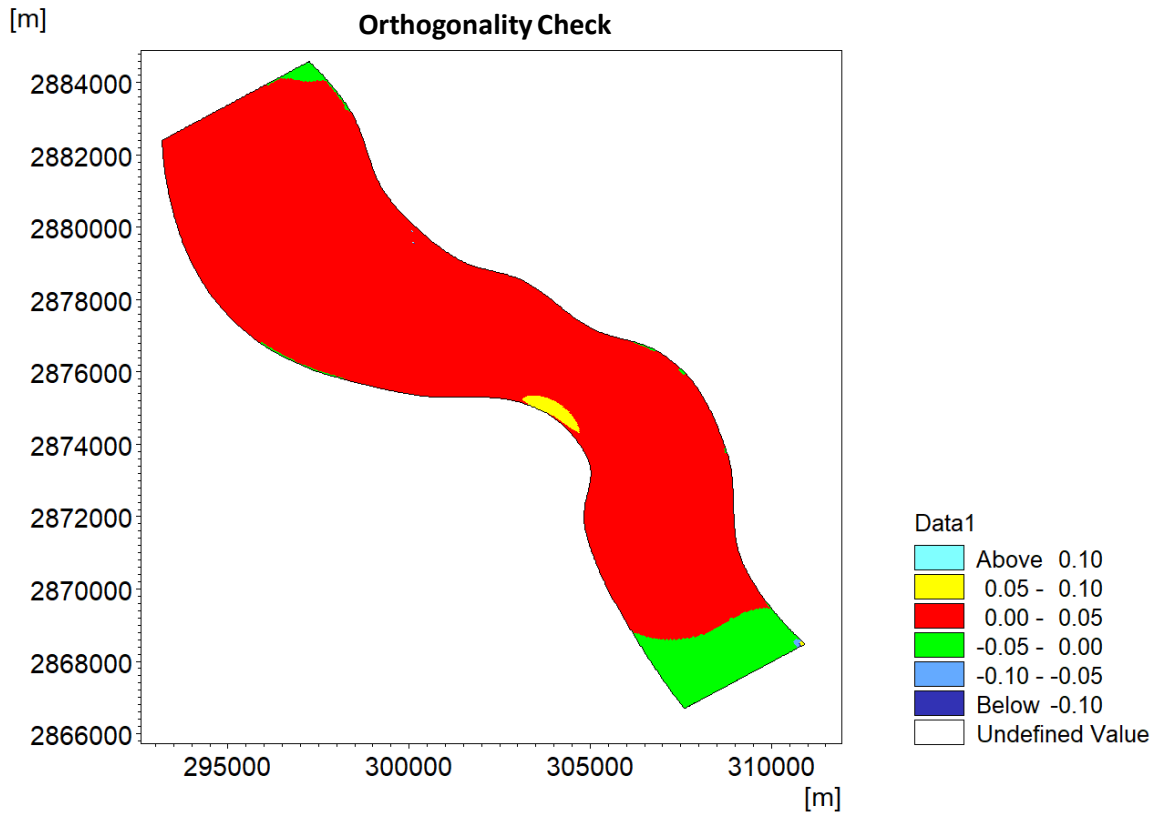

Figure 5.33: Orthogonality for the curvilinear grid.

The centres of the each grid are extracted and the bathymetry is assigned. The bathymetry is computed from the surveyed river cross sections and ALOS PALSAR data as discussed in section 3.3 and shown in Figure 3.15. The elevation corresponding to the centre f each grid is extracted through GIS utility and bathymetry for curvilinear grid is developed. The bathymetry is shown in Figure 5.34.

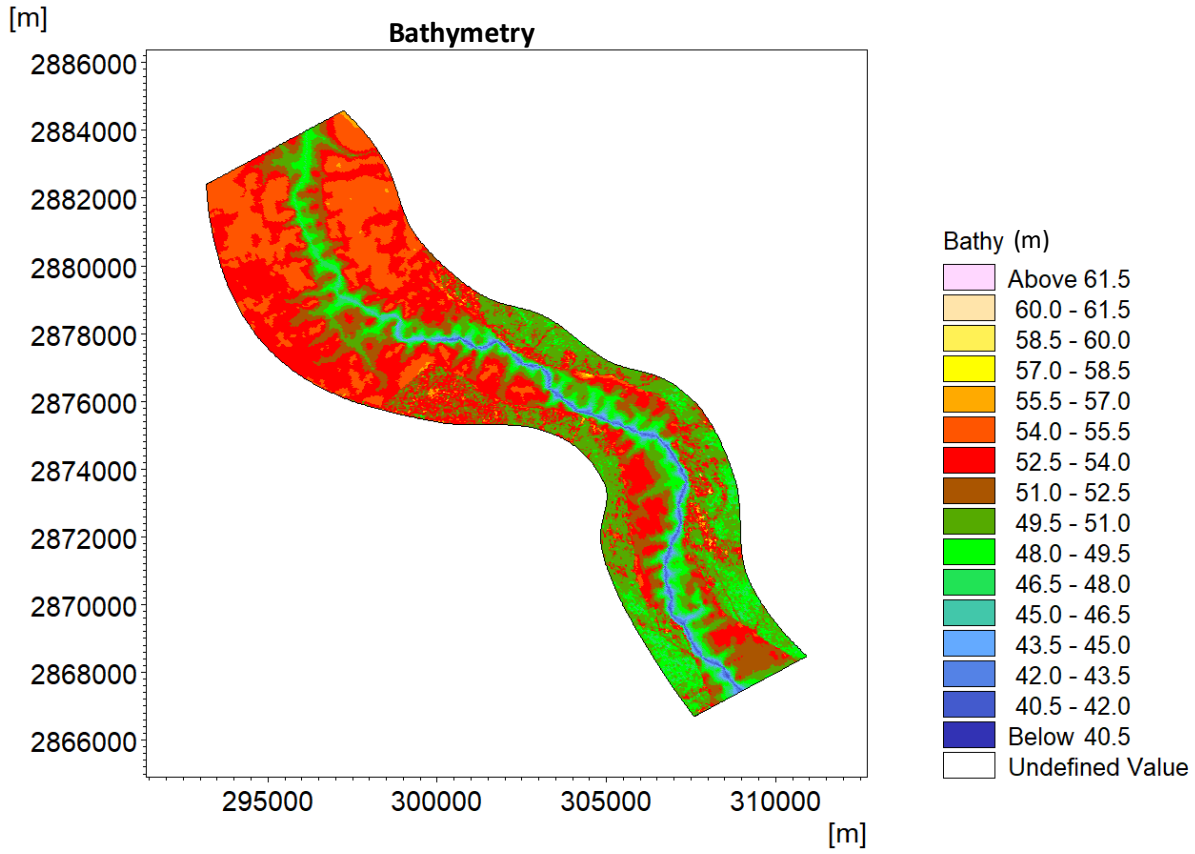

Figure 5.34: The bathymetry of the Gandak river for curvilinear grid.

5.4.2 Flow data for 2D model

The extent of 2D curvilinear flow model is from Kunwari village to Baligaon village. The computed suspended load and discharge at Kunwari village from 1D flow model is initially proposed to use as the upstream boundary condition in the curvilinear grid model. The computed discharge and silt load using MIKE 11 flow simulation for the various flood estimates at Kunwari village is shown in Figure 5.35 and Figure 5.36, respectively. The figures shows that 25- year and 100 Yr flood computed at Kunwari village are about 6000 and 7800 m^3/s, respectively. However, the 25- Yr and 100- Yr flood estimated at Lalganj site is 16779 and 23141 m^3/s, respectively (section 5.2.1 and Table 5.5). The reason for the lower estimates of design flood at Kunwari village may be attributed to the overbank spilling of the flood corresponding to 25- and 100- Yr flood. . The water surface profiles for 25- and 100- Yr flood are plotted as shown in Figure 5.37 and Figure 5.38, respectively. The top of left and right embankment are also shown in these figures and the maximum water level is shown by blue line. These figures show that the flood overtops both the bank at most of the cross sections for 25- and 100 Yr flood, particularly upstream of Kunwari village. Thus the design

flood estimates at Lalganj site have been used in the 2D curvilinear model for further analysis. The design flood estimates used at Kunwari village in 2D curvilinear model is shown in Figure 5.39. However for smaller floods (observed flow during, 2015-2019, the water level at each cross sections remains within the embankment and have been used for estimation of flow at the boundaries of 2D flow domain as proposed.

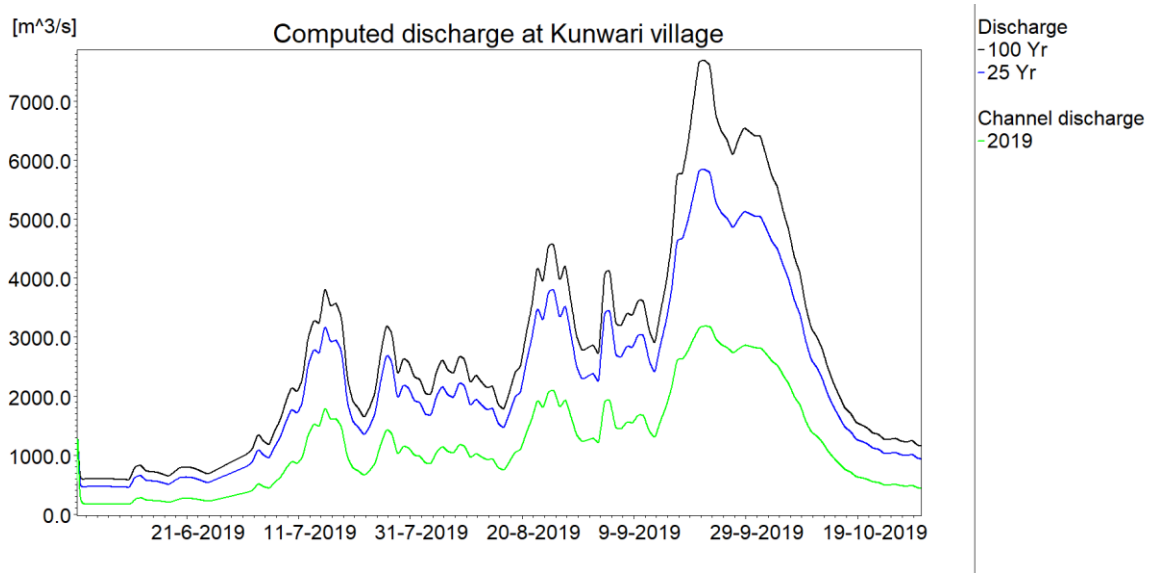

Figure 5.35: Flood estimates at Kunwari village for various return period computed from MIKE 11 simulation.

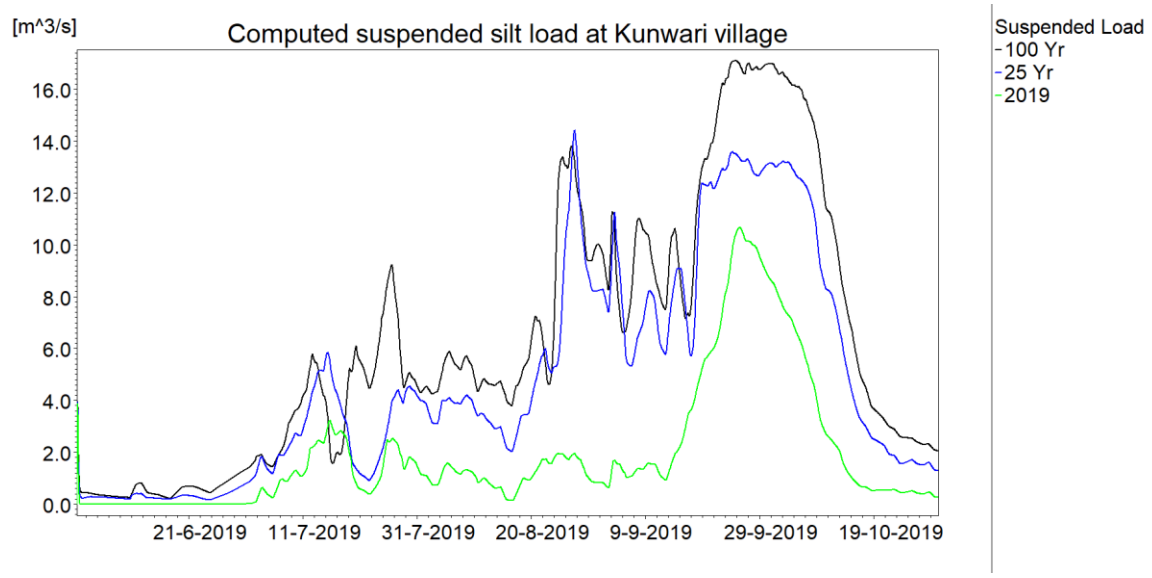

Figure 5.36: Suspended silt estimates at Kunwari village for various return period computed from MIKE 11 simulation.

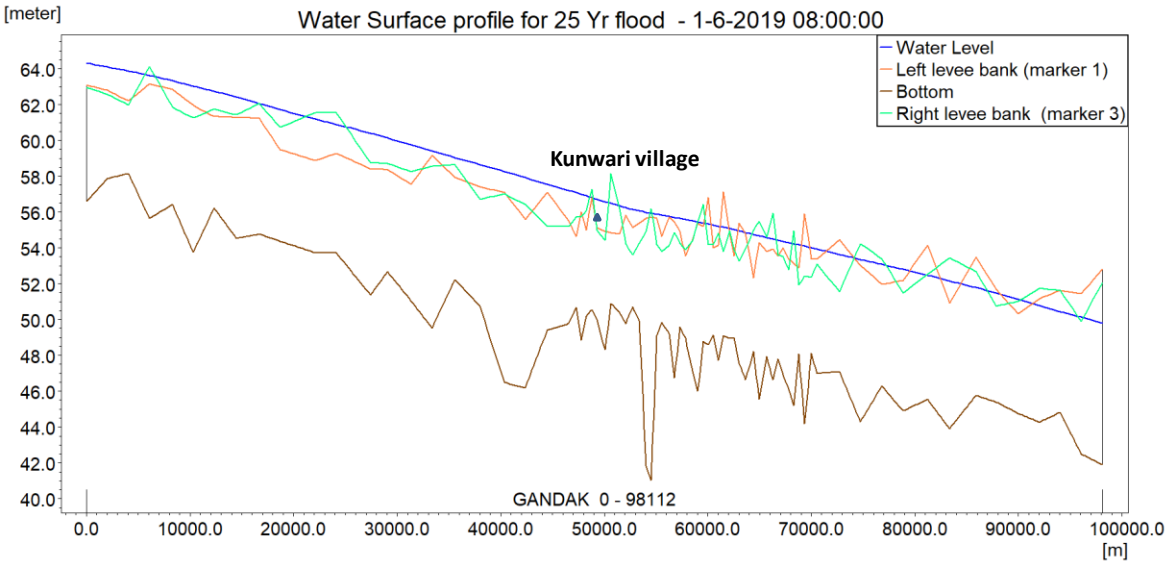

Figure 5.37: Water Surface profile in Gandak river for 25- Yr flood.

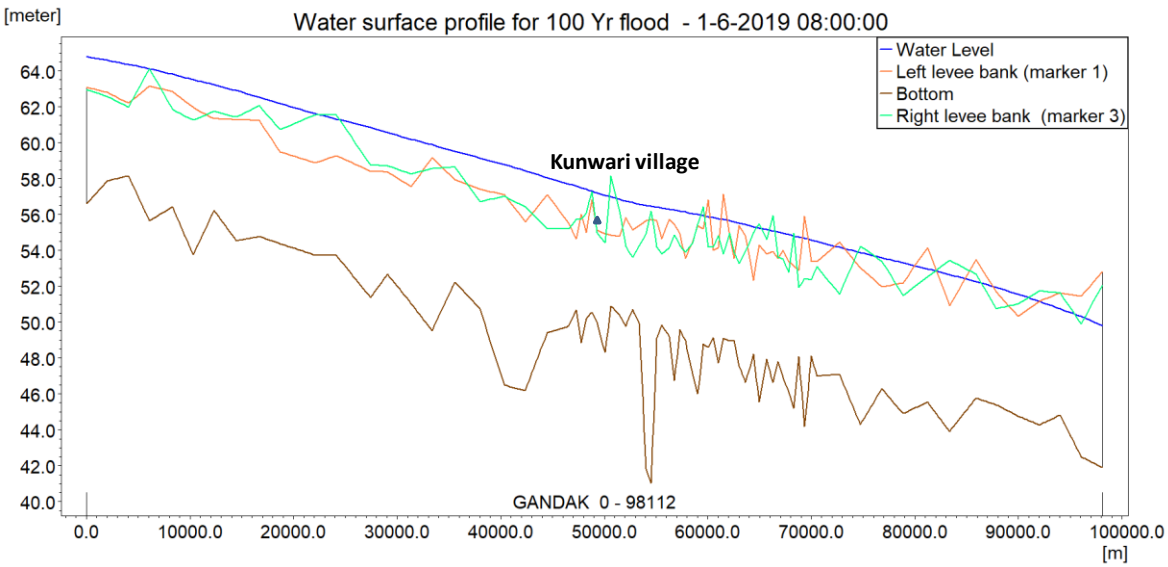

Figure 5.38: Water Surface profile in Gandak river for 100- Yr flood.

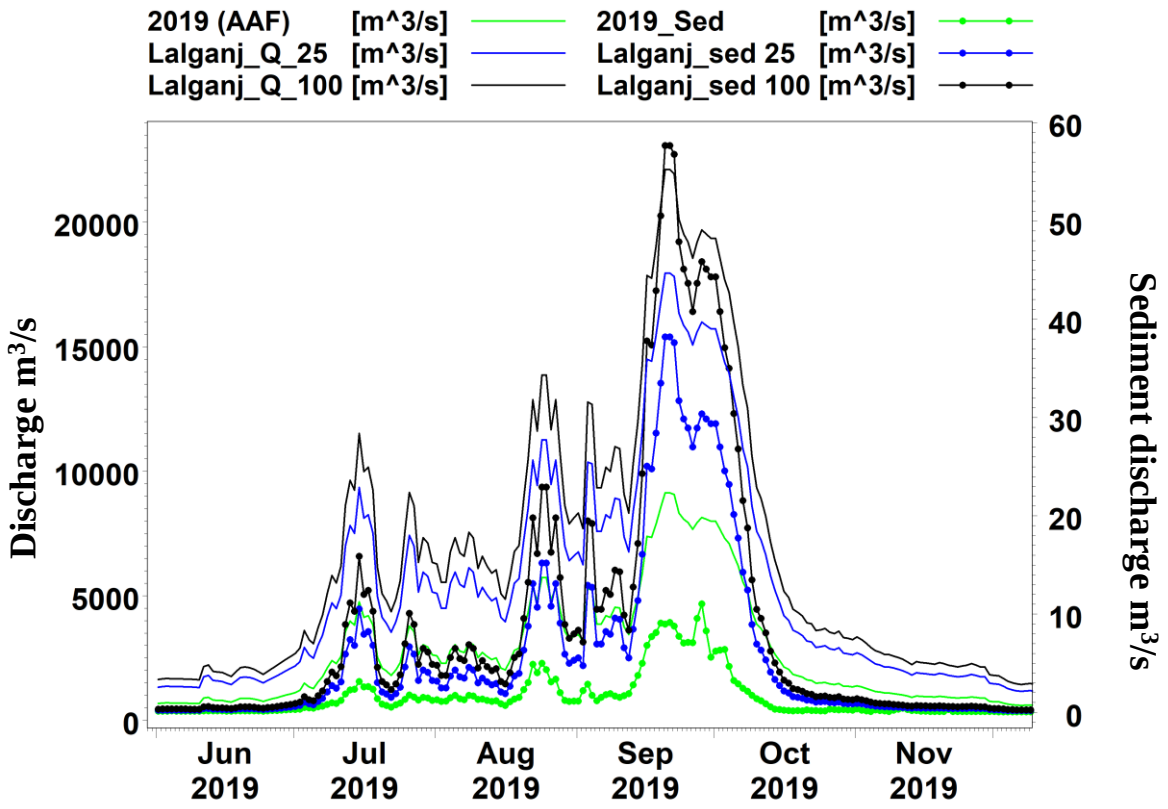

Figure 5.39: Design flood estimates at Kunwari village.

5.4.3 Development of 2D model

2D curvilinear flow model is developed in MIKE 21C. The morphodynamic model has two components, Hydrodynamic and Morphology. The bathymetric data and grid descriptions are defined as described and specified in section 5.4.1. The upstream boundary condition for hydrodynamic model is the discharge at the Kunwari village (upstream end of the 2D model) as described through Figure 5.35 for 2019 flood and Figure 5.39 for the design flood. The downstream flood is boundary condition is the water level near Baligaon (computed from 1D model). The floodplain resistance is defined through spatial grid data using M (invert of Manning's 'n'. The values are 43 (equivalent to 'n' = 0.023) for active river extent and 20 (equivalent to 'n' = 0.05) for floodplain. Model is run with 1 sec simulation time with scaled dynamic HD integration of 0.01 sec. The left and right embankment are defined through structure module using X,Y,Z (longitude, latitude and top elevation of embankments at surveyed cross section locations).

The morphological model is simulated for Helical flow, Sediment transport and morphological updates. The morphological time step frequency of 60 and morphological drying depth of 0.15 m have been used. Non cohesive sediment with porosity 0.35 and density 2650 kg/ m^3 has been adopted. The critical Shield parameter adopted in the model is 0.06. The Grain size of 0.102 mm is defined (Figure 3.12) and Engelund & Hansen transport theory has been adopted for calculation. The bed load fraction of 20% is considered in the model. Single layer of sediment bed has been considered. The upstream boundary condition for morphological model component is defined as the computed sediment discharge at Kunwari village from MIKE 11 sediment transport model (Figure 5.36). MIKE 21C model is calibrated for observed data of 2019 and and validated for 2022 observed data. The flood level at Rewaghat bridge is computed using MIKE 21C model setup and compared with observed water level at Rewaghat site to evaluate the model performance. The simulated water level at the grid located in the mid of the Gandak stream at Rewaghat site is extracted and compared with the observed water level at Rewaghat. The comparison of simulated and observed water level at Rewaghat is shown in Figure 5.40. The model performance is expressed by correlation coefficient of 0.623.

The hydrological data at Baligaon site is computed during the period of 15 June 2024 to 15 October 2022. The flow model is simulated with this observed data and the model results are compared. The comparison of simulated and observed water level at Baligaon site for 2022 is shown in Figure 5.41. The model is also evaluated using the simulated and observed flow velocity at the Baligaon site. Figure 5.42 shows the comparison of two data set. The observation for velocity was carried out at 0.6d (section 3.2.2) while the simulated velocity is the depth average velocity at the specified grid and may be the reason for deviation. Similarly, the comparison for silt load at Baligaon site is also carried to evaluate the MIKE 21C morphodynamic model and shown in Figure 5.43. The figure shows the good agreement between simulated and observed silt load at Baligaon site.

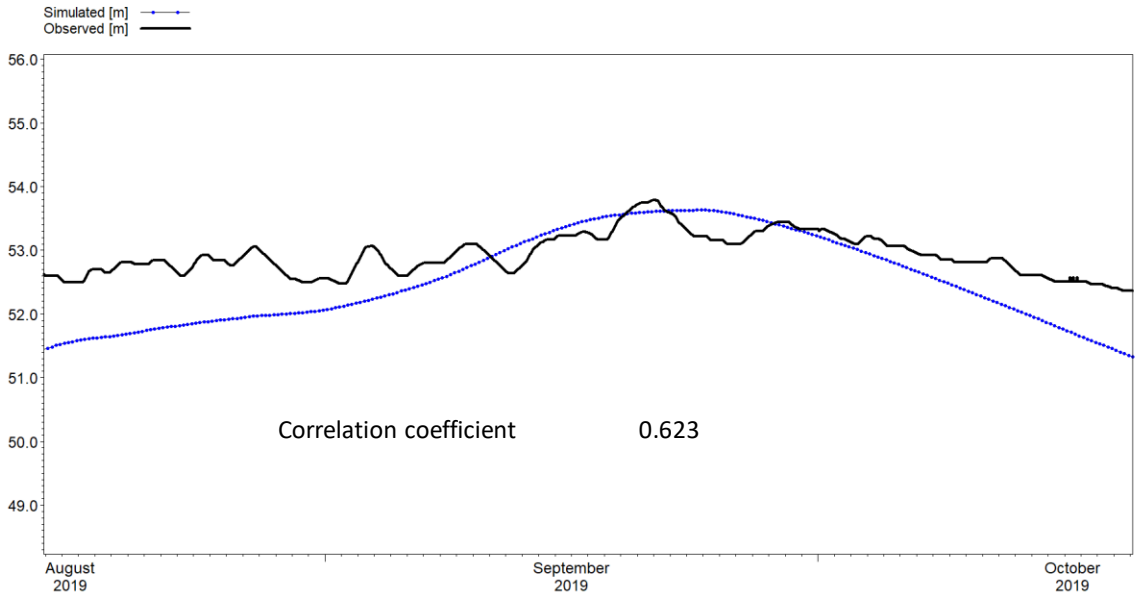

Figure 5.40: MIKE 21C model calibration with 2019 flow data.

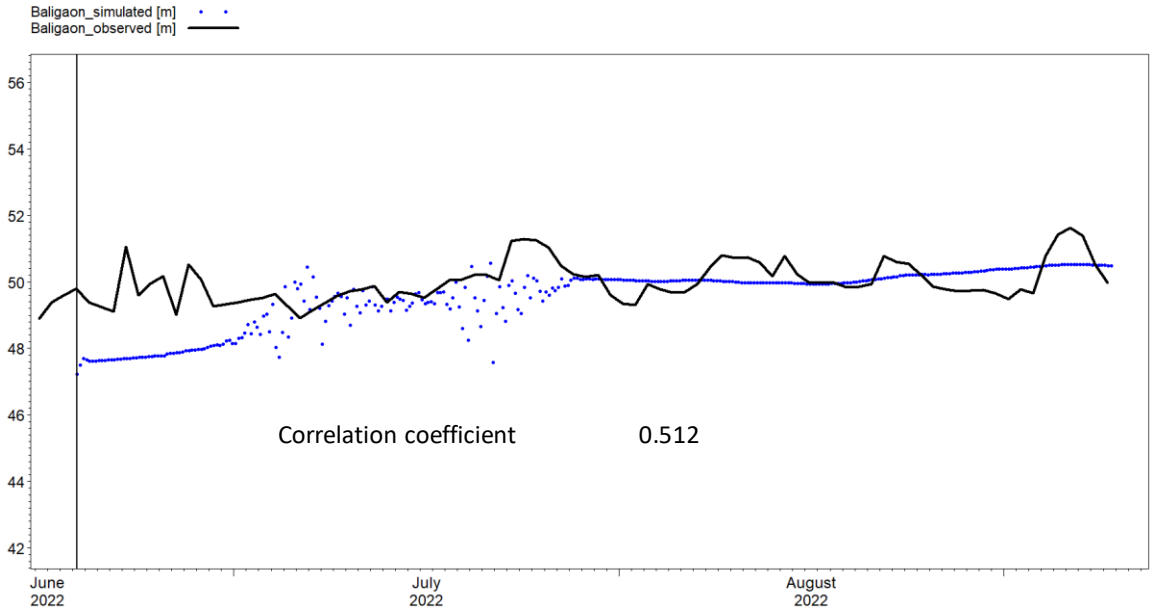

Figure 5.41: MIKE 21C model validation with 2022 flow data.

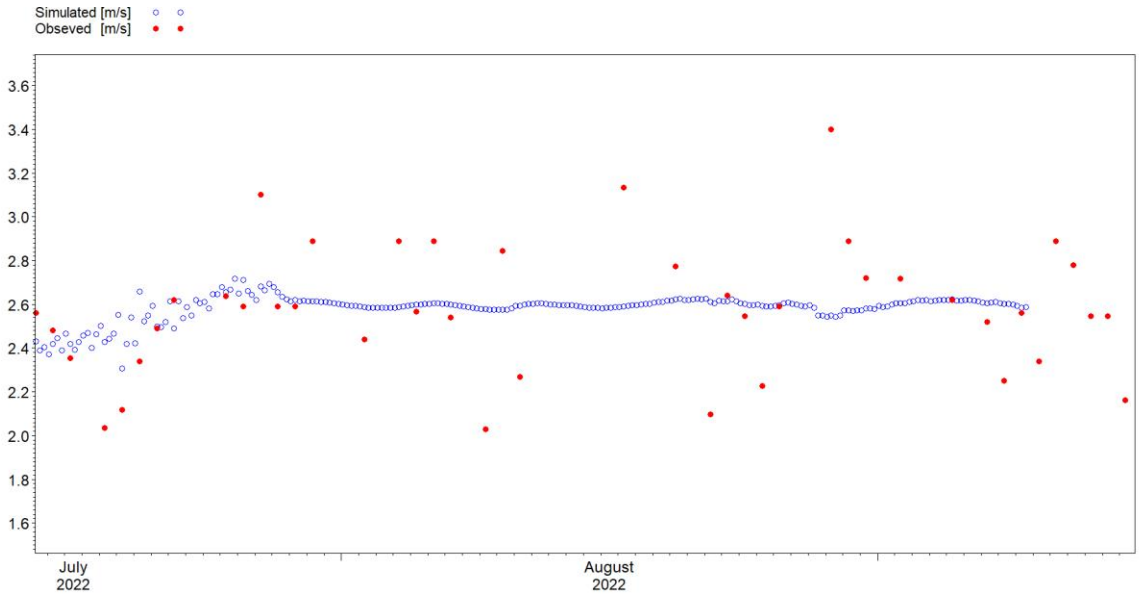

Figure 5.42: Comparison of simulated and observed velocity at Baligaon.

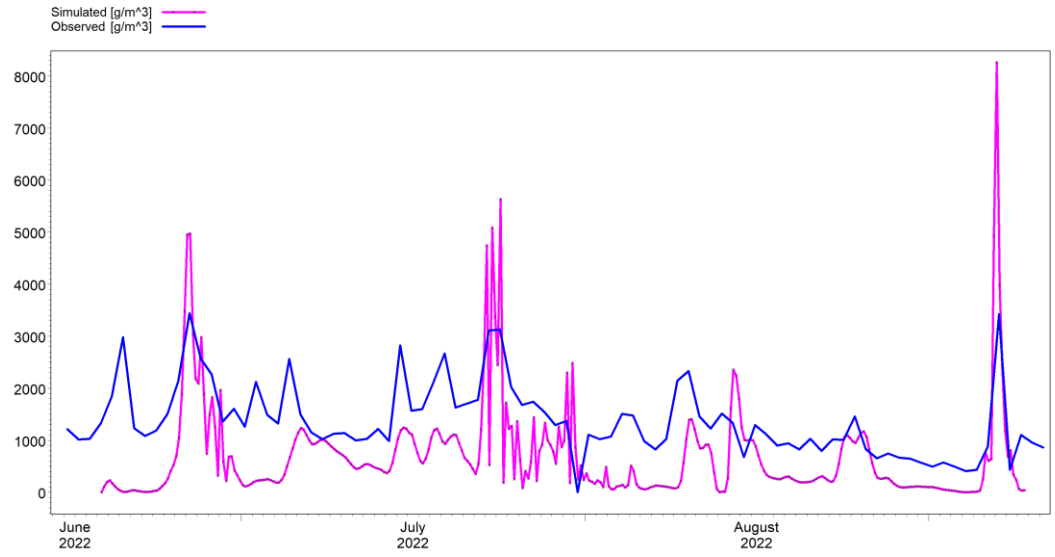

Figure 5.43: Comparison of simulated and silt load at Baligaon.

5.4.4 Velocity distribution along the cross section

For design of the inline structures, the flow velocity along the cross sections are also an essential input data requirement. 2D flow model can be used to estimate the distribution of the flow velocity along a particular cross section. At Baligaon village, two spurs are located (Figure 2.3), the velocity distribution upstream of at 'Spur2' computed from flow model is shown in Figure 5.44. The flow velocity at grids (s=445 and n=38 to 48) have been extracted and shown in this figure. The grid n= 38 is located on right bank 43 in mid stream and 48 in

left bank of the river. The figure shows that the flow velocities at the banks are smaller compared to the mid stream velocity. This difference is more visible for the low flow. At higher flow when most of the river width is occupied, the variation in flow velocity in the middle of river is small.

In addition to the temporal variation of the flood attribute (velocity) at a grid location, the 2D flow model is also capable of describing the velocity distribution in spatial domain as shown in **Figure 5.45**. The figure shows the current speed and flow direction at a specific instant during the simulation through black arrow lines. The length of the black arrow shows the magnitude of current speed. The diversion of flow around the spur and its impact on other banks can be visualized through the flow path. Further, the ineffective flow areas of low velocity can also be identified through such representation.

Figure 5.46 shows the temporal distribution of velocity around the spur. The velocity is plotted at three grid locations; upstream grid (448,42), nose of spur (450,44) and downstream grid (451,43). The figure shows that the velocity at the nose is high (twice compared with upstream grid velocity) while just in the downstream grid, it is very small (ineffective flow area). The spur diverts the flow near the bank, resulting into variation of water surface elevations around it. In the upstream end and at the nose of spur, the water surface elevation is higher compared to the water surface elevation in the downstream reach. The variation of water surface elevation around the spur is shown in Figure 5.47.

The extent of ineffective flow area can be estimated by comparing the flow velocity in successive grids downstream of the spur. Figure 5.48 shows the velocity distribution in successive grids. The small velocities in the downstream grids adjacent to spur {(452,43), (453,43), (454,53)} shows the extent where eddies are formed and velocity breaks. In this extent erosion may occur in the spur side bank due to eddies and circular flow. However, as the flow move further downstream grid (456,44) the flow velocity normalizes and becomes similar to the velocity at the upstream grid (448,42).

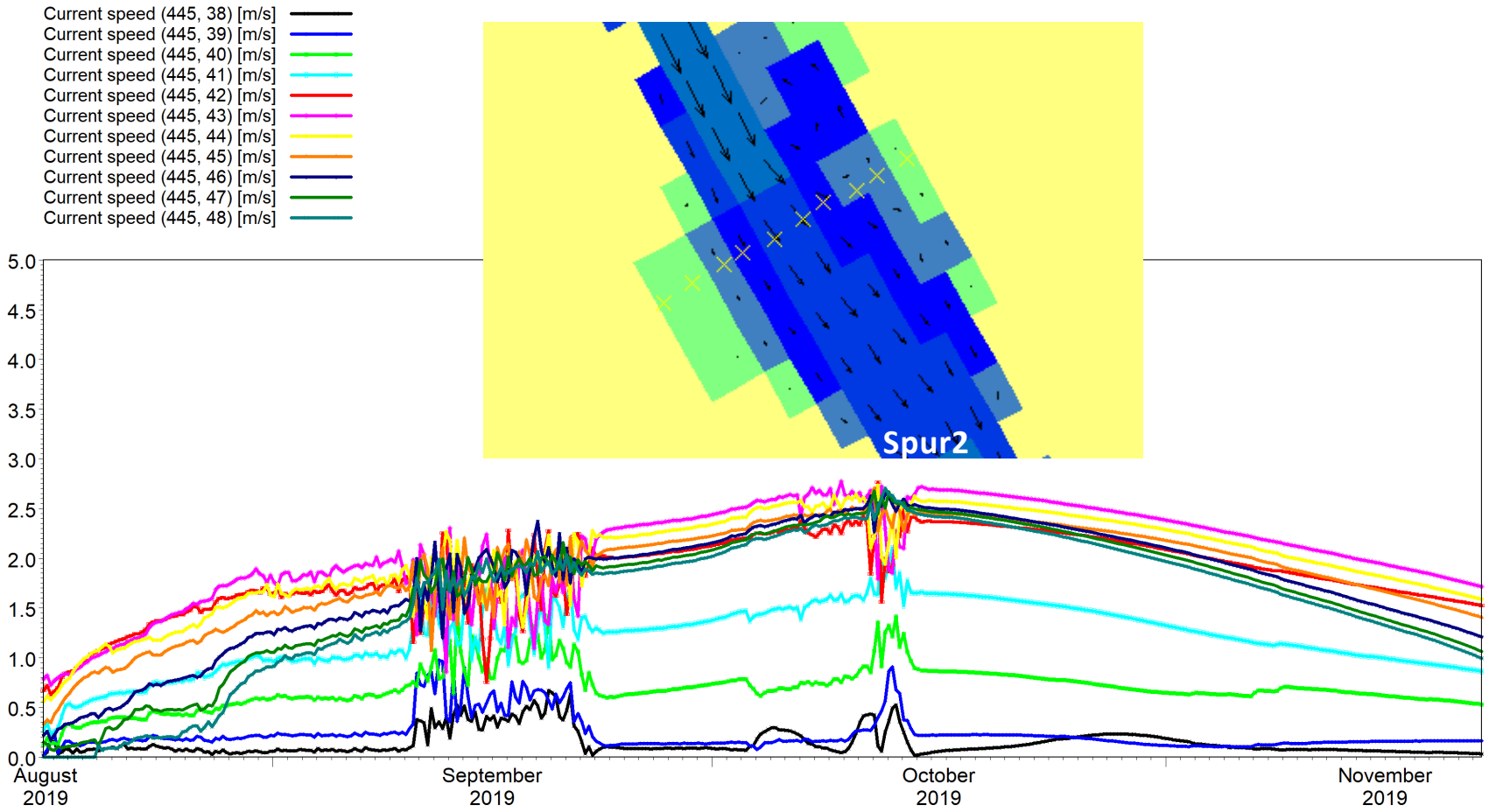

Figure 5.44: Velocity distribution along the cross section near upstream of 'Spur 2'.

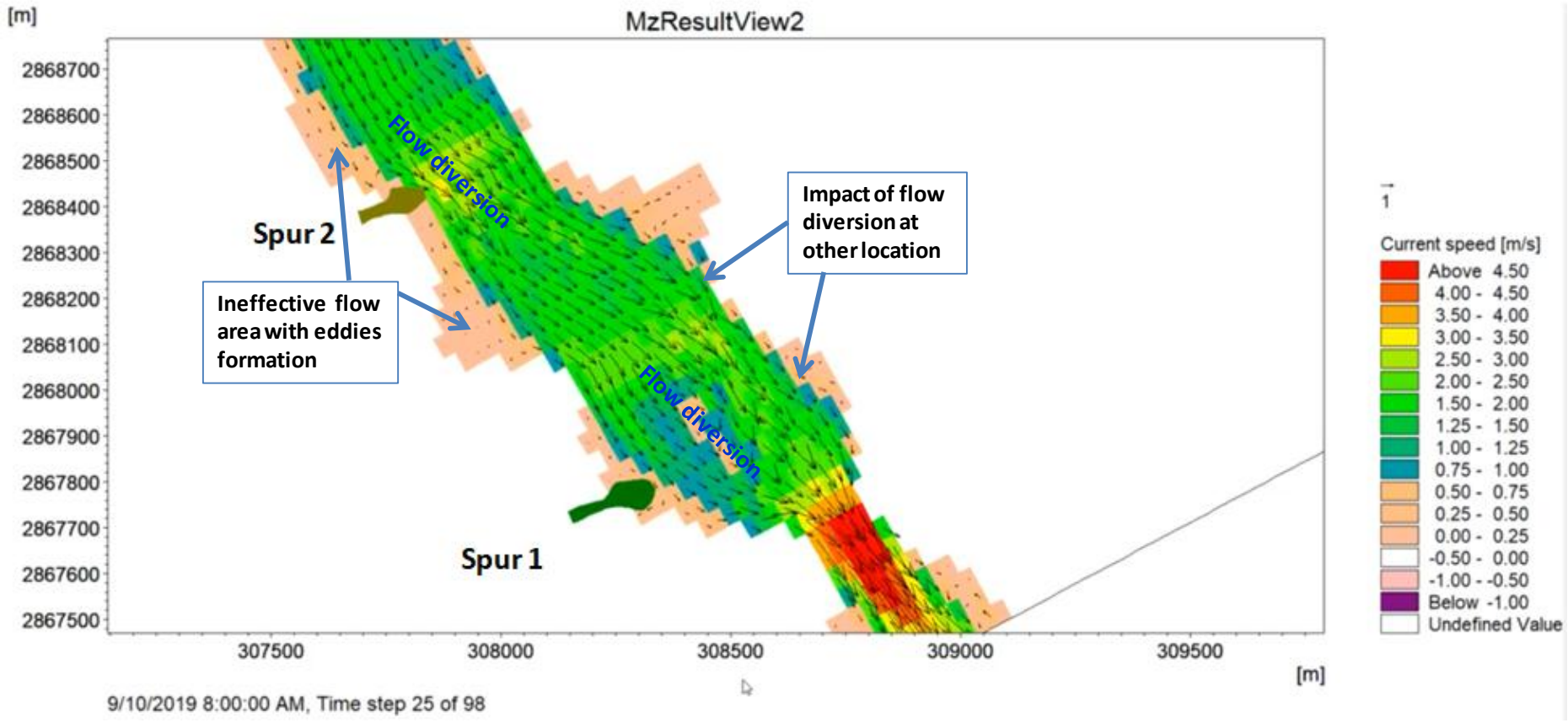

Figure 5.45: Spatial distribution of flow velocity and flow characteristics.

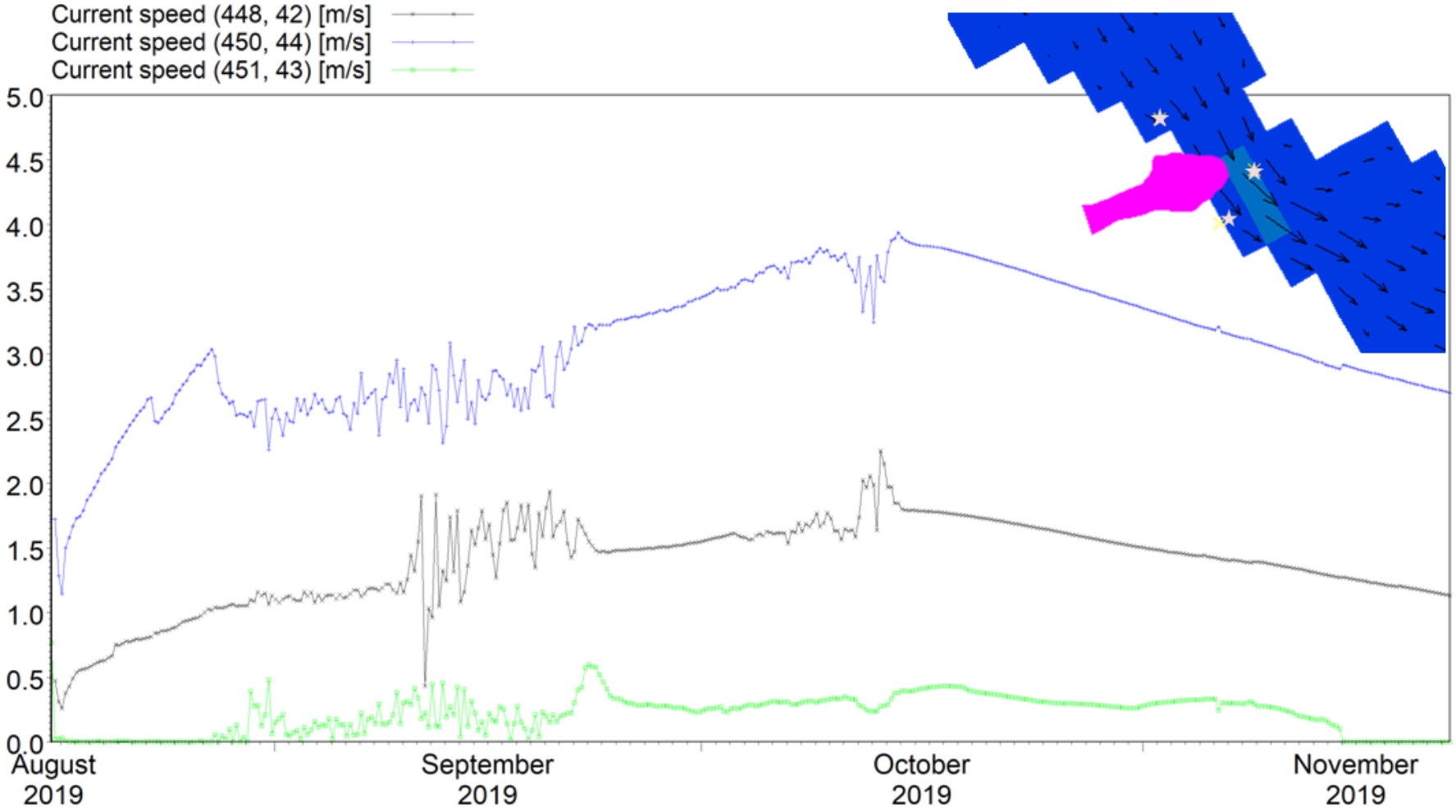

Figure 5.46: Flow velocity pattern near the spur.

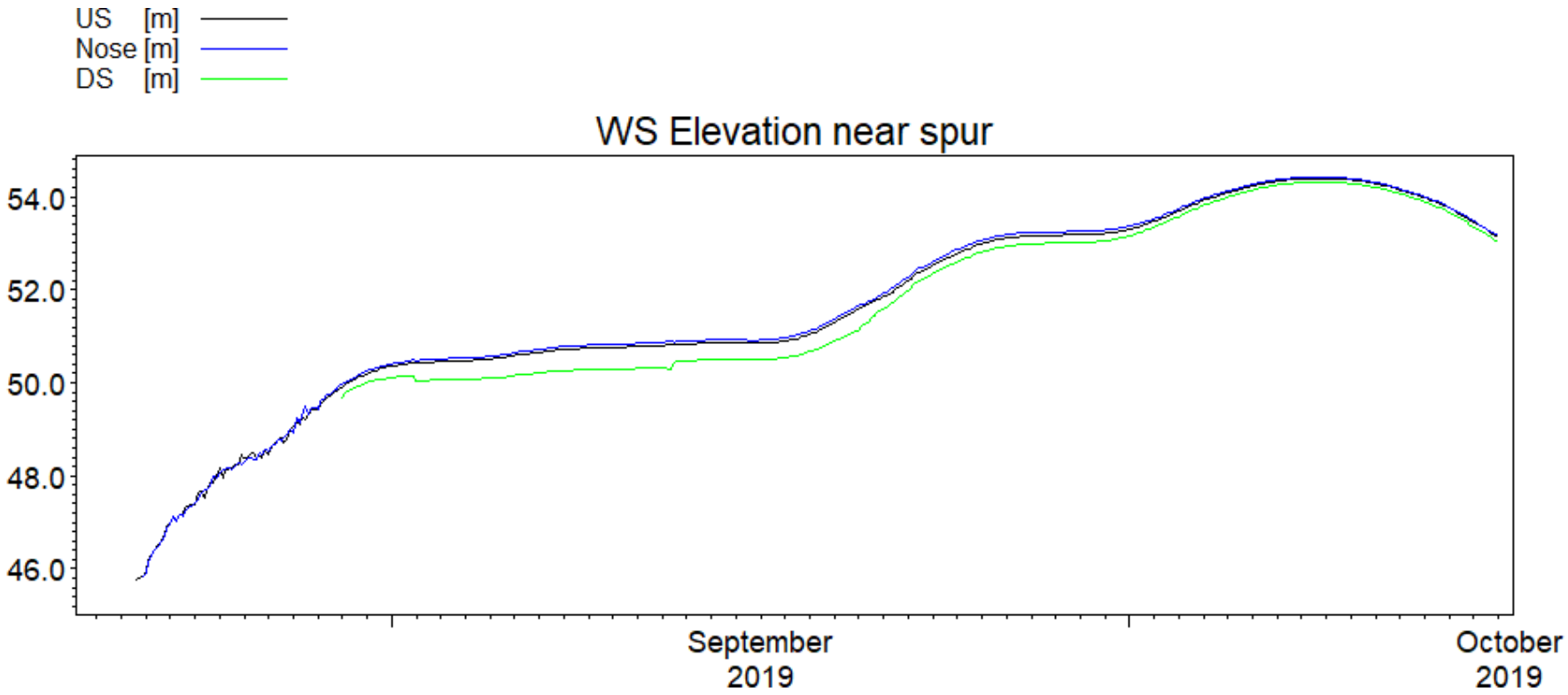

Figure 5.47: Variation of water surface elevation near the spur.

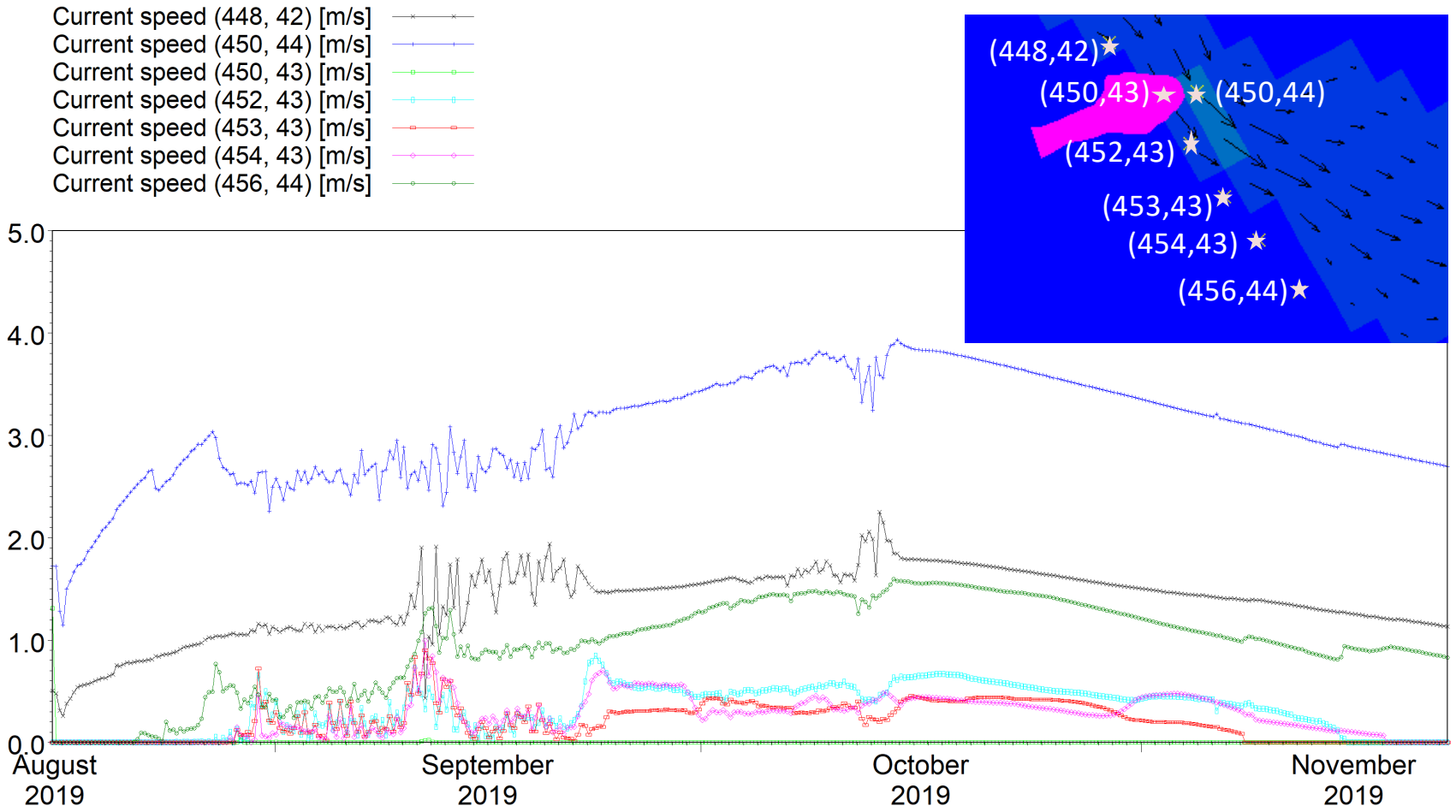

Figure 5.48: Effect of spur in the downstream reach.

5.4.5 Estimation of design parameters using 2D model

As per BIS (12094: 2000) guidelines, the flood protection measures and anti-erosion works are designed for 25- or 100- Yr flood depending upon the nature of area to be protected. The crest level for embankment predominantly for agricultural area is based on 25-yr flood level while for township/ industrial area/ important structures should be based on 100- yr flood level. Further, Stone/boulders used in revetment for bank protection is subjected to hydrodynamic drag and lift forces. These destabilizing forces are expressed in terms of velocity, tractate forces etc. the stabilizing forces acting against these are component of submerged weight of stone and downward component of force caused by contact of the stones. The weight of stones on slopes is the function of v^6, where, v is the velocity corresponding to the design flood. Similar design considerations are also adopted for design of spurs (BIS code 14262:1995). The 2D model results are used to develop the maximum flood level map and maximum flow velocity map. Using such maps, the maximum flood level and maximum flow velocity at any locations can be estimates.

Flow model is simulated for 25- Yr and 100- Yr flood as discussed in section 5.2 and the maximum flood level map and flow velocity maps are generated for 25-yr and 100-Yr flood. Figure 5.49 and Figure 5.51 show the maximum flood level maps for 25- and 100- yr flood, respectively. Similarly, Figure 5.50 and Figure 5.52 show the maximum flow velocity maps for 25- and 100- yr flood, respectively.

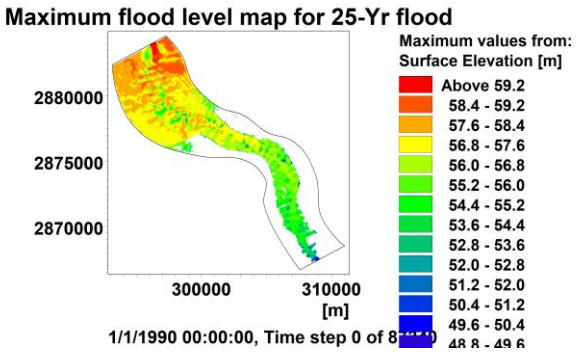

Figure 5.49: Maximum flood level map for 25- Yr flood.

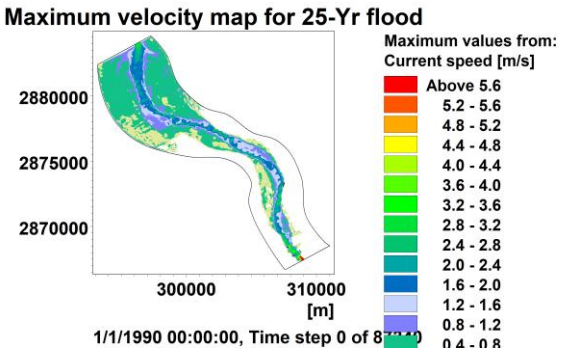

Figure 5.50: Maximum flow velocity map for 25- Yr flood.

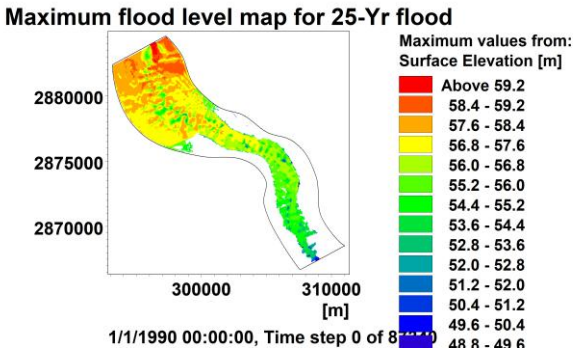

Figure 5.51: Maximum flood level map for 100- Yr flood.

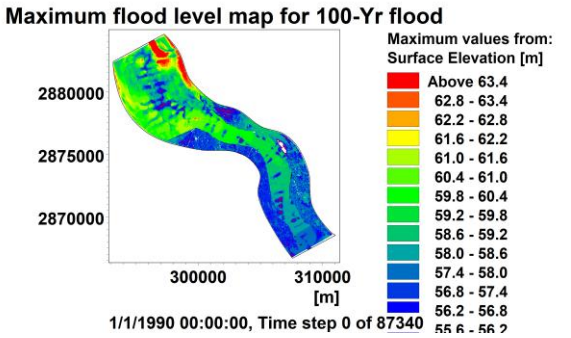

Figure 5.52: Maximum flow velocity map for 100- Yr flood.

In the flow model, two spurs and one bed bars have also been included in the flow model (Figure 2.3). The flood level and flow velocity profiles at these locations have also been plotted and the same has been compared with 1D flow model results given in Figure 5.23 and Figure 5.24. Spur 1 is located near Baligaon where the maximum flood level of 53.83 is estimated by 2D model (Figure 5.53) and maximum flow velocity is computed as 2.1 m/s (Figure 5.54) for 25- Yr flood. The maximum flood level of 54.01 m and maximum flow velocity of 1.43 m/s is estimated for 25- Yr flood using 1D flow model. Thus it is observed that 1D model estimates the slightly higher flood level while the flow velocity estimate is lower. The higher value of flood level may be attributed to (i) confinement of the flow within the bank in 1D model and (ii) average water level across cross section. On the other hand, in 2D simulations, the spills in the floodplain may causes reduction in water level and also the variation of water level across the cross section also occurs. However, the higher velocity in the 2D flow domain may be attributed to the inclusion of secondary flow, particularly at the bends.

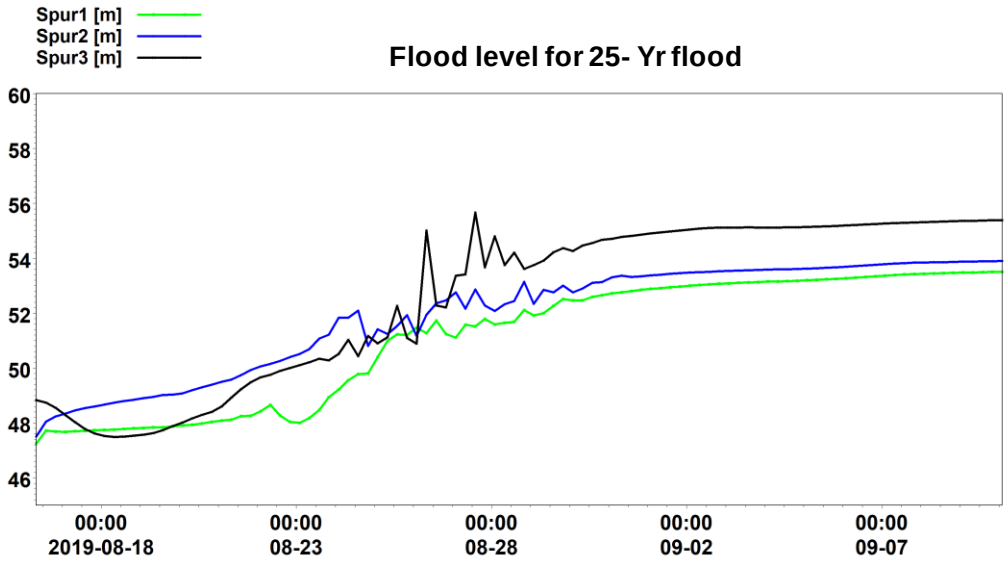

Figure 5.53: Time series of flood level at three anti-erosion works for 25- yr flood.

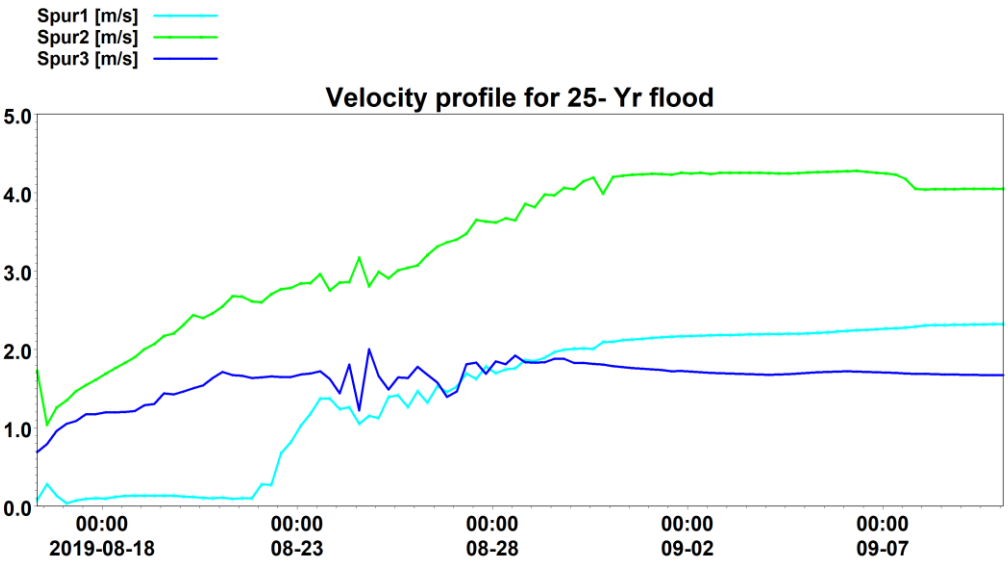

Figure 5.54: Time series of flow velocity at three anti-erosion works for 25- yr flood.

5.4.6 Spatial variation of flood attributes.

As water flows into a meander it takes on a helical or spiral flow which determines where erosion and deposition is concentrated. Centrifugal force draws water toward the outside bank (cut bank) causing erosion. Sediment eroded from the outside bank is deposited on the inside bank and transported downstream. These phenomenons are described through 2D curvilinear flow models. For 25- yr design flood, the maximum Helical map, Sedimentation Concentration map, Maximum Net Sedimentation map and Maximums Shear Stress maps are derived for the study area. The maximum values of flow attributes that has occurred during

the simulation at all the grids are shown in these maps. Helical flow component at the bends could be seen in the downstream reach shown by red polygons in Figure 5.55**Error! Reference source not found.**. These locations having high helical flow are more prone to erosion.

The maximum, sediment concentration map shown in Figure 5.56 shows that higher sediment concentration occurs in the upper reach. Thus the higher availability of sediments may cause sedimentation if other conditions are conducive. The figure also shows the alignment of left and right embankments by blue and red markers. The spacing of the embankments in the upper reach is more and therefore higher cross sectional area (causing fall in velocity) is available for design flood compared to the downstream reach. With higher availability of sediment concentration and higher flow area, the high sedimentation occurs in the upper reach as shown in Figure 5.57.

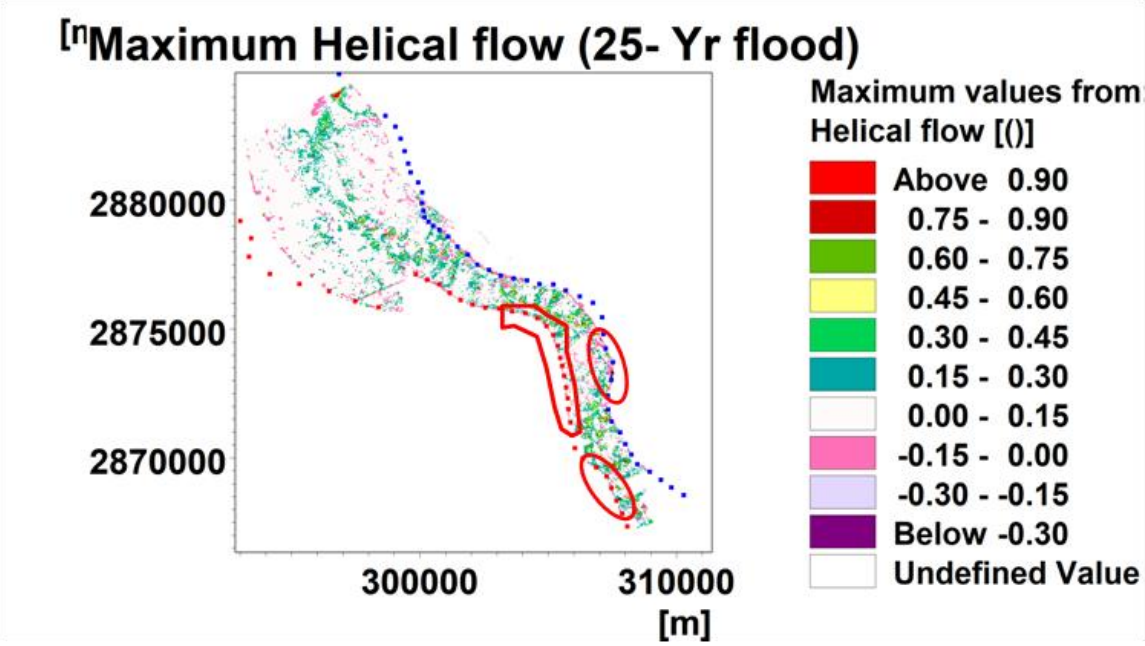

Figure 5.55: maximum Helical flow for 25- Yr flood

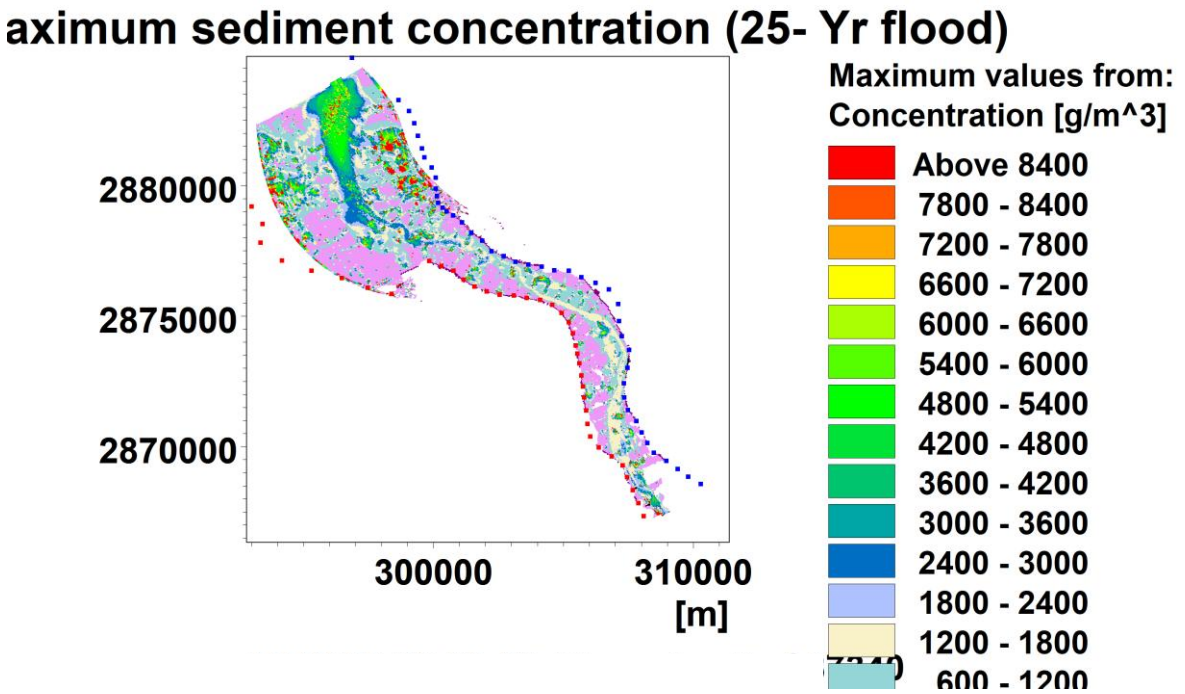

Figure 5.56: Maximum sediment concentration map.

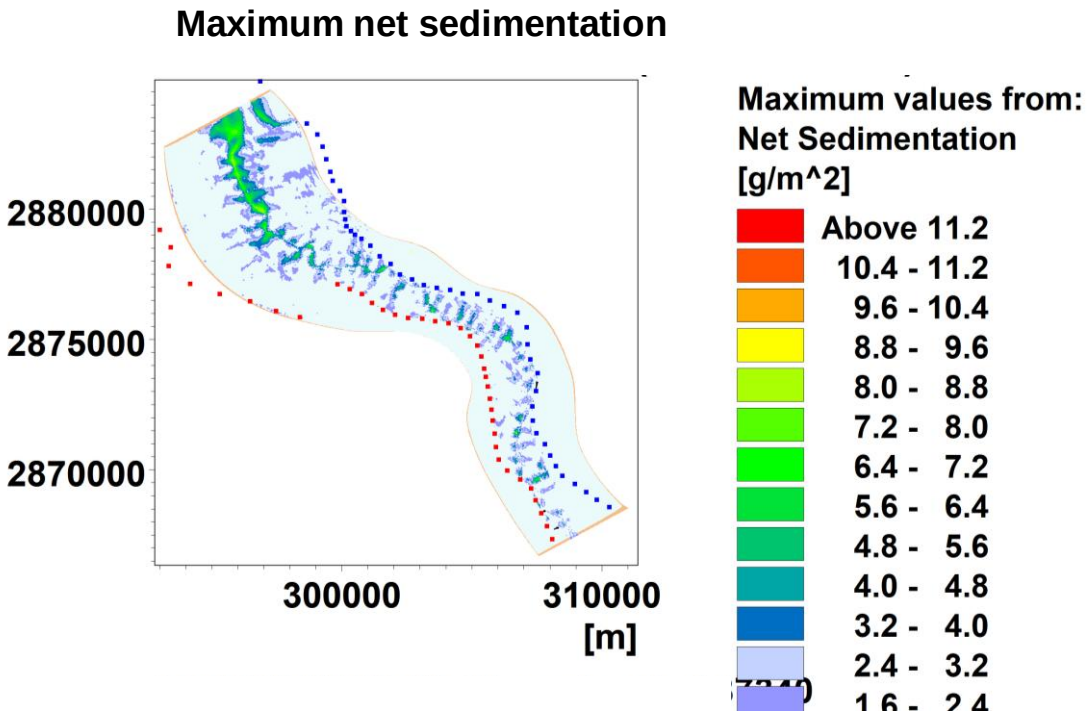

Figure 5.57: Maximum net sedimentation map.

Shear stress is a important parameters that determines the sedimentation and erosion process in alluvial river. In alluvial stream sediments of varying sizes, shapes and densities are

transported through flowing water which exerts shear stress on the bed particles. It is proportional to the velocity and density of the flowing water. The movement of the bed particles is determined by the critical shear stress required to overcome the frictional resistance between the particles and bed surface. When the shear stress acting on the bed particles exceed its critical shear stress, the particle will start to move. Thus the shear stress map represents the spatial distribution of the driving force responsible for bed or bank erosion. The maximum shear stress map for 25- yr flood is shown in Figure 5.58. The map shows that the shear stress is higher in the active flow area of river compared to floodplain. Further, in the downstream reach also, the shear stress is higher shown by red colour that represent the potential sites of erosion.

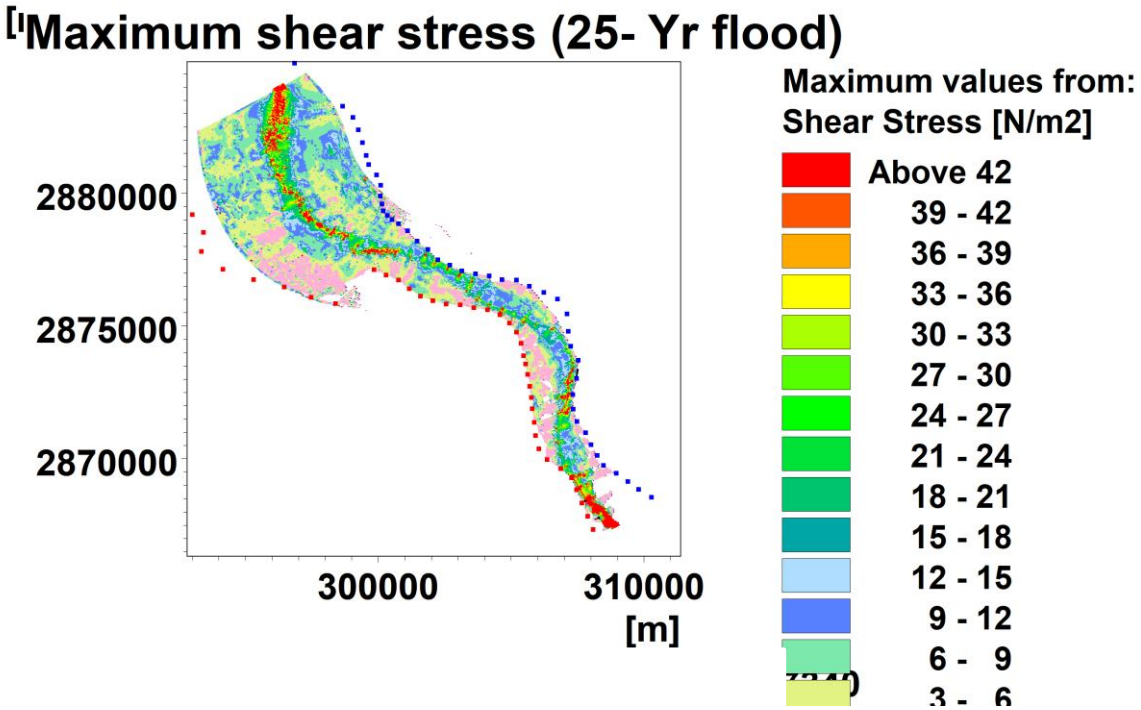

Figure 5.58: Maximum shear stress map for 25- yr flood.

5.4.7 Sediment balance Analysis

The flow simulation result for 2019 flood has been to compute the yearly total sediment passing through a cross section. As discussed earlier, the study stretch is divided into 481x133 (*j x k*) curvilinear grids. The total yearly sediment load is compute at every 50 j lines; namely, j=2, 50, 100, 150, 200, 250, 300, 350, 400, 450 and 479. Thus the Gandak river in the study stretch is divided into 10 zones. Based on the total sediment entering and

releasing from each zone, the sediment balance of the zone is carried out. If the sediment inflow is higher than the sediment outflow, the zone is considered as deposition zone and vice versa. Figure 5.59 shows the total sediment in Million Metric Ton (MMT) passing at various sections during the entire monsoon. Based on the sediment balance, the zone of erosion (E) and deposition (D) is determined and marked on the map.

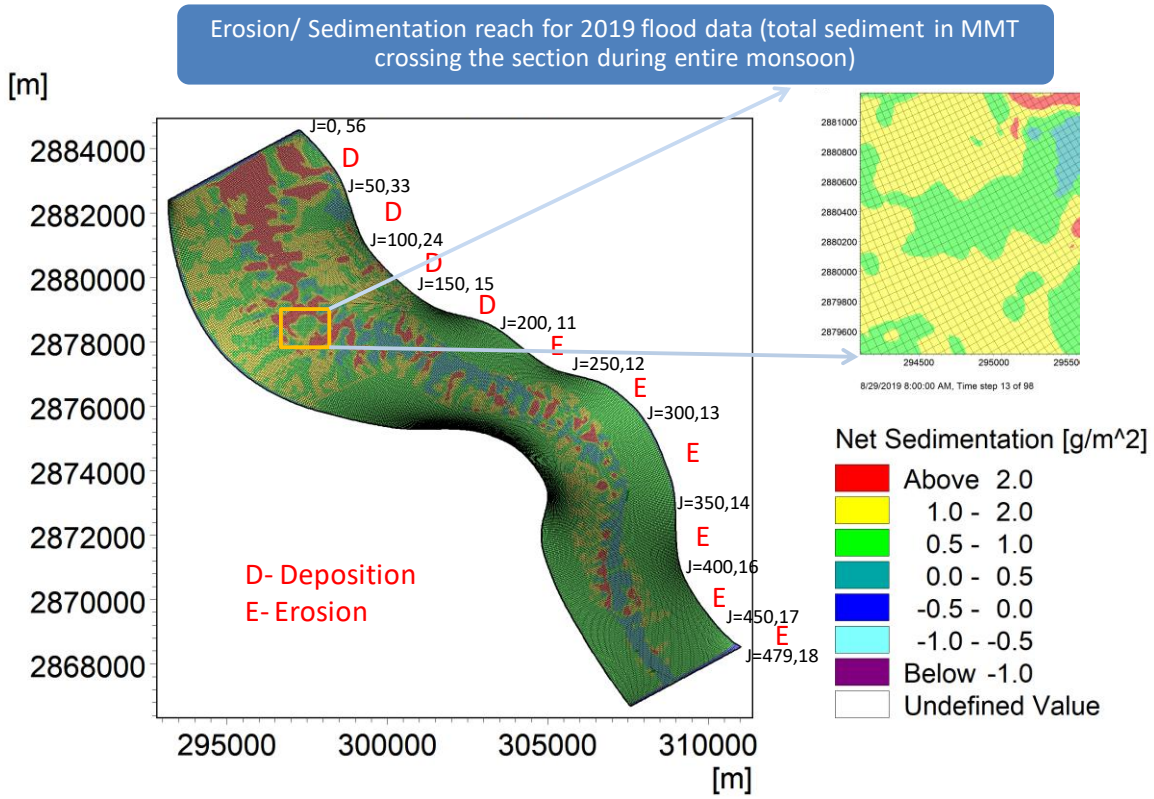

Figure 5.59: Location of erosion and deposition zone.

5.4.8 Short term morphological changes

Similar to the flood forecasting, river erosion prediction can help minimising damage and can help planners and designers to effectively formulate the flood protection measures and anti-erosions works. The flood protection measures are designed for probable flood of 25- or 100-Yr flood depending upon the area to be protected. However, the most frequent flood (annual average flood) are generally selected for predicting the river behaviour. In the study, medium-term (5- years) morphological prediction has been derived for the study stretch. The flood hydrograph of 2019 (which is equivalent to annual average flood) has been repeated for five years to generate the flows shown in Figure 5.60. The figure shows three red dots, corresponding to start of high flood, peak flood (annual average flood) and end of high flood

in each cycle of hydrograph. The flow characteristics at these three time lines in each cycle are extracted to understand the river behaviours.

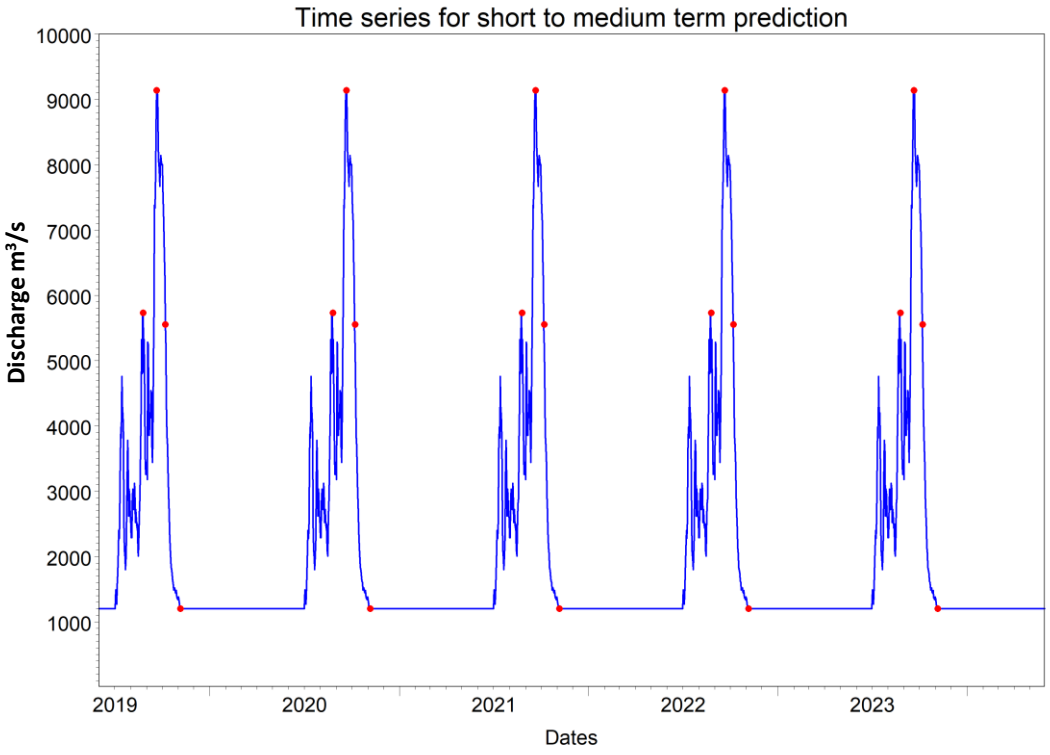

Figure 5.60: Flood hydrograph for short to medium term prediction.

The beginning of the monsoon is the base line condition to evaluate the bed or bank erosion. The start of high flood would generally be associated with start of erosion, increases gradually till the peak flood. At the end of high flood, depositions are expected which would continue till lean period. However, the local hydraulic conditions also govern the erosion and depositions. The bed level changes in the study at these time lines are extracted and monitored to understand the river morphological pattern. The bed level changes during the first year are shown in Figure 5.61. The grids with blue colour show the area of erosion while the green yellow and red colour shows the area of deposition. The figure shows that most of the erosion is concentrated within the main river channel depositions are noticed in the overbank area. The bed level changes at four time line after the second, third, fourth and fifth monsoon are shown in Figure 5.62, Figure 5.63, Figure 5.64, and Figure 5.65, respectively. These figures shows that with the uniform inflow pattern, the sedimentation/ erosion pattern fully develops after third year and very small changes are noticed in the fourth and fifth year. Hence, it may be concluded that such analysis are helpful in predicting short term (upto 3 years) morphological changes.

The absolute maximum magnitude of erosion over the consecutive five monsoons with AAF is shown in Figure 5.66. The figure shows that low to moderate erosion occurs in upper reach, particularly at the bends. Higher erosion is predicted in the lower reach and within the active river width.

The absolute maximum magnitude of deposition over the consecutive five monsoons with AAF is shown in Figure 5.67. The figure shows that the higher depositions occur in the middle reach and low to moderate depositions occurs in the upper and lower reach. Low depositions are also noticed in the floodplain particularly in the upper and middle reach.

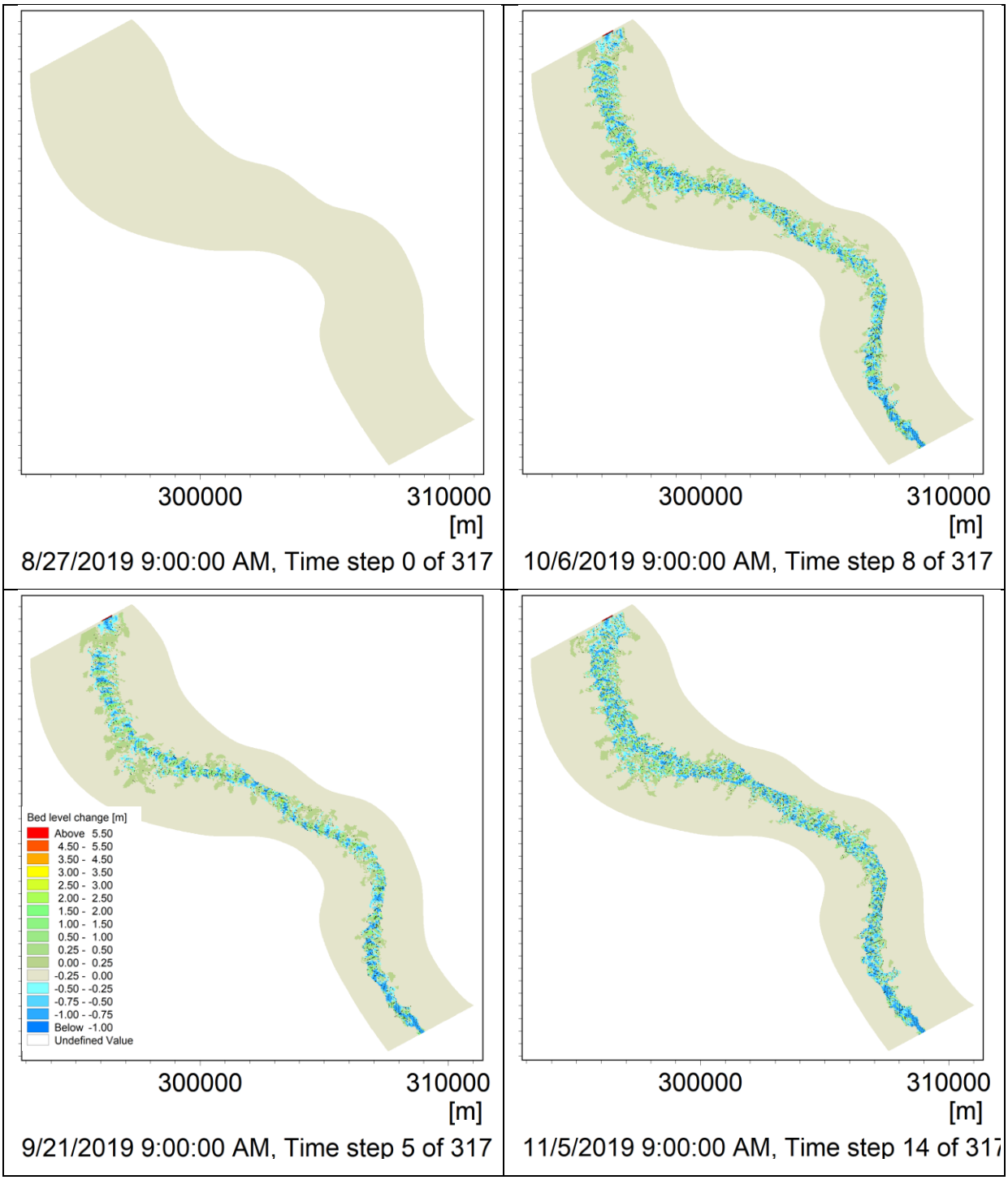

Figure 5.61: Bed level changes after 1st monsoon.

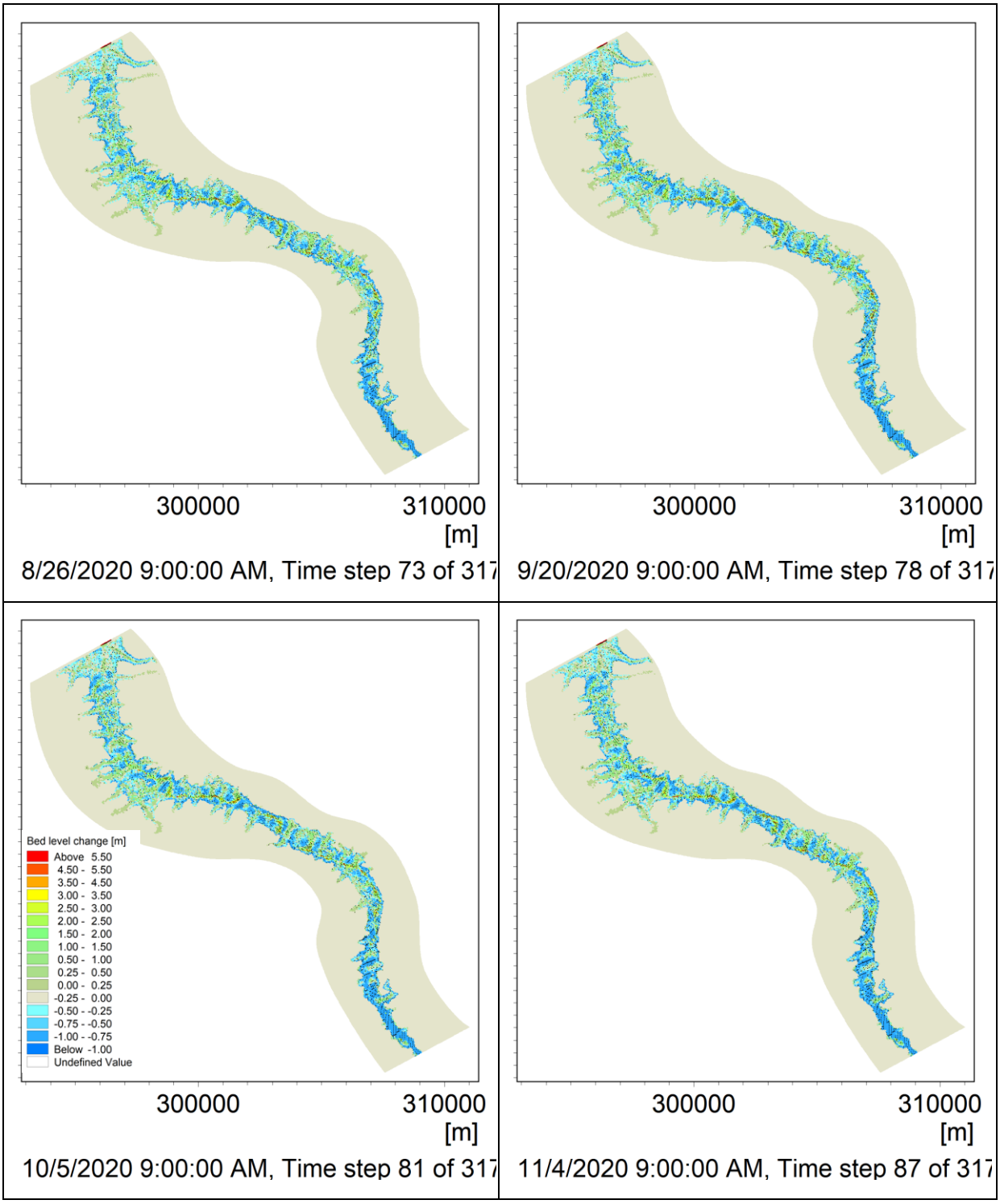

Figure 5.62: Bed level changes after 2nd monsoon.

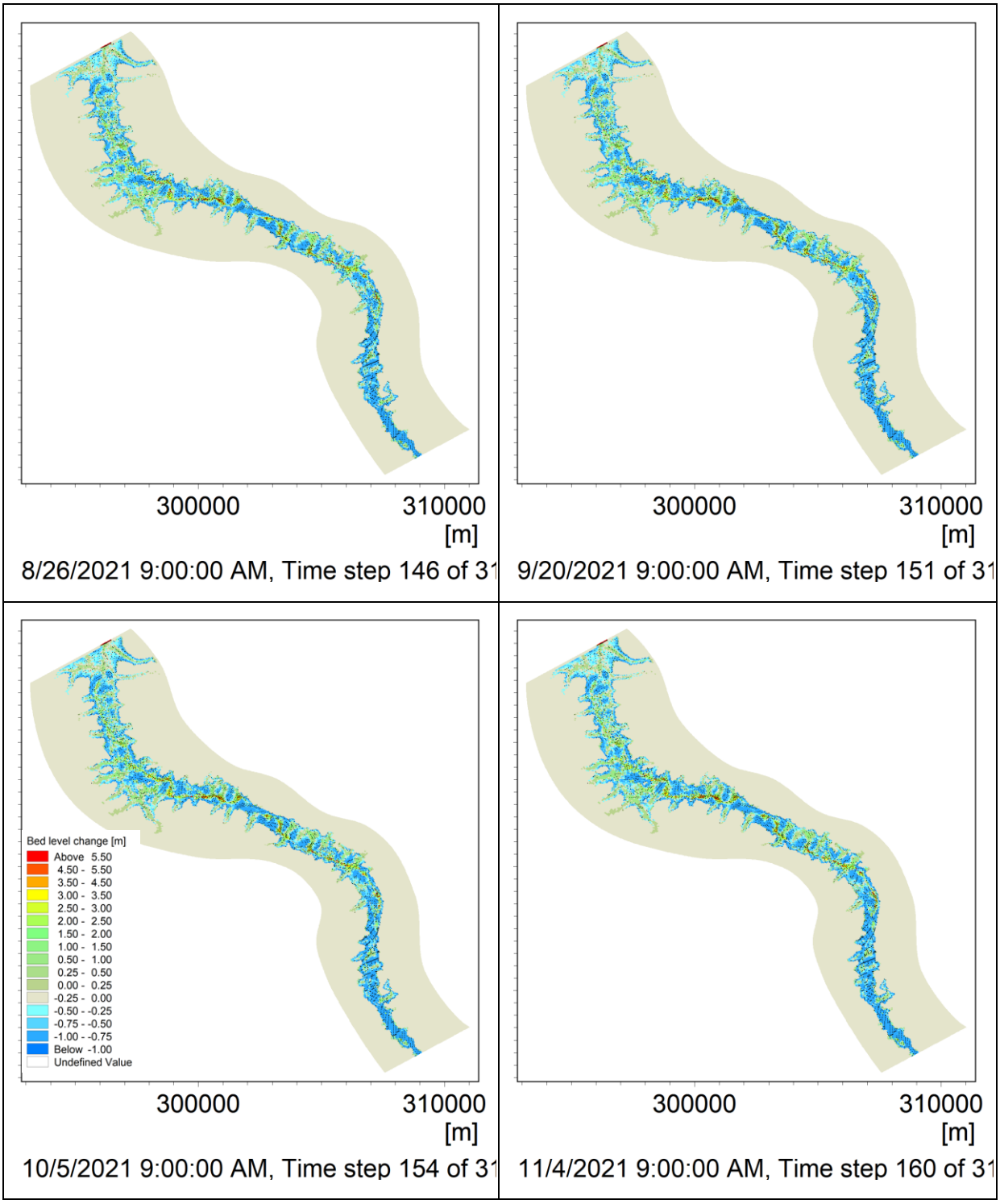

Figure 5.63: Bed level changes after 3rd monsoon.

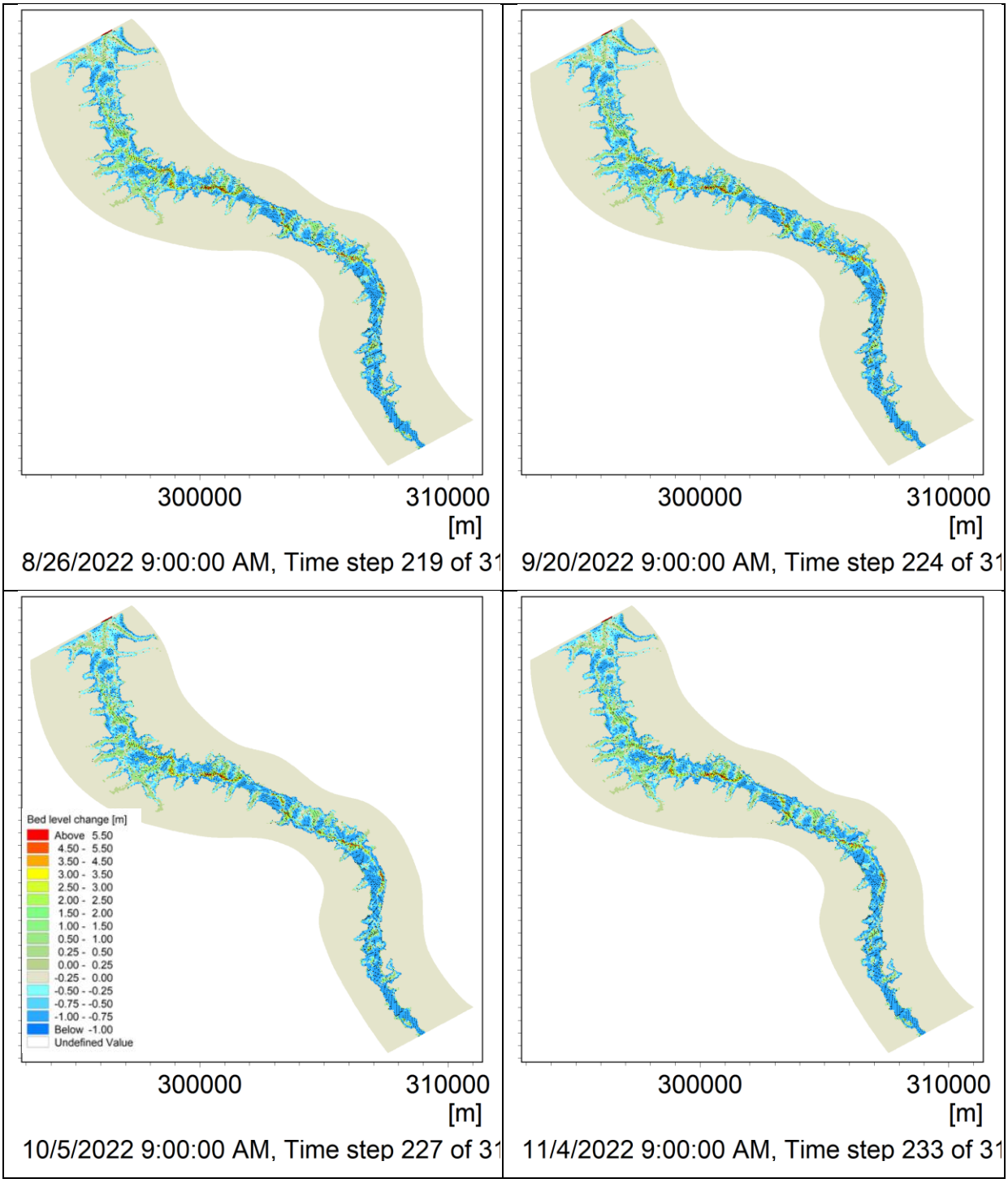

Figure 5.64: Bed level changes after 4th monsoon.

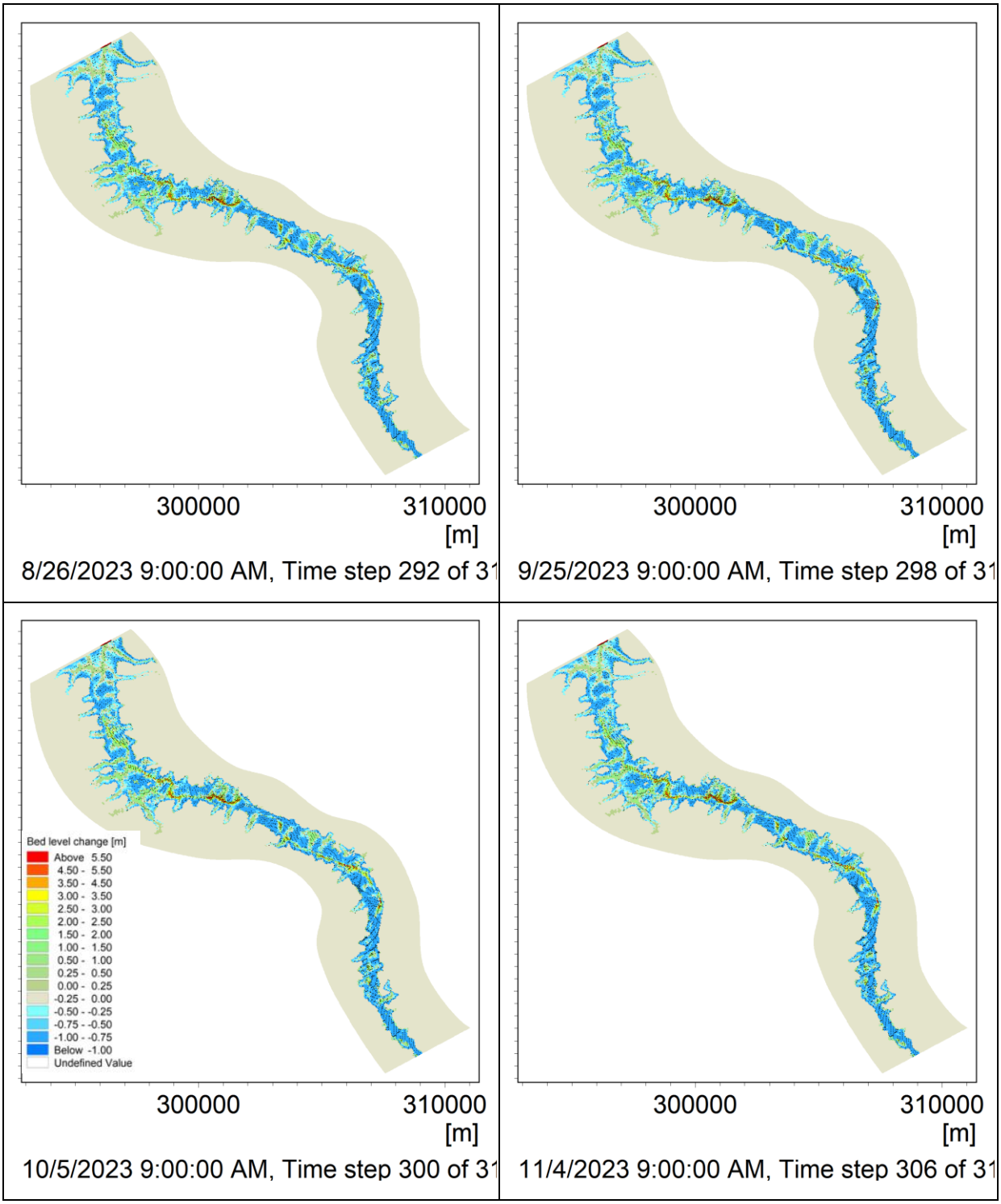

Figure 5.65: Bed level changes after 5th monsoon.

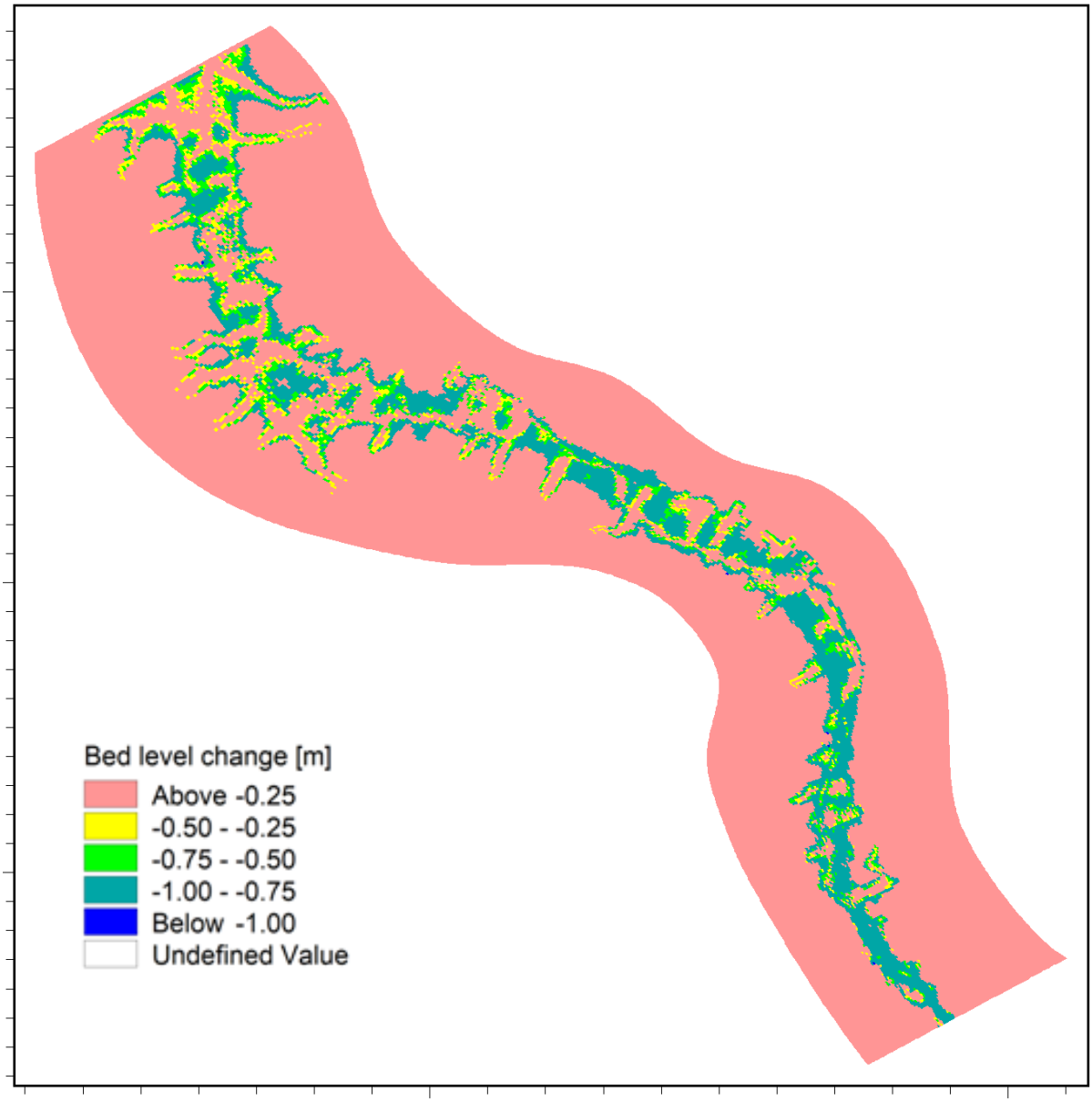

Figure 5.66: Absolute maximum degradation (erosion) predicted over five years of monsoon.

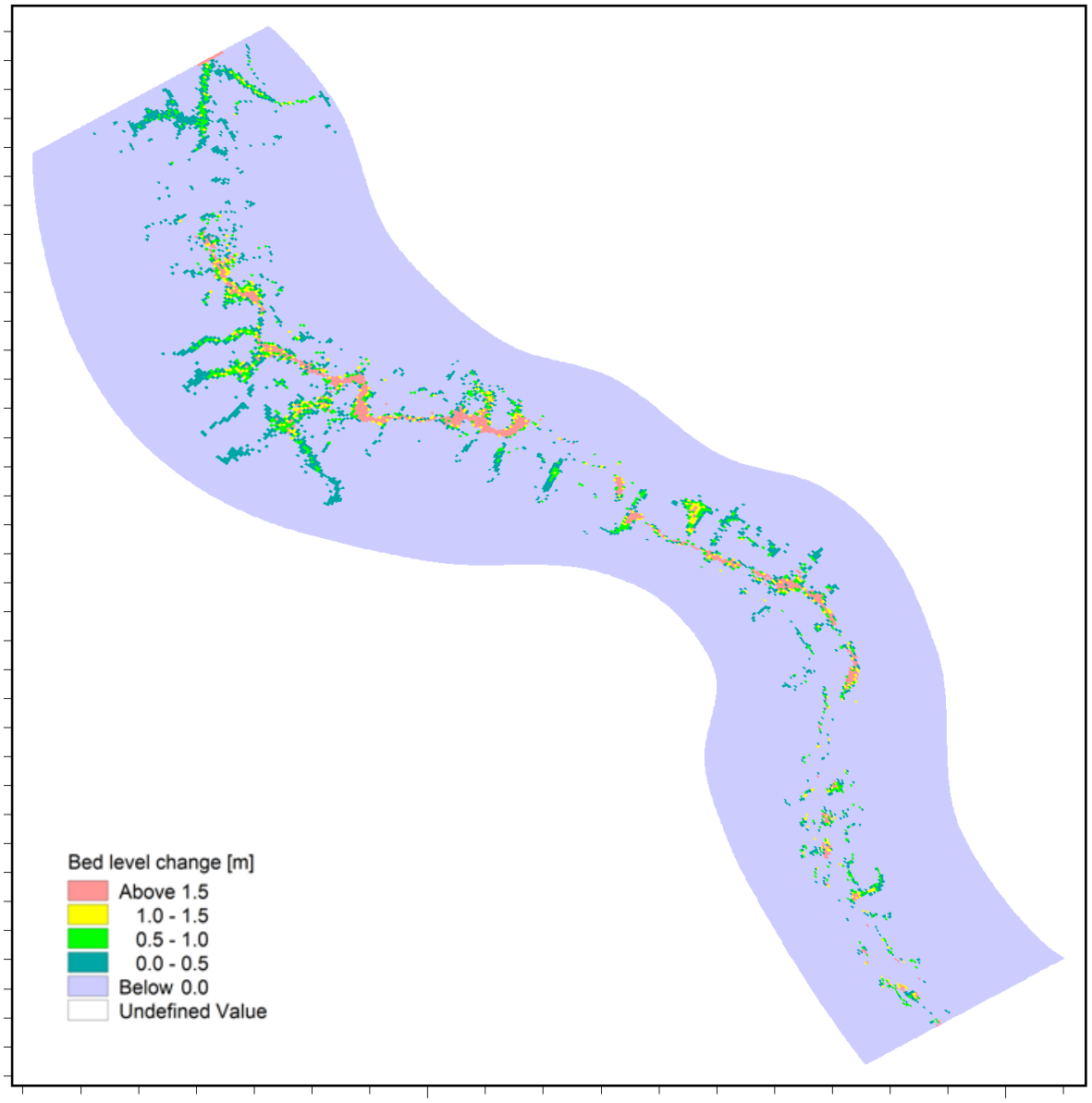

Figure 5.67: Absolute maximum aggradation (deposition) predicted over five years of monsoon.

5.5 Limitations of the 2D Curvilinear Model Study

The followings are the limitation of the study:

1. The bathymetry is based on the river cross section data which is available for the study stretch at the interval of 0.5 km. The average grid size along the river flow is 20-100 m and therefore interpolated river bed elevation has been used.
2. The observed sediment data is available for one year only (at Dumariaghat for 2020 and at Lalganj site for 2019).
3. .

6 SUMMARY AND CONCLUSIONS

The study has been carried out to understand the morphological behaviour of Gandak river in the study stretch. Several approach have been attempted, namely satellite based river morphology study, one dimensional hydrodynamic and morphodynamic model study and two dimensional curvilinear grid hydrodynamic and morphodynamic model study. In this section, the summary of the work of each approach and the conclusions derived thereon are reported.

6.1 Satellite based river morphology study

The river bank erosion, sediment deposition and shifting characteristics of the Gandak river from Dumariaghat to Hajipur is studied using temporal satellite images. The river bank line is delineated for 1975, 1980, 1991, 1995, 2000, 2005, 2010, 2015 and 2020 using open source LANDSAT satellite images. The image of 1975 is used as reference to compute the bank erosion and river shifting. The study stretch of Gandak River from Dumariaghat to Hajipur, is divided into 8 stretches. Three sites of major bank line shifting have been identified. The maximum shift near village Munja on right bank is computed as 2 km since 1975. Similarly, the maximum shift at Gokula Rupali on left bank is computed as 1.8 km since 1995. The third location is near Dharihara village where braiding nature of the river has been identified. At this location, the secondary channel which was prominent up to 1991 appears dormant in images of later date. However, it is seen reappearing again since 2021 images as observed in recent images in Google Earth applications.

The morphological parameters, namely; sinuosity and entrenchment ratio for each stretch is estimated for 2020 image and shown in table Table 6.1 below:

Table 6.1: Morphological parameters computed for different river stretches

River Stretch Name	Length (m)	Sinuosity	Entrenchment ratio
A	8723	1.08	1.58
B	4967	1.02	1.74
C	18644	1.29	1.68
D	6147	1.03	1.77
E	18168	1.23	2.15

F	6741	1.01	1.21
G	20699	1.08	2.68
H	14930	1.01	1.30

6.2 Estimation of Design Flood

The annual peak discharge observed at Dumariaghat and Lalganj sites are used to estimate the floods of various estimate using L moment based flood frequency analysis. The best fit distribution is identified based on Z_i^{dist} Statistic and L- moment ratio. The annual mean flood estimated at Dumariaghat and Lalganj GD sites are 9227 m^3/s and 9819 m^3/s, respectively. The best fit distribution identified for Dumariaghat adnd Lalganj sites are Pearson Type III (PE3) and generalized Logistic (GLO), respectively. The floods of various estimates for two sites are given in Table 6.2 below:

Table 6.2: L- moment based design flood estimate at Dumarighat and Lalganj GD sites.

S. No.	Return period (Years)	Flood Estimate (m3/s)	
		Dumarighat	Lalganj
1	2	8535	9063
2	10	14966	13639
3	20	17245	15956
4	25	17956	16781
5	50	20078	19667
6	100	22117	23143

The analysis shows that the peak of observed flood of 2019 is very close to annual average flood. The design flood hydrograph for various flood estimates are developed using observed time series of 2019 flood.

6.3 1D flow model ling

1 D flow model of Gandak river from Dumarighat to Hajipur GD sites in the stretch of 98 km has been developed in MIKE 11 using 78 surveyed cross section data (embankment to embankment). The model is calibrated and validated using observed flow and discharge data at Dumarighat, Rewaghat and Hajipur for the period of 2015-2020. The model is simulated for 2019 flood (AAR), 25- and 100-yr flood. The analysis shows that the river banks spills even at 25- yr flood at several locations. 1D sediment transport model is also developed for this reach and sediment transport rate (m3/s) is estimated for AAR, 25- and 100- yr flood.

The change in bed level is also estimated for these flooding conditions. The maximum flood level near Kunwari village is computed as 56.58 m and 57.07 m for 25- and 100- yr design flood. The maximum flow velocity at Kunwari village is computed as 1.33 m/s and 1.31 m/s for 25- and 100-yr flood, respectively. The maximum flood level near Baligaon spur site is estimated as 54.01 m and 54.58 m for 25- and 100-yr flood respectively. Similarly, the maximum flow velocity at Baligaon site is estimated 1.43 m/s and 1.49 m/s for 25- and 100-yr flood respectively.

1D sediment transport model shows that for 25-Yr flood, the average variations of bed level are 1.08 m, with maximum and minimum variation computed as 6.15 m and 0.35 m, respectively. Similarly, for 100- yr flood, the average variations of bed level are 1.14 m, with maximum and minimum variation computed as 5.52 m and 0.44 m, respectively. The model results shows that erosion occurs in the upper reach (up to Chainage 16.68 km) and further downstream deposition is estimated.

6.4 2D flow model ling

The 2D curvilinear grid model is generated in MIKE 21C Grid generator for the Gandak river in 20 km stretch from Kumari village to Baligaon village using 481x133 cells. The grid size along the flow varies from 20 to 100 m while the grid size along the cross section varies in the range of 15-80 m. The survey based river cross section data has been used to generate the bathymetry within the river bounds. For floodplain, ALOS PALSAR DEM has been used. The river and floodplain resistance Manning's M is defined as 43 (equivalent to 'n' = 0.023) and 20 (equivalent to 'n' = 0.05), respectively. MIKE 21C flow model is calibrated and validated with observed flow data of 2019 and 2022. Model results for flood level, flow velocity and its distribution across the cross sections and manmade structures (spurs) are analysed and plotted. The flood level and flow velocity at Spur 1 near Baligaon is computed as 53.83 m and 2.1 m/s. However, with 1D flow model, the flood level and flow velocity at the same location is computed as 54.01 m and 1.43 m/s. It is observed that 1D model estimates the higher flood level and lower flow velocity estimate.

The model results are evaluated for the velocity distribution in spatial domain to understand the flow diversion near the spur. The velocity at the nose of the spur is computed as twice the flow velocity in upstream grid. The spatial distribution of velocity also helps in identifying

the ineffective flow area downstream of the spur. The impact of spur in the downstream reach or on the other bank is also estimated through spatial velocity distribution.

Figure 5.46 shows the temporal distribution of velocity around the spur. The velocity is plotted at three grid locations; upstream grid (448,42), nose of spur (450,44) and downstream grid (451,43). The figure shows that the velocity at the nose is high (twice compared with upstream grid velocity) while just in the downstream grid, it is very small (ineffective flow area). The spur diverts the flow near the bank, resulting into variation of water surface elevations around it. In the upstream end and at the nose of spur, the water surface elevation is higher compared to the water surface elevation in the downstream reach. The variation of water surface elevation around the spur is shown in

The extent of ineffective flow area can be estimated by comparing the flow velocity in successive grids downstream of the spur. Figure 5.48 shows the velocity distribution in successive grids. The small velocities in the downstream grids adjacent to spur {(452,43), (453,43), (454,53)} shows the extent where eddies are formed and velocity breaks. In this extent erosion may occur in the spur side bank due to eddies and circular flow. However, as the flow move further downstream grid (456,44) the flow velocity normalizes and becomes similar to the velocity at the upstream grid (448,42).

For 25- yr design flood, the maximum Helical map, Sedimentation Concentration map, Maximum Net Sedimentation map and Maximums Shear Stress maps are derived. These maps shows the spatial distribution of erosion and sedimentation zone and helpful in identifying the erosion/ sedimentation prone reaches/ pockets in the study reach. The results show the higher sediment concentration, net sedimentation and shear stress in the upper reach. Few locations in the downstream reach are also identified as erosion prone following higher sediment concentration and shear stress.

The study reach is divided into 10 zones and the total sediment passing across each zone is computed for the annual average flood. Using the sediment balance concept, zone oe erosion and sedimentations have been identified. In the upper reach, mostly deposition (sedimentation) occurs while in the lower reach, mostly erosion is noticed.

Medium-term (5- years) morphological prediction has been derived with the 5 cycles of annual average flood. The areas of erosion and depositions in short to medium terms are identified by evaluating the changes in bed levels. It is found that most of the erosions are confined to active flow area while depositions are noticed at the banks and overflow section. It is found that with the uniform inflow pattern, the sedimentation/ erosion pattern fully develops after third year and very small changes are noticed in the fourth and fifth year.

BIBLIOGRAPHY

Alekseevskiy, N. I., Berkovich, K. M., & Chalov, R. S. (2008). Erosion, sediment transportation and accumulation in rivers. International Journal of Sediment Research, 23(2), 93–105. doi:10.1016/s1001-6279(08)60009-8

Amoudry, L. O., and Souza, A. J., 2011. Deterministic coastal morphological and sediment transport modeling: a review and discussion. Review of Geophysics, 49, RG2002, doi:10.1029/

Buffington, J.M. and Montgomery, D.R. 1999: Effects of sediment supply on surface textures of gravel-bed rivers. Water Resources Research 35, **3523–30**

CWC, 2018, Comprehensive Flood Management in India, Central Water Commission, Department of Water Resources, River Development and Ganga Rejuvenation, Ministry of Jal Shakti, https://cwc.gov.in/sites/default/files/comprehensive-flood-management-india-2018.pdf.

CWC, 2022, State wise flood damage statistics data, Central Water Commission, Department of Water Resources, River Development and Ganga Rejuvenation, Ministry of Jal Shakti, https://cwc.gov.in/sites/default/files/flood-damage-data-merged.pdf.

Einstein, H. A., 1942. Formula for the transportation of bed load. Transportation ASCE, 107, 561–597.

Gaurav, Kumar, François Métivier, Olivier Devauchelle, Rajiv Sinha, Hugo Chauvet, Morgane Houssais, and Hélène Bouquerel. "Morphology of the Kosi megafan channels." Earth Surface Dynamics 3, no. 3 (2015): 321-331. https://doi.org/10.5194/esurf-3-321-2015 [PDF]

Geschiebebewegung, Mitt. Preuss. Vers. Wasserbau Schiffbau, 26, 5–24.

GFCC (2022), Annual Report of Ganga Flood Control Commission, Department of Water Resources, River Development and Ganga Rejuvenation, Ministry of Jal Shakti, https://gfcc.gov.in/annual-reports

HABERSACK H., BERNHARD SCHOBER B., HAUER C., Floodplain evaluation matrix (FEM): An interdisciplinary method for evaluating river floodplains in the context of integrated flood risk management. Natural Hazards, 75, 2015.

Hudson, P. F. (2017). Fluvial Depositional Processes and Landforms. International Encyclopedia of Geography: People, the Earth, Environment and Technology, 1–9. doi:10.1002/9781118786352.wbi

Luna Bergere Leopold and M. Gordon Wolman, 1957, **River channel patterns: Braided, meandering, and straight,** Professional Paper 282-B, By:, https://doi.org/10.3133/pp282B,

National Statistical Office, 2022 Agricultural Statistics at a Glance 2022, Government of India Ministry of Agriculture & Farmers Welfare Department of Agriculture & Farmers Welfare Economics & Statistics Division, pp. 211–266.

Nelson, J. M., Shreve, R. L., McLean, S. R., and Drake, T. G., 1995. Role of near-bed turbulence structure in bed load transport and bed form mechanics. Water Resources Research, 31(8), 2071–2086,

Rattan, Mehak & Sidhu, G.S. & Singh, Sandeep. (2021). History of Land Use In The Indo Gangetic Plains, India and Its Impact On Population: A Review. Plant Archives. 21. 532-537. 10.51470/PLANTARCHIVES.2021.v21.S1.082.

Richards, K. 1982: Rivers: form and process in alluvial channels. London: Methuen. xi + 358 pp.

Rinaldi, M., Wyżga, B., Dufour, S., Bertoldi, W., & Gurnell, A. (2013). 12.4 River Processes and Implications for Fluvial Ecogeomorphology: A European Perspective. Treatise on Geomorphology, 37–52. doi:10.1016/b978-0-12-374739-6.00321-3

Sehgal, V.K.; Singh, M.R.; Chaudhary, A.; Jain, N. and Pathak, H. (2013). Vulnerability of agriculture to climate change: District level assessment in the Indogangetic Plains. New Delhi: Indian Agricultural Research Institute.

Shields, A., 1936. Anwendung der Ahnlichkeitsmechanik und Turbulenz forschung auf die

Singh 2012, Probable Agricultural Biodiversity Heritage Sites in India:XI. The Upper Gangetic Plains Region, Anurudh K Singh, Asian Agri-History Vol. 16, No. 1, 2012 (21–44.

van Rijn, L. C., 1984. Sediment pick-up function. Journal of Hydraulic Engineering ASCE, 110(10), 1494–1502.

Vanoni, V.A. (1984), Fifty Years of Sedimentation, J. Hyd. Eng. ASCE, Vol. 110, No. 8

Vivekanandan, N.. (2015). Flood frequency analysis using method of moments and L-moments of probability distributions. Cogent Engineering. 2. 1018704. 10.1080/23311916.2015.1018704.

Yang, C. T., 1996. Sediment Transport, Theory and Practice. New York: McGraw-Hill,

ANNEXURES

Annexure I

Office of the Joint Director
Flood Management Improvement Support Centre
Jal Sansadhan Bhawan, Anisabad, Patna

Letter no.-FMISC-30/2017- 660

From,

Er. Anil Kumar
Joint Director

To,

Mr. Biswajit Chakravorty
Scientist G & Head
Centre for Flood Management Studies
National Institute of Hydrology
Walmi, Patna

Patna/dated-28/08/2019

Sub:- Nomination of Principal Investigator (PI) and Co- Principal Investigator (Co-P regarding Purpose driven studies (PDS) under National Hydrology Project.

Ref:- Your Letter no.-CFMS/PDS/50.10/241 dated-06 August 2019

Sir,

As directed, with reference to above letter the following officers from FMISC, WRD, Patna are nominated as Principal Investigator (PI) and Co- Principal Investigator (Co-PI) for study of **"Gandak- From Kunwari village (near 47km. Of Saran Embankment) in u/s of Rewa Ghat up to Baligaon (near 30 km. Of Saran Embankment) in d/s of Rewa Ghat bridge"** regarding Purpose driven studies under National Hydrology Project.

i. Md. Perwez Akhtar, Deputy Director, FMISC, Patna - PI
ii. Er. Bindiya Gupta, Assistant Director, FMISC, Patna - Co-PI
iii. Er. Manish Kumar, Assistant Director, FMISC, Patna - Co-PI

This is for your kind information and necessary action.

Yours faithfully

28/8

(Anil Kumar)
Joint Director

Letter no.-FMISC-30/2017- 660 Patna/dated-28/08/2019

Copy to:- Md. Perwez Akhtar, Deputy Director / Er. Bindiya Gupta, Assistant Director/ Er. Manish Kumar, Assistant Director, FMISC Patna for information and necessary action.

28/8

(Anil Kumar)
Joint Director

b lett-19

Annexure III

Selection of vulnerable sites for ^_PDS^_ Studies under NHP

From: NHP (biharswhp3@gmail.com)

To: mailofpmani@yahoo.com

Date: Friday, 21 June, 2019, 02:38 pm IST

Dear Sir,
Please find the attachment related to lists of the suitable sites/study areas for Modelling and Management of erosion and sedimentation processes in the alluvial river using Morphodynamic modelling under Purpose Driven Studies (PDS) on the River Gandak, Kosi and the Ganges. The lists have been prepared on the basis of proposal received from field officers which are as below:-.

Name of River	Sites/ Study Area
1. Gandak	From Km 22.00 to Km. 24 of P.P Embankment
2. Gandak	From Km 00.00 to Km 3.50 -G-H Reach (P.P Embankment)
3. Gandak	From Ahiraulidan (UP Bihar Border) in u/s of Bettiah Gopalganj Bridge up to Makhsudpur in d/s of bridge
4. Gandak	From Salempur in u/s of Dumaria Ghat bridge up to Bansghat Mansuriya near Mahanrani Chharki in d/s of Dumaria Ghat bridge
5. Gandak	From Bandhauli (near Banhauli- Sitalpur Faijullahpur jamindari bandh to Basa hiya village near 71 km. of Saran embankment.
6. Gandak	From Kunwari village (near 47 km. of Saran Embankment) in u/s of Rewa Ghat up to Baligaon (near 30 km. of Saran Embankment) in d/s of Rewa Ghat bridge
7. Gandak	From Dariyapur (near 10 km. of Saran Embankment) to the confluence of Gandak with Ganga river near Pahleja Ghat
8. Gandak	From Tajpur (near 70km of 7 no Gogra Embankment in u/s of Manjhi bridge to confluence of Ghaghra and Ganga in d/s of bridge near Prabhunath Nagar.
9. Kosi	From Km. 26.88 to km. 27.40 of Eastern Afflux Bandh
10. Kosi	From Km. 10.90 to Km. 11.70 of Eastern Kosi Embankment
11. Kosi	From Km. 20.50 to Km. 20.70 of Eastern Kosi Embankment
12. Kosi	u/s and d/s of Km. 64.2, Km. 64.95 & 78.30 of Eastern Kosi Embankment
13. Kosi	From Km. 6.00 to Km. 6.40, Km. 8.00 to Km. 9.00 Km. 13.20 of ESML
14 Kosi	From Hario to Chorhar on Bagjan Embankment
15.Ganga	Near Ismailpur- Bindtoli embankment

It is requested to suggest 2-3 suitable sites/study areas on a priority basis so that it could be finalized after getting the approval from Department for the PDS proposal.

Regards,

Anil Kumar
Joint Director
FMISC,WRD Bihar
Nodal Office-NHP Bihar(SW)
Anisabad, Patna - 800 002

On Fri, May 17, 2019 at 11:09 AM Pankaj Mani <mailofpmani@yahoo.com> wrote:

> Sir,

I am enclosing the coverining letter and PDS proposal for needful action.

The necessary format for providing consent is given in the PDS proposal.

Thanks

Dr. Pankaj Mani
Scientist E
National Institute of Hydrology
WALMI Complex, Phulwarisharif,
Patna.
phone - 0612-2452219, 2452227.
9471006278, 9334257300 (m),
mailofpmani@yahoo.com, cfmspatna@gmail.com

Morphodynamic Module study letter.pdf
1.3MB

Morphodynamic Module study letter no.-1254, dt.-04.06.2019.pdf
531.6kB

Morphodynamic Module study letter no.-519, dt.-01.06.2019.pdf
487.8kB

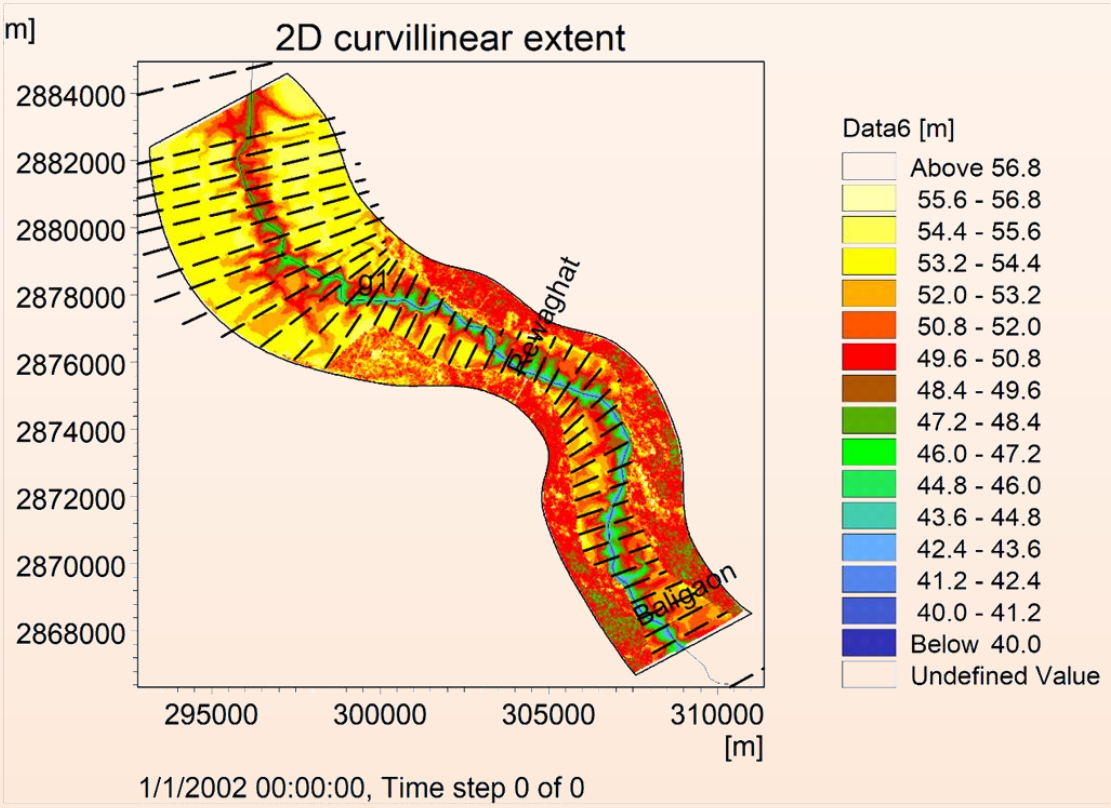

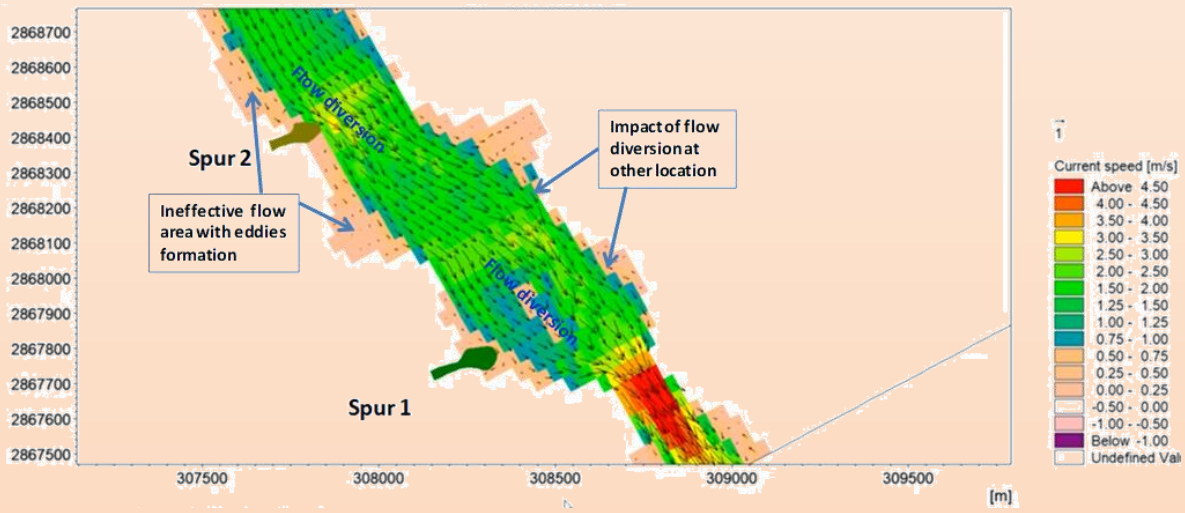

NATIONAL INSTITUTE OF HYDROLOGY

ROORKEE – 247 667, UTTARAKHAND

Website: www. nihroorkee.gov.in